11-17-2017

Wind Loads on Residential Rooftop Solar Photovoltaic Panels

Amir Naeiji
Florida International University, anaei001@fiu.edu

DOI: 10.25148/etd.FIDC006588

FLORIDA INTERNATIONAL UNIVERSITY

Miami, Florida

WIND LOADS ON RESIDENTIAL ROOFTOP SOLAR PHOTOVOLTAIC PANELS

A dissertation submitted in partial fulfillment of

the requirements for the degree of

DOCTOR OF PHILOSIPHY

in

CIVIL ENGINEERING

by

Amir Naeiji

2018

To: Dean John L. Volakis
College of Engineering and Computing

This dissertation, written by Amir Naeiji, and entitled Wind Loads on Residential Rooftop Solar Photovoltaic Panels, having been approved in respect to style and intellectual content, is referred to you for judgment.

We have read this dissertation and recommend that it be approved.

_____
Irtishad Ahmad

_____
Peter Irwin

_____
Arindam Gan Chowdhury

_____
David Garber

_____
Ioannis Zisis, Major Professor

Date of Defense: November 17, 2017

The dissertation of Amir Naeiji is approved.

_____
Dean John L. Volakis
College of Engineering and Computing

_____
Andrés G. Gil
Vice President for Research and Economic Development
and Dean of the University Graduate School

Florida International University, 2018

DEDICATION

I would like to dedicate this dissertation to my beloved wife, parents and brother for their wholehearted support and encouragements.

ACKNOWLEDGMENTS

The author is very grateful to his major advisor Dr. Ioannis Zisis for his supervision and support throughout these years. Because of his initiatives, the research was possible firstly, and his insightful comments and continuous guidance were always a great source of encouragement.

Special thanks to Dr. Peter Irwin and Dr. Arindam Gan Chowdhury that their special expertise and invaluable contributions was vital to this research. Sincere appreciation to the members of my doctoral committee, Dr. Ahmad and Dr. Garber for their valuable participation and accessibility.

Thanks are due to the Wall of Wind Experimental Facility staff Raphael Greenbaum, Walter Conklin, Roy Liu Marques, Maryam Refan and Ashkan Rasouli who provided help on the experimental setup and tests. Sincere thanks to my friends and colleagues, Mohammadtaghi Moravej and Manuel Matus for their help and collaborations.

The support from the International Hurricane Research Center (IHRC) at FIU and Florida Division of Emergency Management is greatly acknowledged. The writing phase of this dissertation has been funded by The Dissertation Year Fellowship (DYF) at FIU.

ABSTRACT OF THE DISSERTATION

WIND LOADS ON RESIDENTIAL ROOFTOP SOLAR PHOTOVOLTAIC PANELS

by

Amir Naeiji

Florida International University, 2018

Miami, Florida

Professor Ioannis Zisis, Major Professor

Solar energy harvesting using photovoltaic (PV) systems has gained popularity in recent years due to its relative ease of use and its cost efficiency compared to the rest of the clean energy sources. However, to further expand the application of PV systems requires making them more desirable than the other competitive energy sources. The improvement of safety and cost efficiency are requisites for further popularization of PV system application. To satisfy these requisites it is necessary to optimally design the system against the environmental conditions. Wind action is one of the main ambient loads affecting the performance of PV systems. This dissertation aims to investigate the effects of wind load on residential scale roof mounted PV panels and their supporting structures as well as evaluating the structural response of the system to the wind-induced vibration. To achieve these goals, several full- and large-scale experimental tests were performed at the Wall of Wind Experimental Facility at Florida International University (FIU). The wind effects on different PV system and roof configurations were investigated in these tests. The

results shed light on the most influential parameters affecting the wind pressures acting on the PV panel surface. In addition, the findings are presented in the form of design pressure coefficients for adoption to future building codes and wind standards. The second phase of the physical testing included the investigation of the actual response of the PV system to the wind action. Because of the dynamic properties of the PV panel, it was expected that the wind induced vibration can affect the dynamic response of the system including the acceleration at the panel surface and support reactions at the racking system to roof interface. To test this theory, two different models of the system were developed, one with the real PV panels and the other one with wooden rigid panels. Comparing the results, it was concluded that the dynamic response of the system was not considerably affected by wind-induced fluctuations. Finally, and to better understand the dynamic response of the system, an analytical model was developed using ANSYS and dynamic analysis was carried out using as input the wind induced pressure data acquired from the physical testing. At the first step, the analytical model was verified by comparing the analytical modal frequencies to the experimental natural frequencies obtained from the hammer test. It was shown that the analytical model can well represent the dynamic properties of the actual model. However, once the reaction output was compared to the loadcell data recorded during the wind tunnel test, there was a considerable discrepancy between the results. It was assumed that the deflection of the supporting structure caused this discrepancy. This assumption was verified and it was concluded that the supporting structure can significantly influence the dynamic response of the system.

TABLE OF CONTENTS

LIST OF TABLES

TABLE PAGE

LIST OF FIGURES

FIGURE PAGE

CHAPTER 1

INTRODUCTION

CHAPTER 1. INTRODUCTION

1.1. Research Motivation

Solar photovoltaic (PV) systems are considered as a cost-competitive source of energy in many markets across the world. The SunShot study, performed by United States Department of Energy, sets a target of generating 302 GW and 632 GW electrical energy in the United States in 2030 and 2050, respectively (1). Figure 1-1 shows the cumulative PV capacity based on the SunShot scenario.

The added capacity of electricity generation only in 2016 was equivalent to installing more than 31,000 solar panels every hour (2). The capacity added to the electric grid by residential rooftop solar PV has increased by a factor of five from 2010 to 2014 (3).

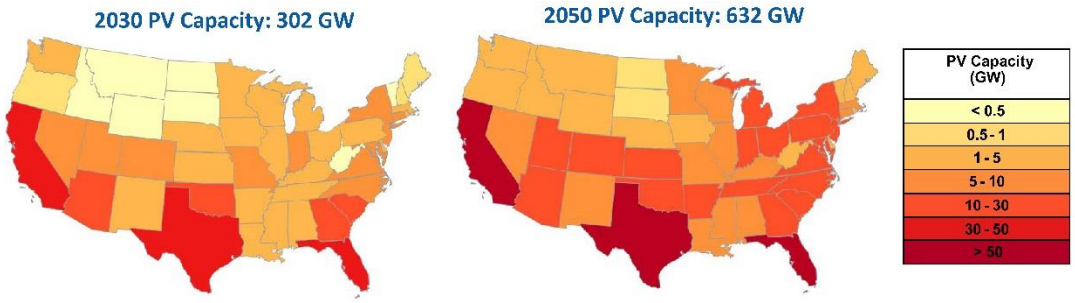

Figure 1-1. Cumulative installed PV capacity in SunShot scenario in 2030 and 2050 (1).

The significant growth rate of solar PV systems along with the widespread interest to further expand the PV electric grid have attracted attention toward the structural design aspects of these systems.

Lack of proper design of these systems can make them quite unreliable in the extreme wind events. Figure 1-2 illustrates the damage of Humacao Solar Farm after the

passage of hurricane Maria. Also, the detached PV compartments can become dangerous projectiles at high wind speeds. Investigations on the aftermath of hurricanes have shown the importance of safe and reliable design of these systems (4, 5).

(a)


(b)

Figure 1-2. Humacao Solar Farm, Humacao, PR. Debris after the passage of hurricane Maria in October 2, 2017. (a) overview and (b) zoom in. (4, 5)

It was only after publishing the ASCE 7-16 (6), that the ASCE 7 standard provides provisions to design solar panels mounted on building roofs. These provisions were mainly based on the wind tunnel studies of rigid small-scale models.

Including the small architectural details is a major challenge of the small-scale wind tunnel studies. In addition, according to ASCE 7 definition of flexible structures as structures with fundamental natural frequency of lower than 1 Hz, solar panels are assumed to be rigid, due to their higher fundamental natural frequencies. However, full-scale experimental tests with actual PV panels have shown the wind-induced vibration of these systems. This observation is contrary to the rigid behavior assumption. As a result, the pressure coefficients suggested by the standard, mainly obtained by wind tunnel tests of small-scale rigid model, needs to be further investigated.

Since there are only a few studies focused on the residential PV systems and there is not a good agreement on the design pressure coefficient for these systems, this dissertation focused on wind effects on residential roof-mounted PV systems.

1.2.Research Objectives

The first part of this study aimed to investigate the effects of different geometric parameters on peak pressure coefficients acting on PV panels. For this purpose, the sensitivity of wind-induced forces to building height, roof type, panel tilt angle and clearance distance was assessed and the most critical parameters were reported.

Another important objective of this research was to propose wind force coefficients for the design of roof mounted PV panels, installed on low-rise residential buildings. To

achieve this goal, enveloping curves of force coefficient versus effective area were presented. These graphs can later be applied in building codes and design guidelines.

Most of the previous studies on PV panels have used scaled rigid models for wind tunnel tests. Little information exists on the effects of wind induced vibration on the PV panel dynamic response. One of the objectives of this study was to investigate the aerodynamic effects which might not be assessed using scaled models. So, full-scale tests were performed on real PV panels and the results were compared to the results of rigid models in order to capture the effects of dynamic vibration.

To further investigate the dynamic behavior of the full-scale PV systems, the numerical model of the PV panels and their racking system was developed and dynamically analyzed under wind induced pressures acting on the panels.

1.3.Organization of Dissertation

The dissertation is prepared in the following five chapters.

Chapter 2 provides a comprehensive literature review of the previous studies performed on investigating the wind effects on PV panels.

Chapter 3 evaluates the effect of different geometrical configuration on the wind induce pressures acting on the residential roof mounted PV systems. The chapter presents the results of several large-scale tests performed at the Wall of Wind Experimental Facility of Florida International University. The design force coefficient suggested based on the experimental tests are presented in this chapter.

Chapter 4 investigates the aerodynamic effects of wind induced vibration on the aerodynamic response of the PV system. The chapter describes the experimental tests performed on two different full-scale models one with real PV panels and another one with wooden panels. The reaction forces at the system supports are compared between these models to capture the effects of wind induced panel vibration.

Chapter 5 presents the analytical evaluation of the PV system dynamic response to wind induced vibration. This chapter describes the details of the numerical model along with the comparison of the analysis results to the experimental results obtained from full-scale tests performed at the Wall of Wind Experimental Facility at Florida International University.

Chapter 6 summarizes the major findings and conclusions of the research.

1.4.References

1. DOE U. SunShot vision study. US DOE. 2012;
2. REN21. Renewables 2017 Global Status Report. Paris, France; 2017.
3. MITei. Future of Solar Energy Study. Energy Initiative Massachusetts Institute of Technology; 2015.
4. Las abrumadoras cifras de la emergencia en Puerto Rico [Internet]. Diario de Puerto Rico. 2017 [cited 2017 Nov 3]. Available from: http://diariodepuertorico.com/2017/10/las-abrumadoras-cifras-de-la-emergencia-en-puerto-rico/
5. Ferrell J. NEXRAD radar, wind turbines, solar farms destroyed in Puerto Rico [Internet]. Accuweather. 2017 [cited 2017 Nov 3]. Available from: https://www.accuweather.com/en/weather-blogs/weathermatrix/nexrad-radar-wind-turbines-solar-farms-destroyed-in-puerto-rico/70002879
6. ASCE 7-16. Minimum Design Loads and Associated Criteria for Buildings and Other Structures [Internet]. Reston, Virginia: American Society of Civil Engineers; 2016. Available from: https://doi.org/10.1061/9780784414248

CHAPTER 2

LITERATURE REVIEW

CHAPTER 2. LITERATURE REVIEW

Based on the mounting configuration PV system can be divided into two groups of ground mounted and roof mounted systems. In the studies by Stathopoulos et al. (1) and Kopp et al. (2) both systems were investigated and it was shown that there is a significant difference between the wind pressures observed on ground mounted and roof mounted systems which is mainly attributed to the effect of building on the wind flow over the panels.

The building effects on pressure distribution over the surface of panels can be dependent on building geometry (height and plan dimensions) and roof type (flat, gable and hip), so another classification of wind studies on PV panels can be defined based on the supporting building structure. According to this classification two main categories can be defined for supporting structure including commercial buildings and residential buildings. Most of the previous experimental studies have investigated the PV systems mounted on commercial buildings, instances of these wind tunnel tests can be found in: (1–9). Currently the design standards use the outcome of these studies to determine the wind loads on PV panels (e.g. SEAOC (10) and Netherland Standard (11)). However, PV panels mounted on small size residential roofs may be differently affected by the wind flow and different design force coefficient may be applicable to these systems.

One of the most comprehensive researches that has considered both residential and commercial buildings is the study presented by Ginger et al. (12). In this study, several geometrical configurations were tested including different roof types (i.e. gable and flat), roof pitch angle, clearance distance between the PV panels and roof surface. The suggested

net force coefficients on PV panels were applied in Amendment No. 2 to AS/NZS 1170.2:2011 (13) for estimation of design wind loads acting on PV panels. However, the experimental tests were limited with low pressure tap resolution on PV panels in addition to mismatched model length scale of 1:20 relative to the wind tunnel length scale.

Stenabaugh, et al. (14) performed another notable study to investigating the wind effects on residential roof mounted PV system. In their research, they tested two building models one gabled roof with 30˚ pitch angle and 15 m x 12 m plan dimensions and another one flat roof with plan dimension of 15 m x 7.5 m. Both models had low eave height of 6 meter and length scale of 1:20. For both roof types, the 0.5 m x 1.455 m panels were arranged in an array of 7 x 4 panels and were mounted parallel to the roof surface. Different configurations with varying clearances (H) and module gaps (G) were tested. It was shown that by increasing the between module gaps and decreasing the clearance distance the net force coefficient on the PV panels decreases. The considerable reduction in C_f values of middle panels caused by sheltering effect, justified application of separate enveloping curve for interior panels. It was concluded that the net force coefficient results of panels mounted on flat and gable roof models were not significantly different, especially for interior panels. In addition to overlooking the effects of panel tilt angle, this study was limited by large length scale of the models compared to the imposed scale by the wind tunnel dimensions.

Another notable research on the residential roof mounted PV panel is the study presented by Geurts and Blackmore (7). In their research, they performed field measurement of real PV panels mounted on full-scale residential building along with the

wind tunnel experiments on scaled down models. The field measurement was performed on a 1.5 m x 1 m panel mounted on a hip roof building with slope of 42˚. In the wind tunnel experiments the PV panel was mounted at different clearance distances on a 1:100 scaled model. The results suggested that the clearance distance does not significantly affect the wind induced pressures. It was also shown that the net wind load on PV panel is considerably lower than the wind load suggested by the building design codes for bare roof surface. These lower net wind loads were justified by the strong correlation between the pressure coefficients acting on the upper and lower surfaces of the PV panel. In this study, the panel tilt angle effect was left uninvestigated. Also, the experiments were limited to a single PV module while in practice PV panels are installed in multi-module arrays that possibly experience different wind flow field over the panels.

Aly and Bitsuamlak (15) published a paper on wind effects on solar panel mounted on residential buildings. They tested two gable roof models with roof slopes of 3:12 and 5:15 and similar plan dimensions of 18.20 m x 9.05 m and roof height of 4.27 m. The 1:15 scaled models were tested at boundary layer wind tunnel with the open-country terrain. PV panels of different dimensions were installed in arrays of different configurations. These configurations consisted of two different set back distances from the roof edges (0 and 1.3m) and two different panel axes alignment relative to the roof horizontal axis (Horizontal and Vertical). The resulted pressure coefficients were compared to the GC_P values recommended for component and cladding by ASCE 7-10 (16). It was concluded that the net pressure distribution over the PV arrays is considerably different from that on the external surface of the bare roof. It was shown that the wind pressures are not significantly affected by roof slope, panel's location and array configuration. This study

did not investigate the effects of panel clearance and tilt angle. Additionally, the experimental wind tunnel tests were limited by incompatibility of the model scale and the imposed scale by the tunnel dimensions.

Ervin et al. (17) investigated the wind loads on residential roof mounted PV panels. The experimental tests were performed using full-scale and 1:12 scaled models. Three building models were used, one with flat roof and the other two with gable roof with slop of 5:12 and 7:12. The flat roof model had an eave height of 3.2 m and plan dimensions of 4.3 m x 4.3 m in full-scale. The gable roof models had the same mean roof height of 3.2 m and the plan dimensions of 3.7 m x 3.7m. A single 1.58 m x 0.95 m PV panel was tested on three different tilt angles of 0˚, 15˚, 45˚ on flat roof model, and two tilt angles of 0˚ and 15˚ on gable roof model. The results were presented as 3-second peak force coefficients averaged over the surface of the panel and comparison were made between the small-scale and full-scale results. The results of the small-scale and full-scale tests showed a good agreement for the 45˚ tilted panel, while for the parallel panels the small-scale tests resulted in lower force coefficients compared to the full-scale tests. Also the force coefficient results were compared to the force coefficients calculated based on the method proposed by Barkaszi and O'Brien (18). It was shown that for flat roof and 7:12 gable roof the full-scale results were compatible with the ASCE 7-2005 (19) procedure for calculation of Main Wind Force Resisting System (MWFRS) given the GC_{pi} range was between +/- 0.1 and +/- 0.03. The major limitation of the experimental test was that they assessed only a single panel, while in practice PV panels are configured in the form of PV arrays and as a result may experience different pressure distribution on their surface.

Since most of the previous studies were limited by the scaling issues, the current study aimed to overcome this limitation by performing wind tunnel tests on large-scale models at Wall of Wind Experimental Facility at Florida International University. The large-scale tests allowed for proper pressure tap resolution and detailed model construction without the limitation imposed by the wind tunnel scale. Additionally, a comprehensive investigation of different geometrical configurations was performed to determine the most influential parameters affecting the wind induced pressures on residential roof mounted PV systems.

2.1. References

1. Stathopoulos T, Zisis I, Xypnitou E. Local and overall wind pressure and force coefficients for solar panels. Journal of Wind Engineering and Industrial Aerodynamics. 2014 Feb 1;125:195–206.

2. Kopp GA, Farquhar S, Morrison MJ. Aerodynamic mechanisms for wind loads on tilted, roof-mounted, solar arrays. Journal of Wind Engineering and Industrial Aerodynamics. 2012 Dec 1;111:40–52.

3. Kopp Gregory A. Wind Loads on Low-Profile, Tilted, Solar Arrays Placed on Large, Flat, Low-Rise Building Roofs. Journal of Structural Engineering. 2014 Feb 1;140(2):04013057.

4. Browne MTL, Gibbons MPM, Gamble S, Galsworthy J. Wind loading on tilted roof-top solar arrays: The parapet effect. Journal of Wind Engineering and Industrial Aerodynamics. 2013 Dec 1;123:202–13.

5. Pratt RN, Kopp GA. Velocity measurements around low-profile, tilted, solar arrays mounted on large flat-roofs, for wall normal wind directions. Journal of Wind Engineering and Industrial Aerodynamics. 2013 Dec 1;123:226–38.

6. Cao J, Yoshida A, Saha PK, Tamura Y. Wind loading characteristics of solar arrays mounted on flat roofs. Journal of Wind Engineering and Industrial Aerodynamics. 2013 Dec 1;123:214–25.

7. Geurts C, Blackmore P. Wind loads on stand-off photovoltaic systems on pitched roofs. Journal of Wind Engineering and Industrial Aerodynamics. 2013 Dec 1;123:239–49.

8. Banks D. The role of corner vortices in dictating peak wind loads on tilted flat solar panels mounted on large, flat roofs. Journal of Wind Engineering and Industrial Aerodynamics. 2013 Dec 1;123:192–201.

9. Wood GS, Denoon RO, Kwok KCS. Wind loads on industrial solar panel arrays and supporting roof structure. Wind and Structures. 2001;4(6):481–94.

10. SEAOC. Report PV2-2012: Wind Loads on Low Profile Solar Photovoltaic Systems on Flat Roofs. Sacramento, California, USA: SEAOC Wind Subcommittee on Solar Photovoltaic Systems; 2012.

11. NEN. NVN 7250: Solar Energy Systems – Integration in Roofs and Facades_Building Aspects. Rotterdam, Netherlands: Netherlands Standardization Institute; 2007.

12. Ginger J, Payne M, Stark G, Sumant B, Leitch C. Investigations on wind loads applied to solar panels mounted on roofs. Rep TS821. 2011;

13. AS/NZS. Amendment No. 2 to AS/NZS 1170.2: Structural Design Actions - Part 2: Wind Actions. Sydney, Australia: Standards Australia/Standards New Zealand; 2012.

14. Stenabaugh SE, Iida Y, Kopp GA, Karava P. Wind loads on photovoltaic arrays mounted parallel to sloped roofs on low-rise buildings. Journal of Wind Engineering and Industrial Aerodynamics. 2015 Apr 1;139:16–26.

15. Aly Aly Mousaad, Bitsuamlak Girma. Wind-Induced Pressures on Solar Panels Mounted on Residential Homes. Journal of Architectural Engineering. 2014 Mar 1;20(1):04013003.

16. ASCE 7-10. Minimum Design Loads for Buildings and Other Structures [Internet]. Reston, Virginia: American Society of Civil Engineers; 2010. Available from: https://doi.org/10.1061/9780784412916

17. Erwin James, Bitsuamlak Girma, Chowdhury Arindam Gan, Barkaszi Stephen, Gamble Scott. Full Scale and Wind Tunnel Testing of a Photovoltaic Panel Mounted on Residential Roofs. Advances in Hurricane Engineering [Internet]. [cited 2017 Aug 16]; Available from: http://ascelibrary.org/doi/abs/10.1061/9780784412626.041

18. Barkaszi S, O'Brien C. Wind load calculations for PV arrays. Solar American Board for Codes and Standards Report. 2010;

19. ASCE 7-05. Minimum Design Loads for Buildings and Other Structures [Internet]. Reston, Virginia: American Society of Civil Engineers; 2005. Available from: https://doi.org/10.1061/9780784408094

CHAPTER 3

WIND LOADS ON RESIDENTIAL SCALE ROOFTOP PHOTOVOLTAIC PANELS

(A paper published in Journal of Wind Engineering and Industrial Aerodynamics)

CHAPTER 3. WIND LOADS ON RESIDENTIAL SCALE ROOFTOP PHOTOVOLTAIC PANELS

Amir Naeiji[1], Farzaneh Raji[2], Ioannis Zisis[3]

3.1. Abstract

The vast application of rooftop photovoltaic (PV) panel arrays on residential buildings has increased the importance for reliable and efficient design of racking systems. Adequate design guidelines assure proper function of the system as well as safety implications on the surroundings during extreme wind events. During such events, the distributed pressures on PV panels' surface can lead to considerable structural damage which can result in partial or total loss of the PV array as well as potential damage to nearby properties. In this study, large-scale models of PV systems installed on residential structures were tested in the Wall of Wind Experimental Facility. The findings revealed that the critical wind directions that induced the worst maximum and minimum peak force coefficients were dependent on roof type and panel tilt angle. Overall, the panel tilt angle was found to be the most critical parameter on the resulting peak pressure coefficients. Finally, the resulting force coefficients from all tested configurations were codified and

[1] [Corresponding author] Department of Civil and Environmental Engineering, Florida International University, Miami, FL, USA. E-mail: anaeiji@fiu.edu

[2] Department of Civil and Environmental Engineering, Florida International University, Miami, FL, USA. E-mail: fraji@fiu.edu

[3] Department of Civil and Environmental Engineering, Florida International University, Miami, FL, USA. E-mail: izisis@fiu.edu

presented for different effective areas while comparison was made between the outcomes of this study and the results of previous investigations.

Keywords: Wind load; Photovoltaic panel; Residential building; Large-scale; Wall of Wind

3.2. Introduction

Reduction in construction and installation costs of PV panels and inverters has led to widespread use of residential rooftop PV modules. According to the report by Massachusetts Institute of Technology Energy Initiative (1), the capacity added to electric grid by residential rooftop PV, has increased by a factor of five from 2010 to 2014. Propagation of solar energy harvesting and development of more efficient PV systems have increased the attention toward the structural design aspect of these systems and in particular the design for wind forces. Over the past decade, numerous studies have been performed and guidelines for estimating wind loads on industrial and residential structures have started to be included in some building codes and wind standards. Instances of these guidelines can be found in SEAOC 2012 (2), Amendment No. 2 to AS/NZS 1170.2:2011 (3), NVN 7250 (4) and more recently in ASCE 7-10 (5). Although these guidelines provide pressure or force coefficients that are more reliable than previous methods - which treated the PV panels the same way as either the bare roof or as components and cladding - there are still incomplete due to various limitations.

First of all, some of these guidelines are solely developed based on studies performed for industrial buildings with considerably larger plan dimensions compared to residential buildings. Considering the effect of building dimensions on the peak wind

forces acting on the PV panels, application of the pressure coefficient obtained from large industrial buildings might be erroneous for small residential dwellings. Secondly, most of these guidelines are based on limited number of tests which do not in capture all different possible building roof types as well as different configurations of panel installations. Thus, generalization of force coefficients obtained from limited testing to all photovoltaic systems, including residential structures, would possibly introduce errors in the design procedure. The third limitation is related to the model scale that is used when roof mounted PV panels are tested in typical boundary layer wind tunnel laboratories. In typical wind tunnels the test section width and height range between 2-2.5 m, therefore when the whole depth of atmospheric boundary layer is modeled (which generally requires a length scale in the range of 1:200 to 1:400), the specimen dimensions get too small. As a result, the construction of detailed architectural features (i.e. racking system, clearance, panel thickness, fitting of tubing, distance between pressure taps etc.) becomes impractical and in some cases, it is even not representative of prototype solar array structures. Often, in order to capture the architectural details, some studies use larger model scales (in the range of 1:20 to 1:50) which results in mismatches in the wind power spectra and improper simulation of the integral length scale. Also, the effects of Reynolds number might have an important influence on the experimental findings. The lower Reynolds number of scaled models can be problematic especially for the flow between the panel and roof surface.

The above issues are confirmed when a comparison between the different experimental studies is attempted (6). Moreover, there is an apparent discrepancy between the pressure coefficients suggested by different guidelines. To remove these limitations more studies should be performed to obtain more consistent design pressure coefficients

for estimating the peak wind loads on different configurations of PV systems mounted on different residential building types.

3.3. Previous Studies

The studies on PV panel systems can be categorized in three main groups, namely ground-mounted, commercial roof-mounted and residential roof-mounted systems. While some studies are dedicated to investigation of wind effects on ground-mounted systems only (7,8), some others included both ground-mounted and roof-mounted systems and provided the data for comparison between the wind load effects acting on these two systems (9,10). The majority of the previous roof-mounted experimental studies have been performed on commercial buildings (9–17).

Since, the main attention so far has been on commercial buildings most of the current guidelines (e.g. NEN, 2007 (4); SEAOC, 2012 (2)) may not be appropriate for PV panels mounted on residential building. Beside the fact that the design wind pressures for PV panels may vary for residential dwellings due to the smaller size of the building, another concern is that the pressure coefficients suggested for commercial buildings are generally developed considering a conservative set back from the building edges to prevent the high suction zones, while for residential buildings avoiding these critical zones might be impractical. On the other hand, the dimensions of commercial building did not allow for large enough scaled models which can lead to limitation in respect to in capturing the architectural details and flow characteristics. Considering this gap in knowledge the objective of this study was to concentrate on the investigation of the wind load effects on PV panels mounted on residential buildings by testing large-scale models.

Ginger et al. (18) carried out wind tunnel tests using two building models; one representing commercial buildings with flat roof and another one representing residential buildings with gable roof slope of 7.5˚, 15˚ and 22.5˚. The findings from this study were adopted by AS/NZS 1170.2:2011 (3). The tests were performed in the wind tunnel laboratory at James Cook University which has a 2 x 2.5m test section and the selected model scale was 1:20. For the gable roof models, the panels were installed parallel to the roof surface at two different array sizes of 1 x 7 panels and 2 x 7 panels, then several tests were performed with altering the locations of array on the roof, clearance distance between the panels and roof surface (0.1 m and 0.2 m) and wind angle of attack. It was shown that clearance distance and array size do not have a significant effect on the wind forces acting on PV panels, while roof pitch angle, panel installation tilt angle and location of panels on the roof can significantly affect the observed wind forces. It should be noted that in this study each panel was instrumented with only four pressure taps (two taps at top surface and two taps at bottom surface) which limits the ability to capture the actual pressure distribution over the surface of the 1.7 m x 1 m panel. Another limitation of this study was the mismatch between the integral length scale of turbulence and the rather large model scale selected for the model (1:20). Such discrepancy may have led to inaccurate peak pressure estimation. Also, in this study for the residential model the panels where mounted only in parallel configuration and the effect of panel tilt angle was not investigated.

Another important study that used a residential building configuration is the research performed by Stenabaugh et al. (10). Two low-rise building models, one with gabled roof and another one with flat roof were tested in the wind tunnel of University of Western Ontario using a length scale of 1:20. Several combinations of clearance distances

and gap between modules were examined. An important finding of this study was that the large gap between modules and small clearance distance will lead to smaller net force coefficient on PV panels. As with Ginger et al. (18) the model scale was larger than the integral scale imposed by the wind tunnel dimensions. Also, the effect of panel tilt angle was not investigated.

Geurts and Blackmore (14) performed field measurements on a residential building with instrumented PV panels. This study also included wind tunnel tests on a 1:100 scaled model of the actual building. The building had a 42˚ pitch roof with a single 1.5 m x 1 m panel mounted parallel to the slope. For the scaled-down wind tunnel model five different clearance distances of 0.025 m, 0.05 m, 0.1 m, 0.2 m and 0.3 m were tested. It was observed that the clearance distance had relatively small effects on wind pressures on the PV module. The limitation of the field study was mainly the lack of an array configuration; i.e. the wind pressures were observed over the surface of a single panel. The effect of panel tilt angle was also not considered. In the wind tunnel tests, and due to the small scale of the models, the equivalent full-scale panel thickness was considerably thicker than a real panel. Also, the small model dimensions can lead to laminar cavity flow between the panel and roof surface which is not the case in reality.

Aly and Bitsuamlak (7) presented the results of the boundary layer wind tunnel tests performed on two gable roof models with roof slope of 3:12 and 5:15. Both models were built in 1:15 scale and had plan dimensions of 18.20 m x 9.05 m and roof height of 4.27 m (equivalent full-scale). Three different panel sizes were used with common dimension of 1.5 m and altering dimension of 0.9 m, 2.4 m and 2.7 m Panels were mounted parallel to

the roof surface in multi-array arrangements on both sides of the gable roof. The results of pressure measurements were presented as GC_P coefficients and when compared to the ASCE 7-10 (5) suggested values for component and cladding considerable discrepancies were identified. Roof slope, panel's location and array configuration were found out to be important parameters affecting the wind-induced pressures. Similar to the previous studies, there was a significant discrepancy between the scale required by the wind tunnel dimensions and the model scale. Also, the effects of panel tilt angle and clearance distance were not investigated.

The study by Ervin et al. (19) also focused on the investigation of wind loads acting on panels mounted on low-rise residential buildings. Full scale tests at Wall of Wind Experimental Facility at Florida International University (FIU) and 1:12 scaled tests at RWDI's boundary-layer wind tunnel were carried out in order to investigate Reynolds Number (Re) effects as well as aerodynamic response of the PV panel and its support structure. For this study, a single 1.58 m x 0.95 m PV panel was mounted on a flat roof building at three different tilt angles of 0˚, 15˚, 45˚, and on a gable roof model at 0˚ and 15˚ tilt angles. It was concluded that for the 45˚ tilted panels there was a good agreement between the small-scale and full-scale results, while for parallel and low tilt panels the results of small-scale tests were generally reported values lower than full-scale tests. The main limitation of this study is related to application of single panel instead of arrays of panels.

In summary, most of these studies were performed on scaled models that in some cases were even larger than the scale constrained by the wind tunnel facility where the tests were

carried out. One of the objectives of the current study is to address such scaling limitations by using large-scale models that can incorporate smaller architectural details of PV systems without violating flow scaling rules that existed in previous studies.

3.4. Methodology

3.4.1. Experimental considerations

One of the first steps of performing experimental tests at any wind tunnel is to decide on the model length scale. Several considerations should be kept in mind when choosing the scale. For instance, one of the problems related to modeling low-rise buildings at typical boundary layer wind tunnel laboratories is that due to small dimensions of the test section, when the whole depth of atmospheric boundary layer is modeled, the specimen dimensions gets too small and construction of detailed architectural features becomes impractical. To capture the architectural details, researchers use larger model scales and simulate only partial depth of the atmospheric boundary layer. This will result in missing the low frequency end of turbulence spectrum (large turbulence eddies) and improper simulation of integral length scale. In the Wall of Wind Experimental Facility, the low frequency part of turbulence is not included in the spectrum (20) therefore the PTS method is applied to estimate the peak values (21). As a result, the tests in partial simulation are free of integral length scale constraints and there is no limitation imposed on model scale by integral length scale. Another confining parameter for length scale selection is the blockage ratio. Based on ASCE 7-10 (5) the blockage ratio is limited to 8% for the boundary layer wind tunnel tests. Aly et al. (22) concluded that 16% blockage ratio at Wall of Wind Experimental Facility leads to accurate pressure distribution on the roof surface. Having these considerations in mind, for this study which aims to investigate the pressure

distribution over the surface of roof mounted solar panels, the length scale of 1:6 that results in 16% blockage ratio was deemed acceptable.

Simulation of the actual characteristics of the flow pattern between the lower surface of the panels and the roof surface (cavity flow) is another consideration that needs to be taken into account. In reality, cavity flow has Reynolds Number (Re) highly greater than 2000 (23). For example, with wind design speed of 70 m/s, characteristic length (distance between the roof surface and lower surface of PV panels) of 0.3 m and the air viscosity of 1.5×10^{-5} m^2/s the Reynolds number would be 1.4×10^6 ($Re= (70\times0.3)/ (1.5\times10^{-5}) =1.4\times10^6 >> 2000$) which is characterized as turbulent flow. Most of the previous studies, which were performed at small wind tunnel laboratories, were incapable of providing large enough gap between the panels and the roof to allow for turbulent flow (10,18,23). However, the large dimensions of the test section at Wall of Wind Experimental Facility allowed for adopting a larger scale, equal to 1:6, which resulted in more realistic turbulent flow characteristics between the lower surface of panels and roof surface (e.g. model-scale: $Re= (25\times0.05)/ (1.5\times10^{-5}) = 83333 > 2000$).

3.4.2. Testing facility

The tests were carried out in the 12-fan Wall of Wind Experimental Facility at Florida International University (FIU). This open jet boundary layer wind tunnel has a test section of 6 m wide and 4 m high which allows for large to full scale testing, similar to the one performed for this study. Figure 3-1 shows the mean wind speed (V_z) as well as turbulence intensity (I_u) profiles of the simulated flow. The obtained mean wind speed

profile can be represented by the power low relation with the exponent of 0.18 which corresponds to a relatively open terrain exposure.

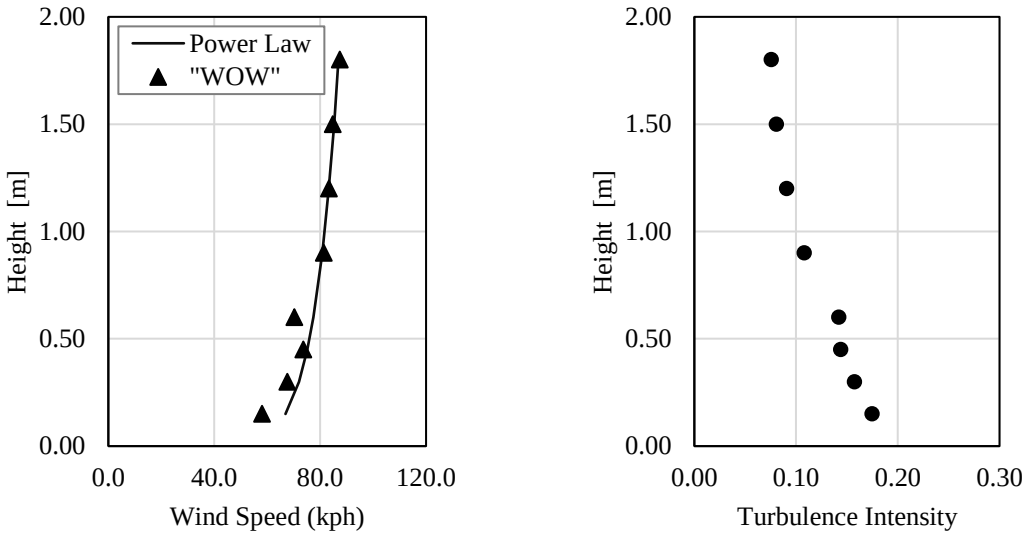

Figure 3-1. Mean velocity and turbulence intensity profiles.

3.4.3. Experimental set up

For this study, building models with flat, gable and hip roof types, which are the most common roof types for residential buildings, were tested. For each roof type, effects of building height, panel clearance distance (the gap between the panel lower edge and the roof surface) and panel tilt angle were investigated. All models were built with plan dimensions of 9.1 m (width) and 13.7 m (length) in full scale. To investigate the effect of building height, models were built with mean roof heights of 6.55 m and 10.59 m for flat roof, and 7.13 m and 11.16 m for gable and hip roofs, which are referred to as 2-story and 3-story buildings respectively. The equivalent full-scale size of the panels was 2 m length, 1 m width and 0.15 m thick. It should be noted that this thickness is considerably smaller and more realistic when compared to PV models used in other small-scale wind tunnel

tests; e.g. Stenabaugh et al. (23) study used PV panels of 0.30 m thickness in full-scale. Panels were mounted at two clearance distances of 0.3 m and 0.45 m. For flat roof models, the panels had three different tilt angles of 20˚, 30˚ and 40˚. Gable roof and hip roof models had a slope of 3:12 and panels were mounted either parallel to the roof or inclined at a 14° positive angle relative to the roof surface. Each model configuration was tested at sixteen different wind directions starting from 0˚ (the wind attacking the south wall of the model) and increasing by 22.5˚ increments in counter clockwise direction.

As shown in Figure 3-2, the panels were mounted in multi-array arrangements on the roof surface of building models. For all roof types only eight of the panels were instrumented and the rest of them were dummies. The instrumented panels were numbered as displayed in Figure 3-2.

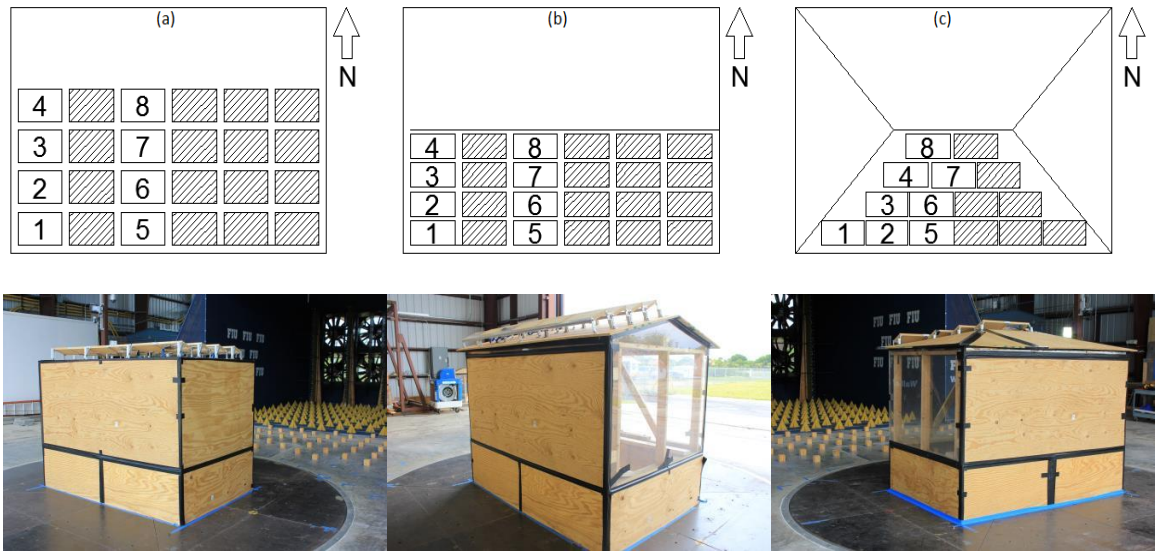

Figure 3-2. Panel configuration schematics and model of the flat (a), gable (b) and hip (c) roof buildings.

A schematic of the scaled instrumented PV panel is shown in Figure 3-3. Each dot in this figure represents the location of two pressure taps, one at the top surface of the panel

and another one at its bottom surface. Each panel was instrumented with total of 30 pressure taps (15 at top surface and 15 at bottom surface). It is important to mention, that the larger scale of the model allowed for a more refined pressure tap arrangement (i.e. more pressure taps per PV panel) which consequently resulted on a more accurate characterization of pressure gradients (24). This model characteristic addresses some of the limitations of previous studies (e.g. Ginger et al. (18); Stathopoulos et al. (10)) in which a lower number of pressure taps was adopted due to the limited size.

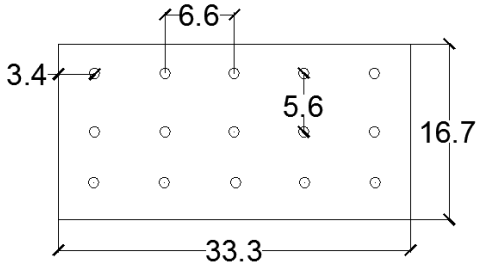

Figure 3-3. Scaled pressure tapped panel dimensions (cm).

3.4.4. Data treatment

Conventionally the pressure measurements are presented in the dimensionless form of pressure coefficients (C_p) to facilitate comparison between the scaled models and prototypes. In this paper, the pressure coefficients are calculated using the following equation:

$$C_p = \left(P - P_a\right) / \left(0.5 \rho U^2\right) \tag{3-1}$$

In this formula, C_p is the pressure coefficient; P is the pressure acquired at each pressure tap (N/m^2); P_a is the ambient atmospheric pressure; ρ is the air density (kg/m^3); U is the 3-second wind gust at mean roof height (m/s). To obtain the net pressure coefficient

at each tap location the pressure coefficient of bottom pressure tap ($C_{p,b}$) is deducted from pressure coefficient of top pressure tap ($C_{p,t}$) at each time (i.e. sampling) step of the test.

Beside the local pressure coefficients, in this paper force coefficient (C_f) values are also reported. Generally, the force coefficients describe dimensionless form of wind forces obtained by area averaging of net pressure coefficients over any specific number of pressure tap locations. In the following sections, the panel C_f values refer to the force coefficients averaged over all fifteen pressure tap locations on the panel.

Since, the frequency spectrum of the simulated flow lacks the fluctuations in the low frequency range, the Partial Turbulence Simulation (PTS) approach was selected for peak estimation (24). In the PTS method, it is assumed that the velocity turbulence of the wind flow is composed of two separate parts, a low frequency part (that is not included in the simulated flow) and a high frequency part (that is actually simulated). In this method, the realistic peak pressure coefficient (the one that can be observed at atmospheric flow) can be estimated using Fisher-Tippett type I probability distribution and assuming Gaussian distribution for low frequency turbulence fluctuations. The slope and mode parameters for Fisher-Tippett type I distribution is calculated based on pressure data obtained from simulated high frequency flow. To obtain these parameters the sampling time is divided into several time intervals and peak C_p values for each time interval are selected. Finally, Gumbel method is applied and slope and mode parameters are calculated.

3.5. Results

3.5.1. Effect of geometrical properties on panel force coefficients

The experimental study produced a vast amount of data which were evaluated in order to examine the effect of each of the geometric parameters that were considered during this study. In this section, a brief overview and discussion on the effect of these parameters is presented in order to select the most influential one and further interpret the results in the subsequent sections. A comprehensive comparison of the peak force coefficients for all tested geometrical parameters is presented in Naeiji et al. (25). The presented peak net panel force coefficients are critical values; i.e. worst peak values observed on the most critical panel under the most critical wind direction for each geometric configuration.

3.5.1.1. Effect of building height

Figure 3-4 shows the effect of changing the building height of the flat roof model on the peak force coefficients averaged over the surface of one panel. The results indicate that both net maximum and net minimum C_f values are not much affected by increasing the building height. Overall, a small reduction in minimum net force coefficient can be observed (about 10% in average) for the 3-story building height whereas the maximum net force coefficients show even smaller difference (less than 2% in average) and there is no apparent trend for this variation. For the gable roof and hip roof models the results did not follow any specific patterns and the only inferred conclusion was that the building height does not significantly influence the peak force coefficients.

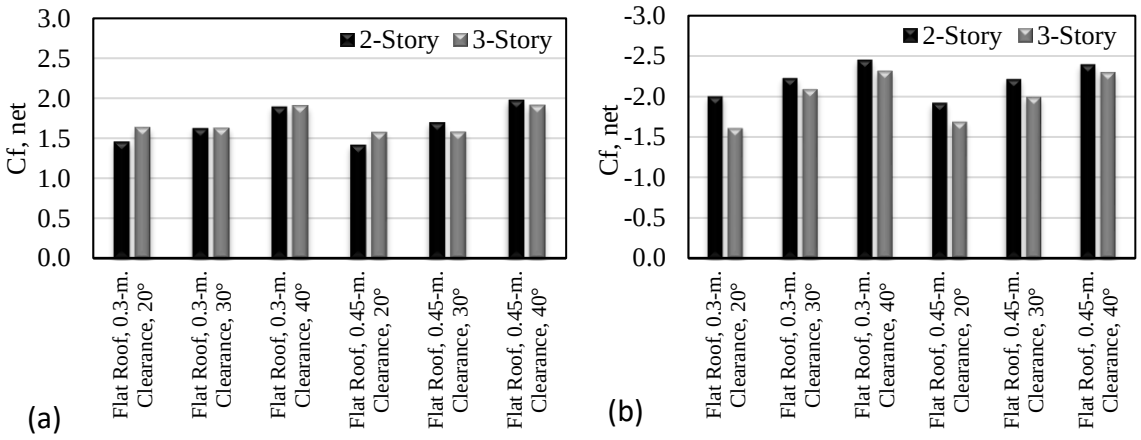

Figure 3-4. Effect of building height on the most critical peak force coefficients for flat roof models; (a) Maximum Net C_f, (b) Minimum Net C_f.

3.5.1.2. Effect of roof clearance

The effect of clearance (distance between roof and panel) on peak net force coefficients can be observed from Figure 3-5 for flat roof models. It can be concluded that increasing the clearance from 0.3 m to 0.45 m does not significantly affect the peak net force coefficients (at most 5%). Overall, no general trend was observed when the clearance was varied. Similar to the flat roof building, the results for the other two roof configurations (gable roof and hip roof) did not reveal any particular influence of the building height.

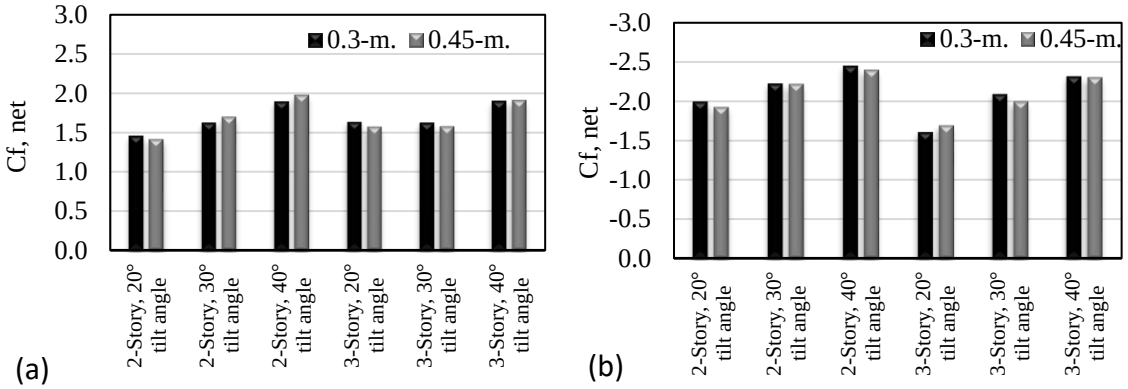

Figure 3-5. Effect of clearance distance on the most critical peak force coefficients for flat roof models; (a) Maximum Net C_f, (b) Minimum Net C_f.

3.5.1.3. Effect of tilt angle

Figure 3-6 and Figure 3-7 show the effect of increasing the panel tilt angle for flat roof and gable roof models, respectively. It can be observed that increasing the tilt angle has led to generally higher minimum net force coefficients for both flat roof (up to 43% increase from 20˚ to 40˚) and gable roof models (up to 40% increase). In the case of maximum net force coefficients, the flat roof models experience higher values at higher tilt angles (up to 40% increase) whereas for gable roof models there is not much difference due to panel tilt angle (8% at most). Considering the above results, it can be concluded that the tilt angle is the most significant parameter affecting the peak force coefficients observed over the surface of roof mounted PV panels.

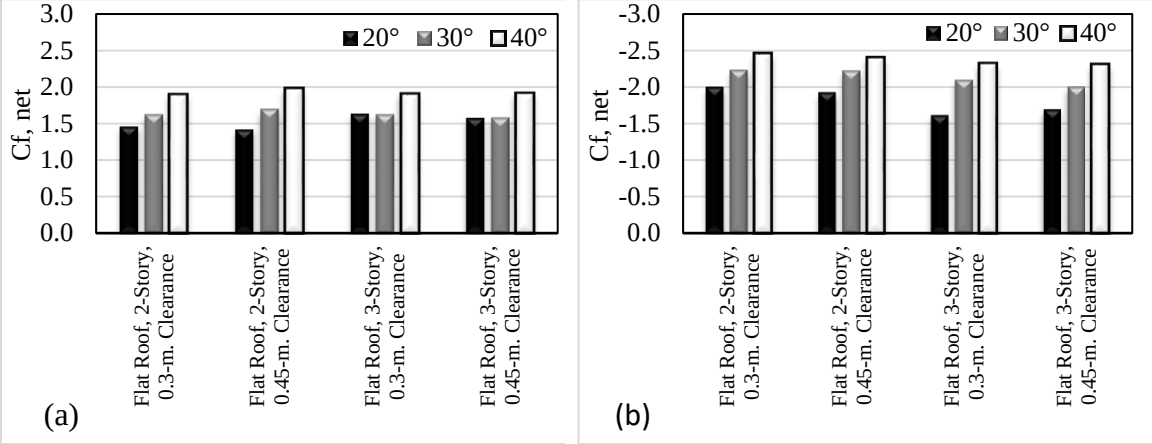

Figure 3-6. Effect of tilt angle on the most critical peak force coefficients for flat roof models; (a) Maximum Net C_f, (b) Minimum Net C_f.

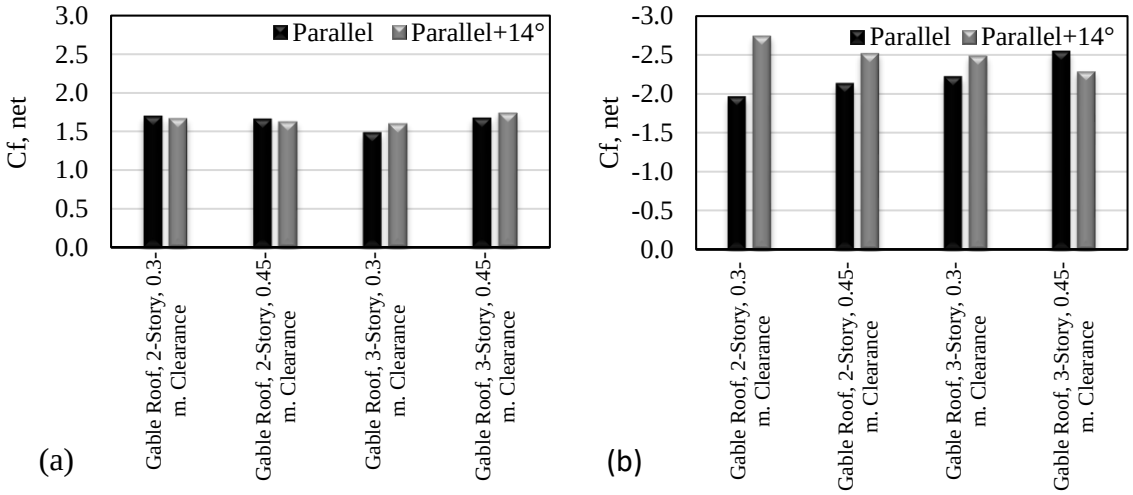

Figure 3-7. Effect of tilt angle on the most critical peak force coefficients for gable roof models; (a) Maximum Net C_f, (b) Minimum Net C_f.

3.5.2. Comprehensive results on the effect of tilt angle

3.5.2.1. Flat roof

The variation of the peak net force coefficients with wind direction is presented in Figure 3-8 for all flat roof models. The presented peak values are net force coefficient acting on the most critical panel. In this picture four graphs are presented. Each graph shows the results of three models with identical configurations except for the panel tilt angle to identify tilt angle effects while maintaining other parameters constant.

It can be observed from all four graphs that maximum net C_f values for all tilt angle models occur at the 315˚ - 337. 5˚ wind direction range. Also, at 337.5˚ wind direction increasing the tilt angle leads to higher maximum net C_f. For minimum peak values, it can be noted from all graphs that the worst suction values occur at the 202.5˚ - 225˚ wind direction range and by increasing the tilt angle the minimum net C_f increases. The above

wind directions will be considered to investigate in detail the distribution of local peak pressure coefficient on the top and bottom panel surfaces as well as the overall net effect.

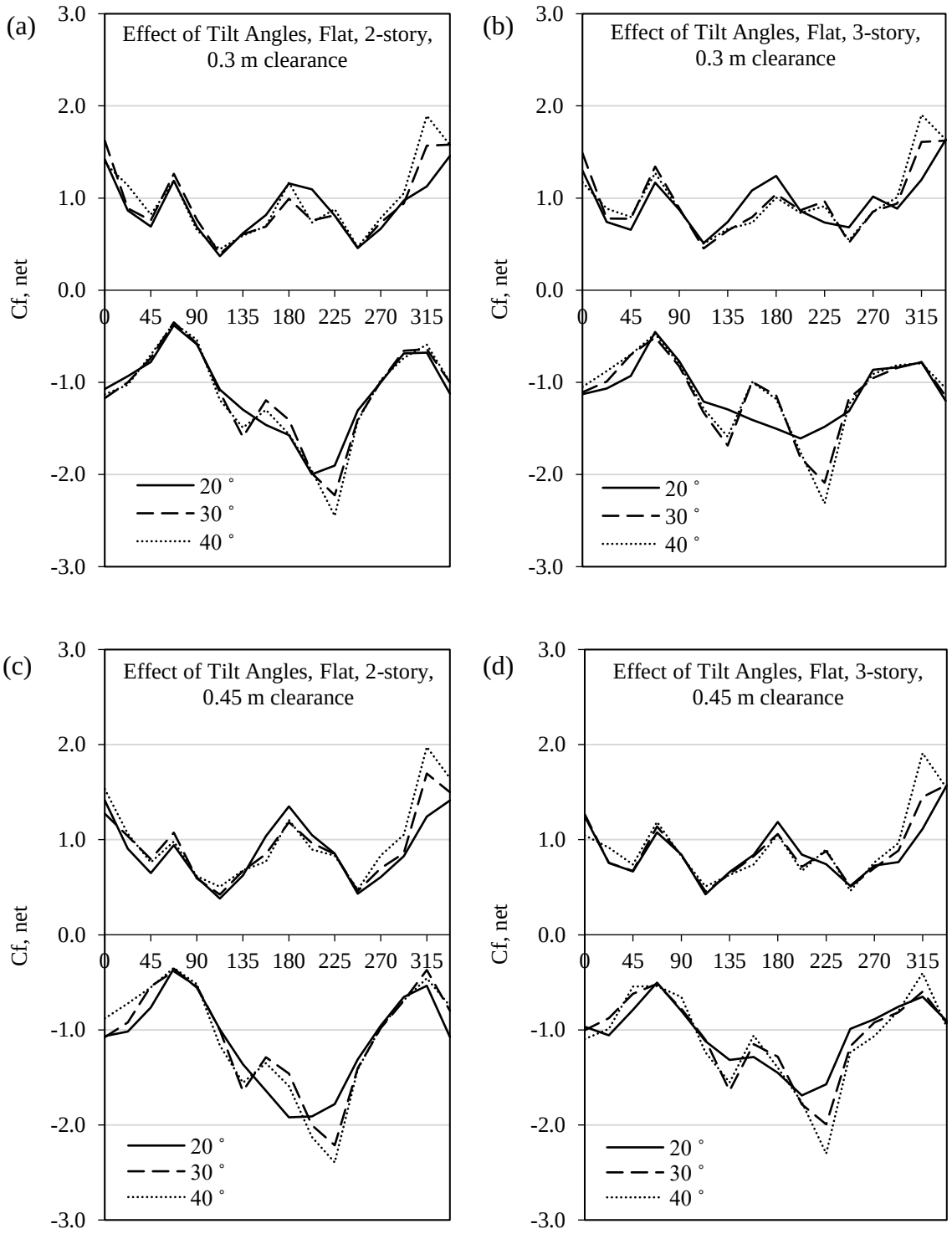

Figure 3-8. Variation of peak net force coefficient with wind direction (flat roof).

The peak pressure distribution over the surface of instrumented panels mounted on flat roof, 2-story, and 0.3 m clearance models with 20˚ and 40˚ and for 315˚ wind direction is shown in Figure 9. As shown in Figure 3-8, 315˚ wind angle of attack leads to high peak net force coefficient for both tilt angles, but the maximum net C_f values observed at 40˚ were considerably higher compared to 20˚ tilt angle. The same conclusion can be inferred from Figure 3-9. More specifically, for both tilt angles the panels located at the west edge of the roof experience the highest maximum net pressure but the observed peak values for panels at 40˚ tilt angle are noticeably higher compared to the 20˚ tilt angle case. On the other hand, the panels located on the middle column have the maximum net pressure coefficient values almost in the same range for both 20˚ and 40˚ tilt angles. This comparison indicates that increasing the tilt angle for the critical wind direction affects predominantly the panels located at the leading edges of the roof which are immediately affected by the wind flow. This observation can be also confirmed when the peak local pressures on upper and lower surfaces of the panels are considered separately (see Figure 3-9). Considering the sign convention for net pressure calculation, it is expected that maximum net values be resulted from highly correlated maximum pressures at top surface and minimum pressures at bottom surface of the panels. For both tilt angles, it can be noted that the maximum pressures are not highly variant over the top surface of the panels, while the peak suction at bottom surface of panels noticeably decreases for panels located at the middle column on the roof. Although the high suctions at bottom surface of leading edge panels can be due to flow separation at panel edges the reduction in lower surface suction for sheltered panels can be justified by dissipation of wind energy as it passes through leading panels.

Increasing the tilt angle has led to slightly higher suction at the bottom surface of near west edge panels, on the other hand the pressures at top surface of these panels almost double by increasing the tilt angle. Without considering the correlation between the top and bottom time histories, it is reasonable to expect higher net maximum values for 40˚ tilt angle at the panels located close to east edge of the roof.

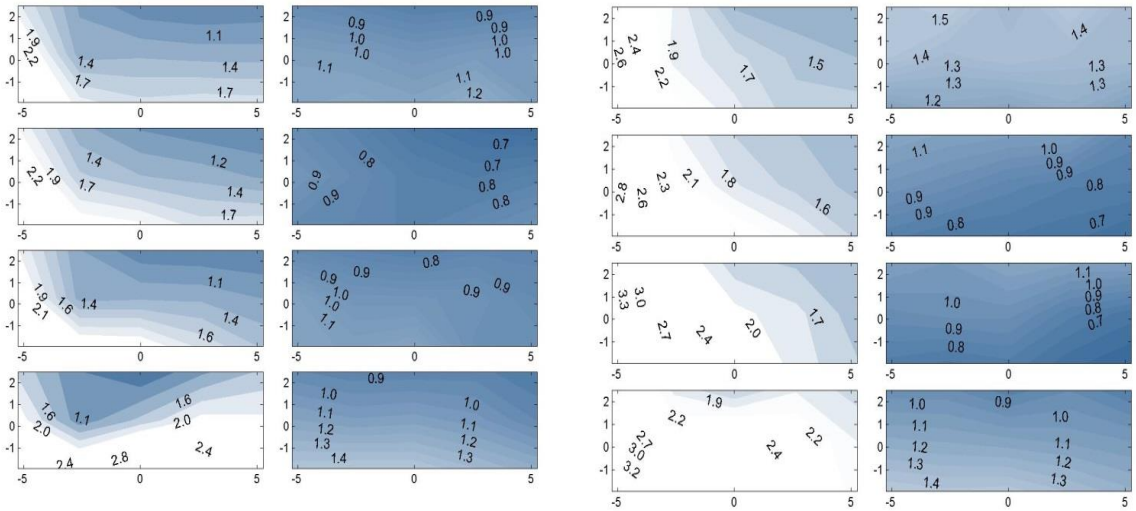

Maximum net values

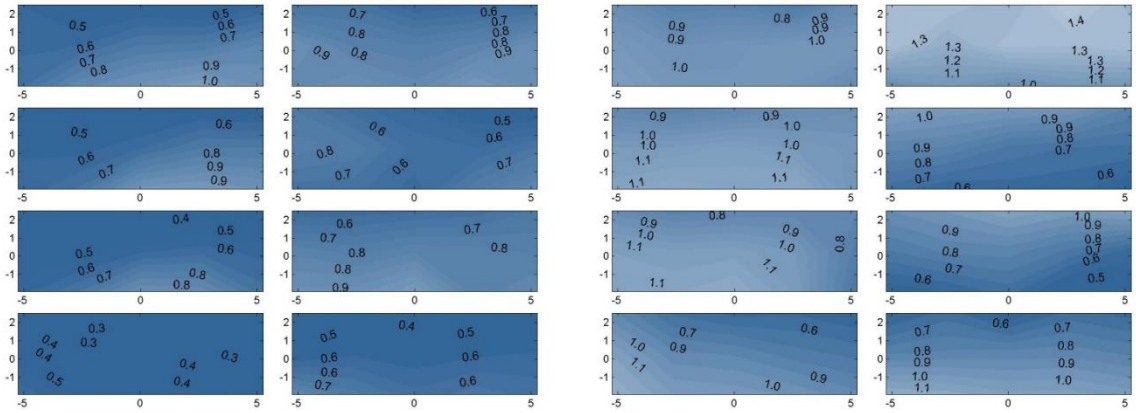

Top surface maximum values

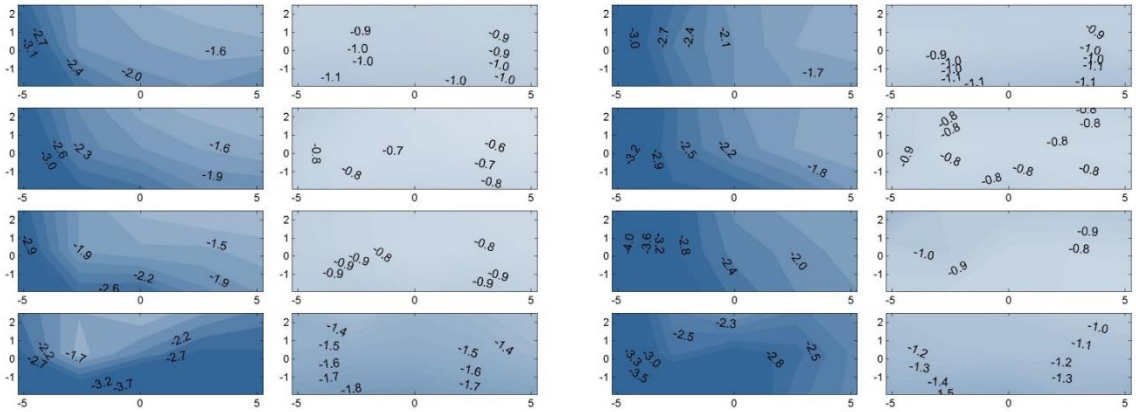

Bottom surface minimum values

Figure 3-9. Peak C_p recorded at 315˚ wind direction on 2-story, 0.3 m clearance flat roof models with (left) 20˚ tilt angle and (right) 40˚ tilt angle.

The minimum net C_p values along with top surface minimum and bottom surface maximum pressure coefficients for the 2-story, 0.30 m clearance models with tilt angles of 20˚ and 40˚ are presented in Figure 3-10. The results are specific to the critical wind direction of 225˚. According to Figure 3-8, the net minimum force coefficients at 225˚ wind direction for 40˚ tilt angle models were somewhat higher compared to 20˚ model and the net minimum C_p contour plots presented in Figure 3-10 are compliant with this observation. More specifically, the worst minimum net pressure coefficients occurred at the windward corner panel (wind approaching from NW) for both tilt angles. This critical effect can be partially justified by two major flow characteristics for the specific wind direction; 1) the top surface of the panel is leeward to the approaching wind (NW) so the flow separation at panel edges can amplify the suction at top surface and 2) the corner panel is located where the oblique NW wind generates corner vortices and leads to higher roof suctions. As the tilt angle increases the panel-induced turbulence expands the high suction area to the whole top surface of the windward corner panel which results in somewhat higher net uplift forces for the 40˚ tilt angle panel compared to that with 20˚ tilt angle. When the top and bottom surface pressure coefficients are considered separately, the increase on the panel tilt angle results to less significant differences particularly for the maximum bottom pressure coefficients. Although, one would expect that as the panel tilt angle increases more positive pressure is sustained by the lower surface of the panel, for the 225˚ wind direction the flow separation at the roof edge is upstream to the location of the panel and therefore the arrays are located within the rood shear layer.

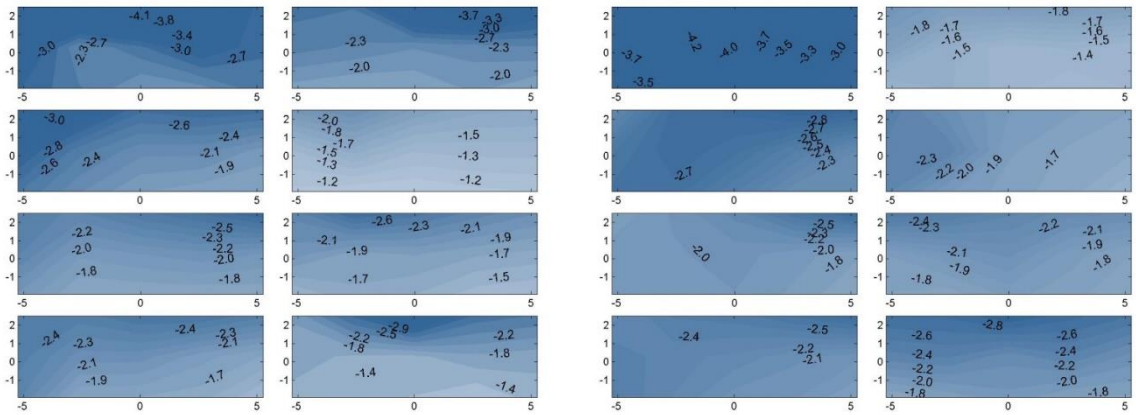

Minimum net values

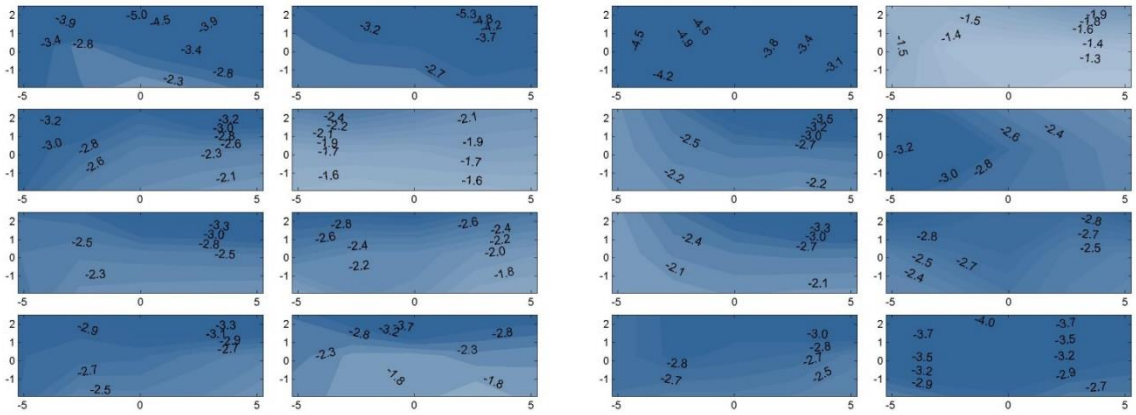

Top surface minimum values

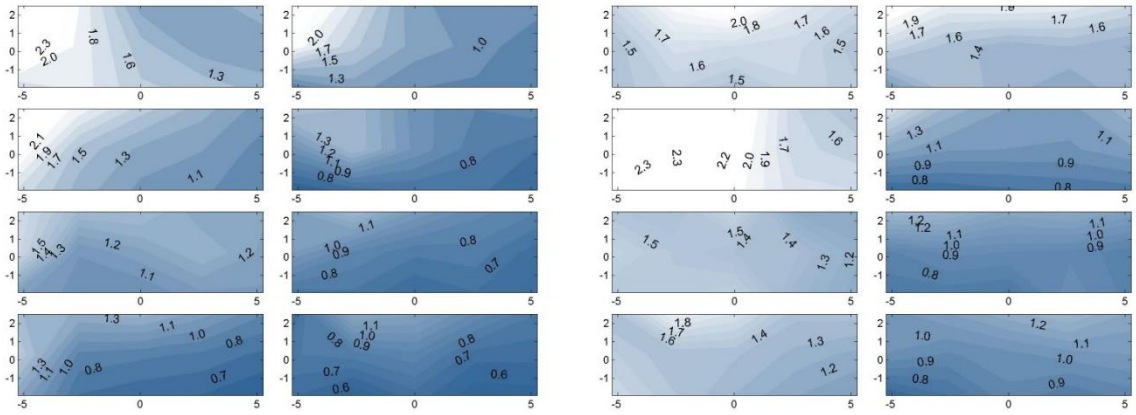

Bottom surface maximum values

Figure 3-10. Peak C_p recorded at 225˚ wind direction on 2-story, 0.3 m clearance flat roof models with (a) 20˚ tilt angle and (b) 40˚ tilt angle.

3.5.2.2. Gable roof

The maximum and minimum net force coefficients with respect to wind direction are presented in Figure 3-11 for all gable roof models. The presented peak values are net force coefficient acting on the most critical panel. In each graph, the parameter that varies is the panel tilt angle; i.e. the two presented configurations in each graph have identical building height and roof-to-panel clearance.

When considering the maximum force coefficients, it can be observed that for all models with parallel tilt angle the most critical wind angle is 247.5˚, while for all parallel+14 models, except the 3-story, 0.45 m clearance model (Figure 3-11 d), the maximum cases occur at 315˚. It should be noted that although the change in tilt angel has led to different critical wind direction, it has not considerably affected the maximum values and both parallel and parallel+14 cases have similar peaks (maximum net C_f value approximately 1.7). Another interesting observation is that although the variation of the maximum net C_f for both tilt angles has a similar trend, for 315˚ wind direction the parallel models experience considerably lower values compared to parallel+14 models.

In the case of minimum net C_f values, a similar characteristic - change in critical wind angle due to altering the panel tilt angle - can be observed. For all parallel models, the wind direction that results in critical minimum net C_f values is 180˚, while for parallel+14 models the critical wind direction is 225˚. Also, it can be observed that, in all cases except for the 3-story, 0.45 m clearance model (Figure 3-11 d), increasing the panel tilt angle to parallel+14 results into an increase on the absolute value of the minimum net C_f.

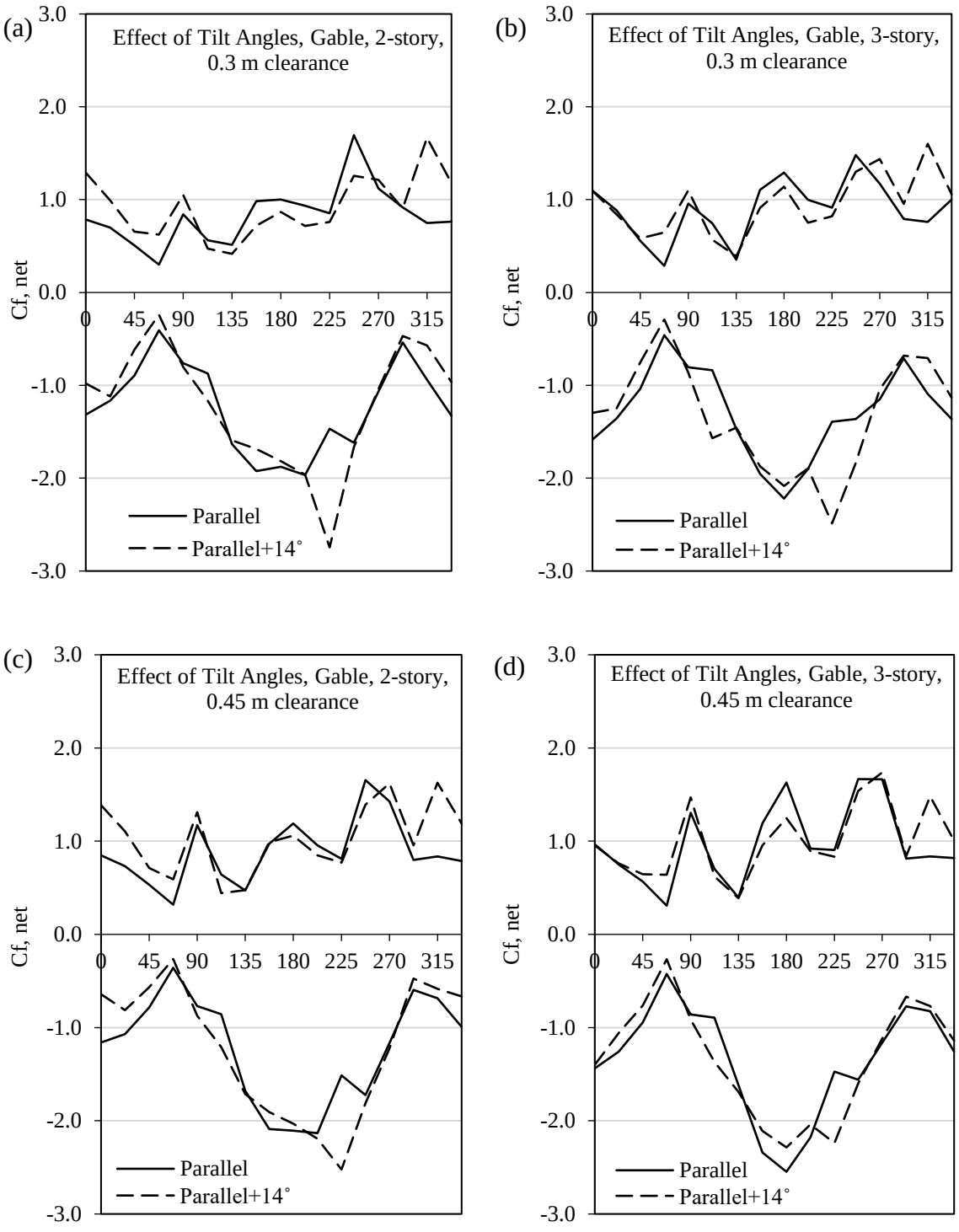

Figure 3-11. Variation of peak net force coefficient with wind direction (gable roof).

Figure 3-11 clearly reveals the difference between the most critical wind directions for the models with parallel versus parallel+14 tilt angle panels. To further investigate the flow and consequently the wind-induced pressures and suctions on the panel's surfaces, the maximum and minimum pressure coefficients (local C_p's) are presented separately for each of the critical wind directions and for models with identical configurations except for panel tilt angle. The net, top and bottom pressure coefficient results are compared for parallel and parallel+14 panel tilt angle for the representative case of the 2-story, 0.3 m clearance model and for wind directions of 315˚ and 225˚.

For 315˚ wind angle of attack (Figure 3-12), the net pressure distribution over the surface of the panels is significantly different for parallel and parallel+14 tilt angle. To better understand the mechanism causing this difference, the peak maximum pressures at top surface and peak minimum pressures at bottom surface of the panels are also presented in Figure 3-12. Considering the maximum peak pressures at top surface it can be observed that increasing the tilt angle has expanded the high-pressure zone from only first windward row at parallel tilt angle to all instrumented panels for parallel+14 tilt angle. While the high maximum pressures at first row of parallel panels is mainly due to the turbulence generated by flow separation at building edge, for parallel+14 model higher peaks at top surface of panels might be justified by two mechanisms. The first one is the panel generated turbulence which amplifies the wind fluctuations caused by flow separation at building edges. The other one is the windward upper surface of the panel which is affected by direct downward flow as the tilt angle increases. For the peak minimum pressures at bottom surface increasing the tilt angle has led to considerable increases in suction at all near edge panels, while the sheltered panels are left unaffected. The increase in high suction at bottom

surface of leading panels can be due to the turbulence caused by flow separation at edges of tilted panel. As the flow passes underneath these panels the fluctuations drop considerably and thus the pressure distribution at lower surface of sheltered panels are the same for both tilt angle models.

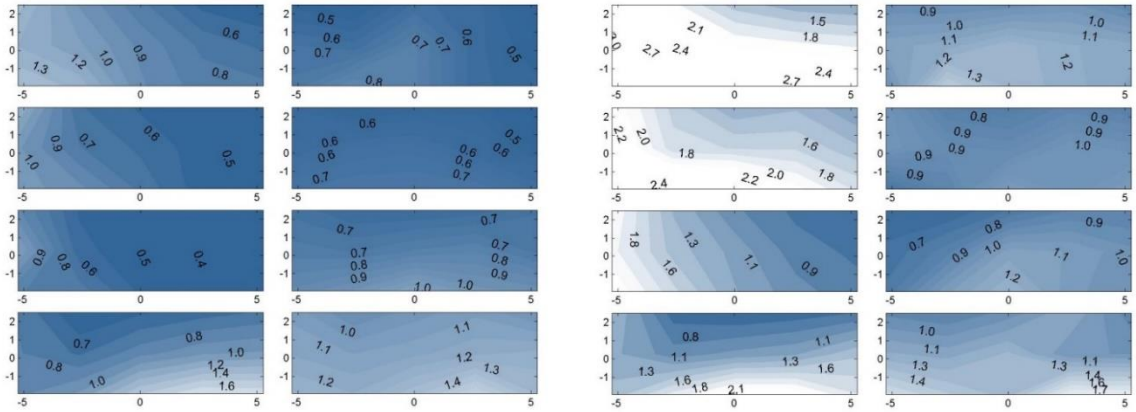

Maximum net values

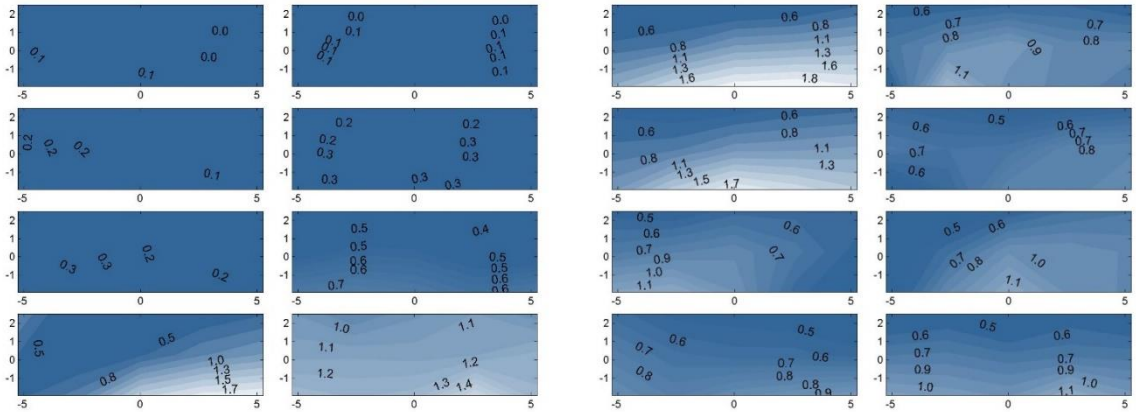

Top surface maximum values

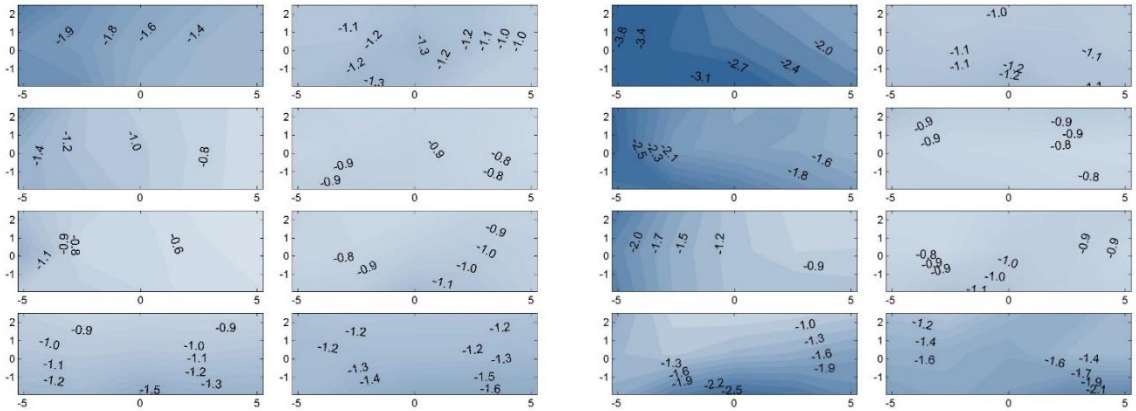

Bottom surface minimum values

Figure 3-12. Peak C_p recorded at 315˚ wind direction on 2-story, 0.3 m clearance gable roof models with (left) parallel tilt angle and (right) parallel+14˚ tilt angle.

The critical wind direction for the minimum net force coefficient was 225˚ (see Figure 3-11) therefore the minimum net, minimum top and maximum bottom C_p results for both tilt angles of the same gable roof model (i.e. 2-story, 0.3 m. clearance) for the same wind direction are presented in Figure 3-13. As shown in this figure the panel close to ridge and gable edge of the roof is the one that experiences the highest suction peaks at both parallel and parallel+14 models. This can be primarily justified by the flow separation at building ridge for the 225˚ wind direction which leads to high suction at the leeward side of the roof. Another important observation is that increasing the tilt angle has led to considerable increase in high suction pressures at all panels except for near ridge panels which remain relatively at same levels for both tilt angles. By further studying the minimum pressures at upper surfaces, the same pattern can be noted which indicates that the top surface suctions have considerable influence on the overall – net – wind-induced effect. This behavior can be possibly attributed to the panel generated fluctuations that amplify the building generated turbulence after flow separation at building ridge and expand the high uplift zone further in to the roof. Lastly, by increasing the tilt angle on the panels, a considerable increase is observed on the lower surface maximum pressures especially for those panels that are located near the gable edge.

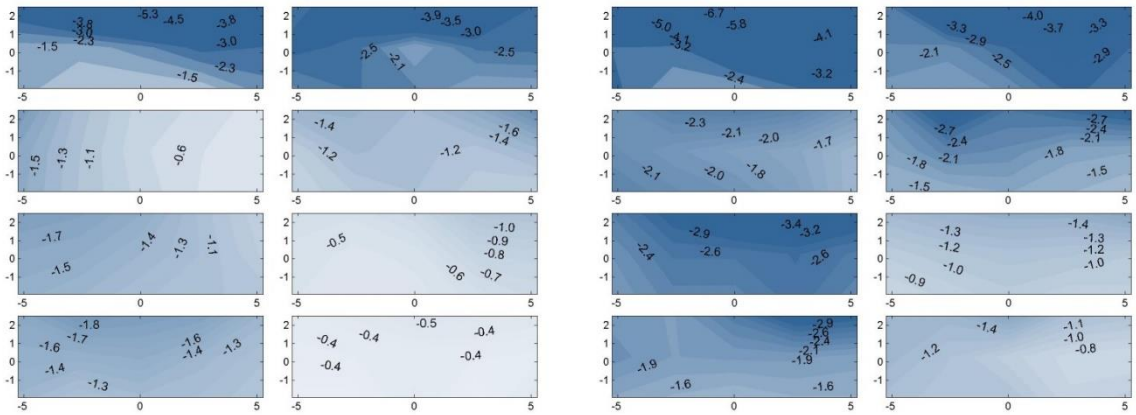

Minimum net values

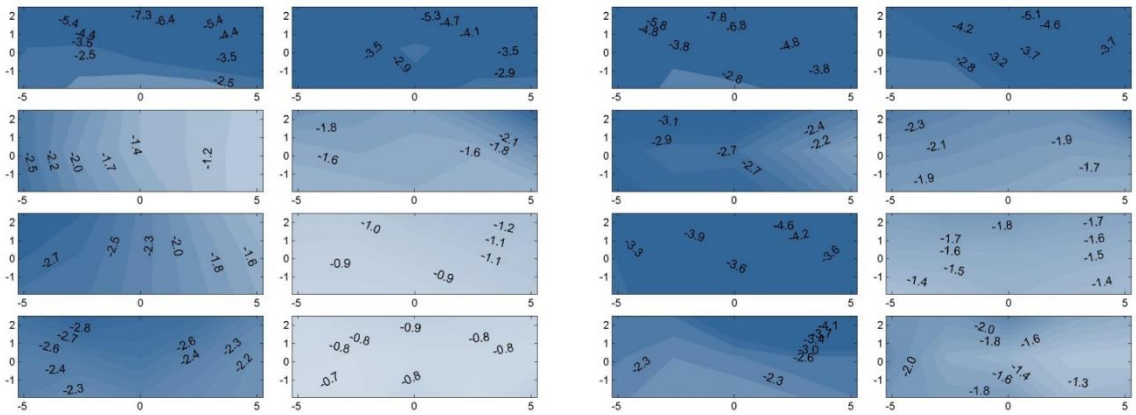

Top surface minimum values

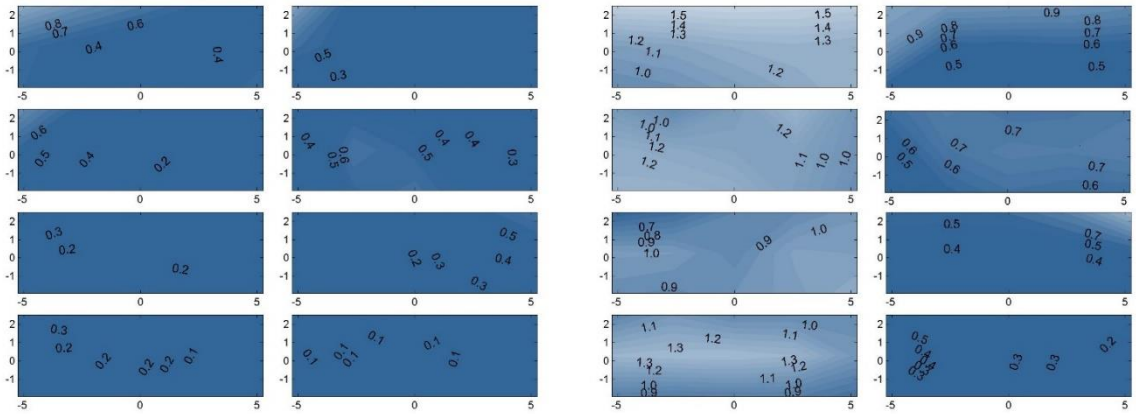

Bottom surface maximum values

Figure 3-13. Peak C_p recorded at 225˚ wind direction on 2-story, 0.3 m clearance gable roof models with (a) parallel tilt angle and (b) parallel+14˚ tilt angle.

3.5.2.3. Hip roof

The maximum and minimum net force coefficient calculated for hip roof models at different wind directions are presented in Figure 3-14. The presented peak values are net force coefficient acting on the most critical panel and each graph shows the results of two models with identical configurations except for the panel tilt angle.

For the maximum net force coefficients, it can be observed that for parallel models the 180˚ wind direction is the most critical one while for parallel+14 models the critical wind direction is the range 337.5˚-0˚. When the minimum net C_f values are considered, it can be observed that the critical wind direction for almost all cases has shifted from 180˚ to 225˚ by increasing the panel tilt angle by 14˚. Finally, in all configurations and for both maximum and minimum net C_f values the variation with respect to wind direction shows a very similar trend between the two tilt angles.

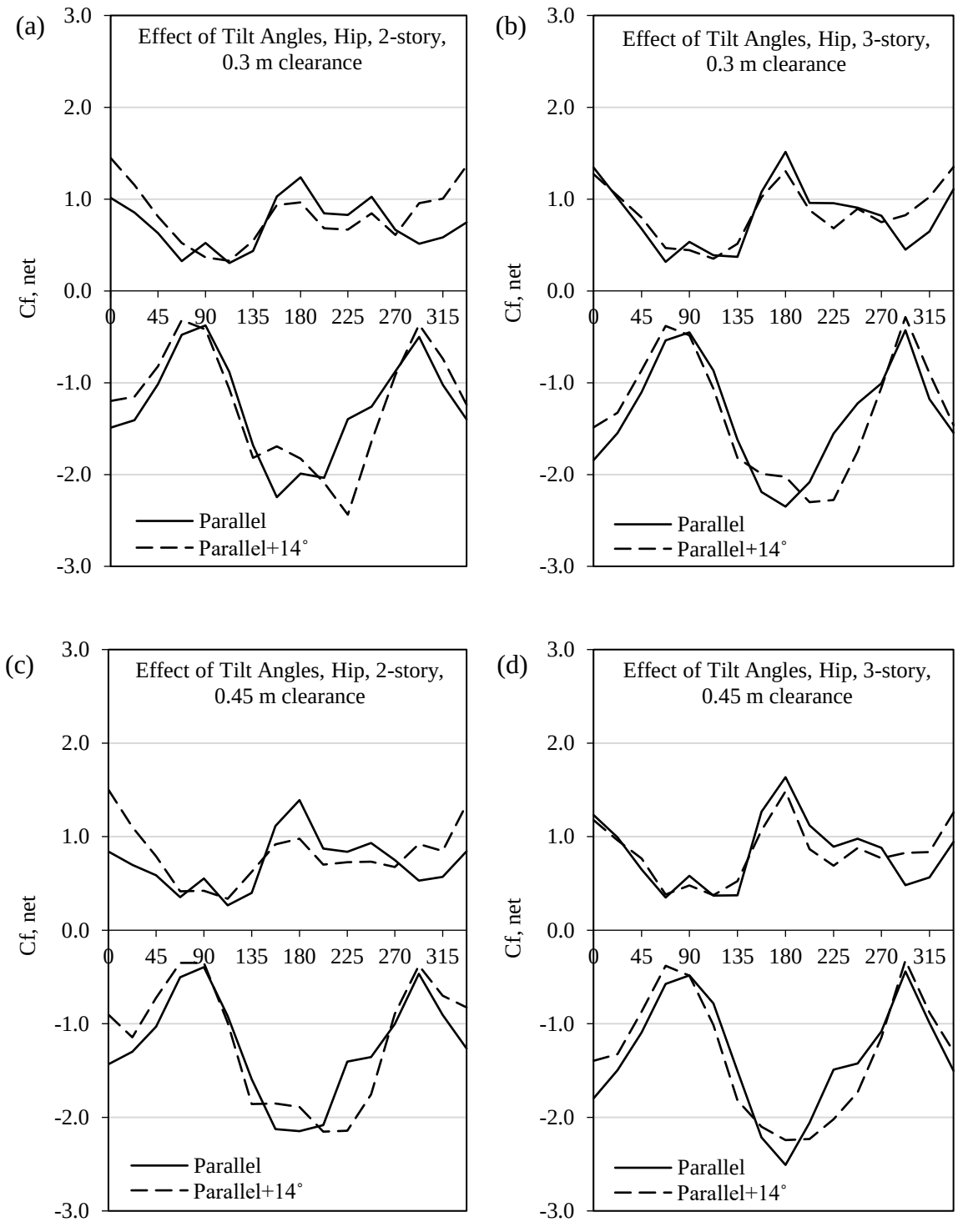

Figure 3-14. Variation of peak net force coefficient with wind direction (gable roof).

Taking into consideration the critical wind directions for the peak net force coefficients, the same wind angles of attack are considered to further discuss the distribution of the net peak values in terms of local pressures and suctions. According to Figure 3-14, at 180˚ wind angle of attack the highest peak maximum C_f values occurred for parallel panels mounted on hip roof building while parallel+14 models 180˚ was not necessarily the worst case. To investigate this observation further the distribution of maximum net C_p values recorded at 180˚ wind direction is compared for parallel and parallel+14 models in Figure 3-15 for the representative case of the 2-story and 0.3 m clearance model. The results indicate that by increasing the panel tilt angle there is an apparent change on the location of the critically loaded panel; ridge edge panel for parallel case and second row from ridge and hip edges panel for the parallel+14 case. While the high positive net pressures at near ridge panel can be attributed to building generated fluctuations the considerable increase in second top row of panels is possibly due to turbulence generated by near ridge panels.

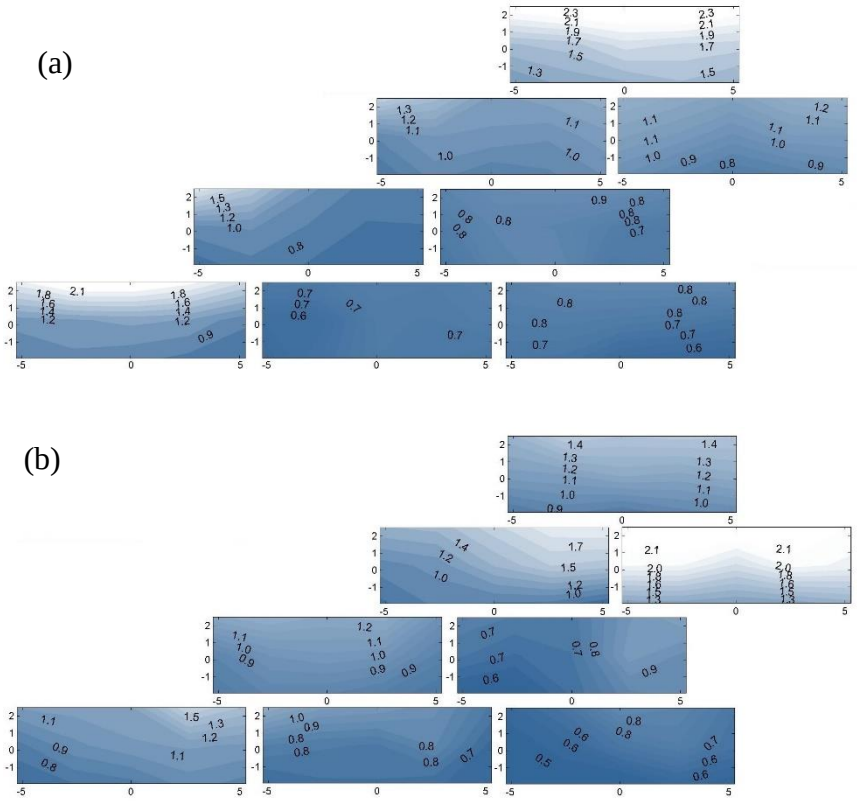

Figure 3-15. Peak net maximum C_p recorded at 180˚ wind direction on 2-story, 0.3 m clearance hip roof models with (a) parallel tilt angle and (b) parallel+14˚ tilt angle.

By investigating the critical wind direction with respect to minimum net panel C_f, it was revealed that for parallel panels the 180˚ wind angle of attack led to worst results while for parallel+14 panels the most critical wind direction was 225˚ (see Figure 3-14). To better comprehend the flow characteristics as well as the local pressure effects a comparison is made between the minimum net pressure distributions for 2-story, 0.3 m clearance hip roof models with different tilt angle at 180˚ (Figure 3-16). The results of minimum net C_p values reveal a similar behavior, in terms of critical panel location, to the maximum net C_p results discussed previously. For the 180˚ wind direction, the increase of the tilt angle results to the transfer of the critical pressure location to the middle panel, at

second top most row instead of the ridge panel. This similarity strengthens the assumption that increasing the tilt angle intensifies the panel generated turbulence that leads to higher peaks at more centrally located panels.

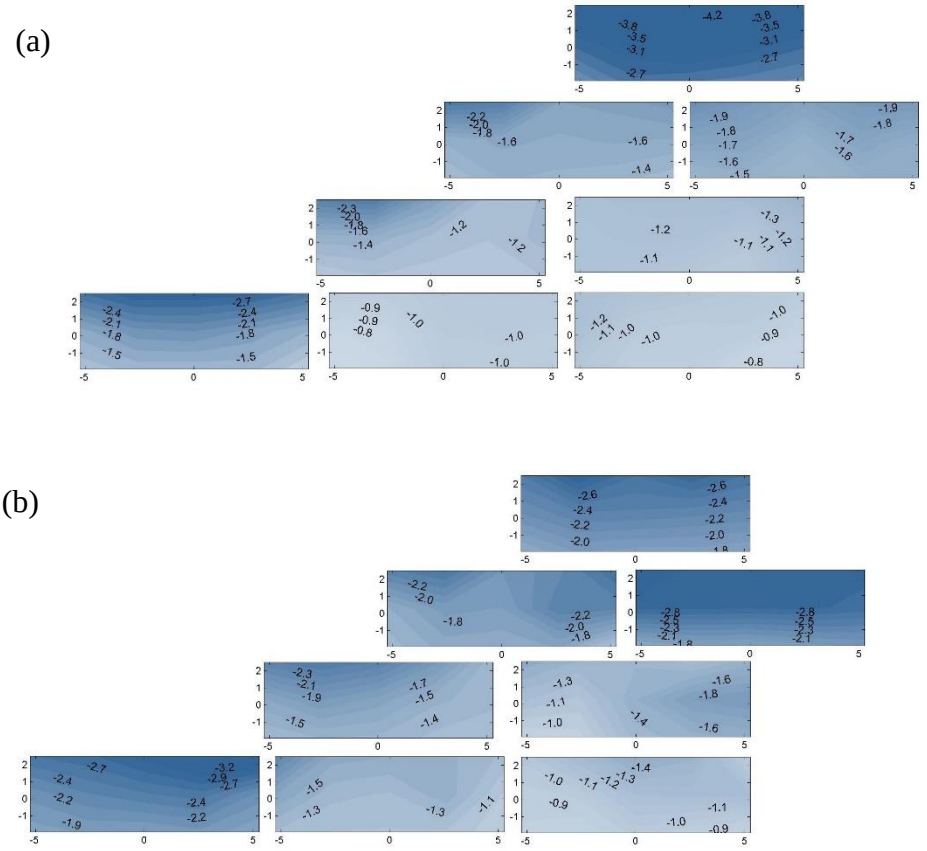

Figure 3-16. Peak net minimum C_p recorded at 180˚ wind direction on 2-story, 0.3 m clearance hip roof models with (a) parallel tilt angle and (b) parallel+14˚ tilt angle.

3.5.3. Single Panel Critical Force Coefficients

3.5.3.1. Flat roof

Figure 3-17 shows the most critical net C_f values for all instrumented panels as well as the corresponding – critical - wind direction for which the critical value occurred. The highest maximum force coefficient is observed on the panel located at southwest corner of

the roof due to cornering wind. The panels located at west edge of the roof (the shaded panels in Figure 3-17b) also experience high pressures, while the rest of panels have relatively lower peaks (less than 80% of the maximum value). As it is shown in Figure 3-17a, the worst suction force coefficient is observed at the shaded panel close to northwest corner of the roof due to cornering wind. The minimum net value at this panel is significantly higher than the rest of the panels with C_f less than 80% of the most critical panel. It can be concluded that the worst location for panel installation is at roof corners.

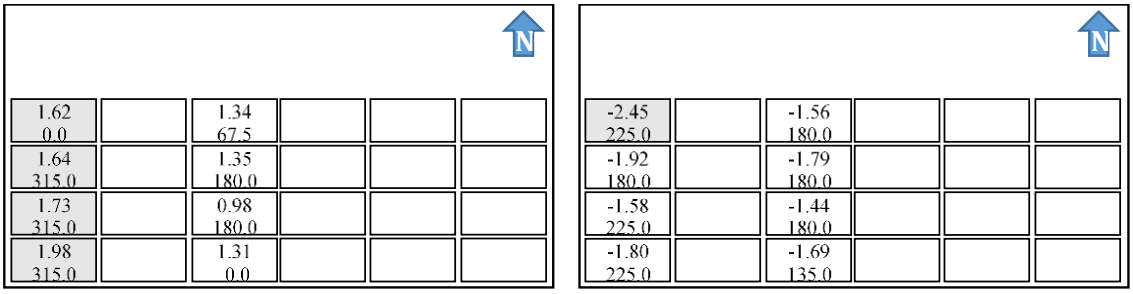

(a) (b)

Figure 3-17. Critical peak net C_f values and corresponding wind direction for each panel on the flat roof models (a) maximum peaks and (b) minimum peaks.

3.5.3.2. Gable roof

The most critical net force coefficients observed for gable roof models are presented in Figure 3-18. As can be observed from this figure the most critical location for panel installation is near the roof ridge (shaded panels in Figure 3-18a and b). Except for the panels located at this critical zone the rest of panels experience relatively lower peaks (less than 80% of the highest peaks).

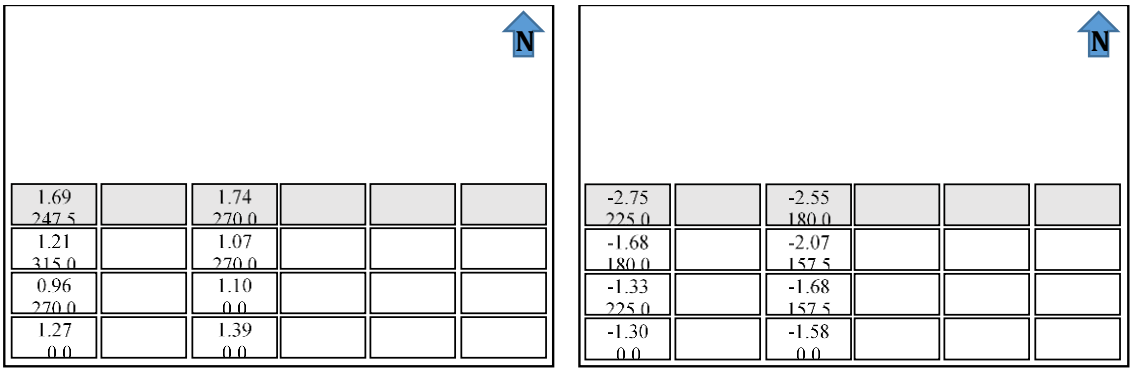

(a) (b)

Figure 3-18. Critical peak net Cf values and corresponding wind direction for each panel on the gable roof models (a) maximum peaks and (b) minimum peaks.

3.5.3.3. Hip roof

Figure 3-19 shows the highest net force coefficients recorded at panels on hip roof building models. The most critical zones where both maximum and minimum peaks have occurred are intersection of hipline with roof edge and roof ridge lines (shaded panels in Figure 3-19a and b). The maximum and minimum peaks at the rest of panels are less than 80% of the critical C_f values at high pressure and suction zones.

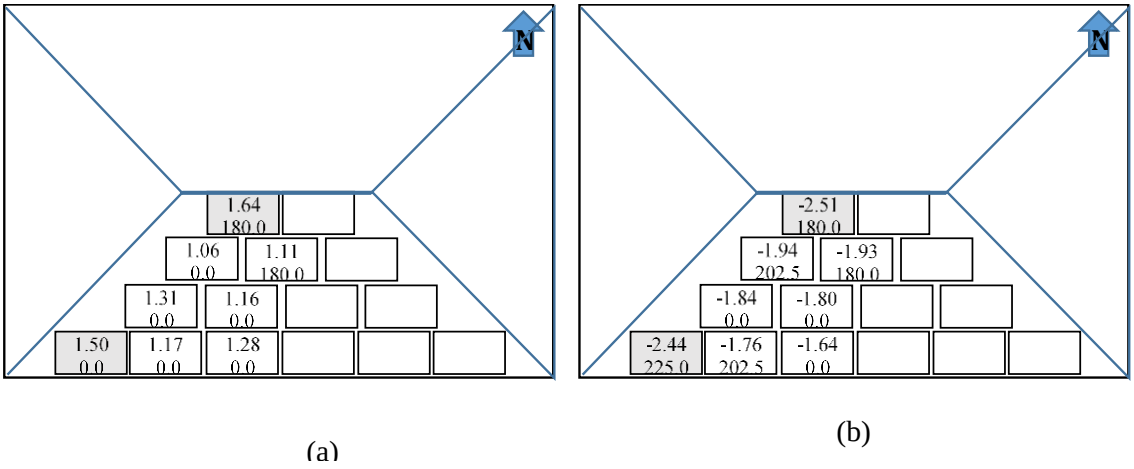

(a) (b)

Figure 3-19. Critical peak net C_f values and corresponding wind direction for each panel on the hip roof models (a) maximum peaks and (b) minimum peaks.

3.6. Enveloping curves and Codification

So far, the local pressure coefficients as well as panel force coefficients were discussed. Because of the turbulent nature of the wind the peak pressures do not occur simultaneously at all locations over the surface of PV panels. Larger monitoring areas will lead to lower chance of correlated peaks and as a result lower area averaged force coefficient. On the other hand, the racking systems are usually designed to support an array of PV panels instead of a single panel, so considering the non-coincident peak C_f for all panels in an array will result in unnecessary conservatism. For this reason, design guidelines usually suggest enveloping curves of force coefficient as a function of the effective area. In this section, the effect of panel tilt angle on area averaged peaks is investigated and individual enveloping curves are proposed for each roof type. To obtain these enveloping curves for each model configuration area averaging was performed for all possible combinations of pressure taps associated with any specific effective area and the highest force coefficient was assigned to the related effective area. After obtaining the area average force coefficients for each model configuration the results were grouped into several model categories. Then the enveloping curves which surpassed all force coefficients at all effective areas were developed for each model category.

Since for each roof type the panel tilt angle is the most important parameter affecting the critical panel force coefficient, in order to develop the enveloping curves, the building models were categorized based on roof type and panel tilt angle. Figure 3-20 shows the resulted envelopes for flat, gable and hip roof models. These curves envelope the force coefficients averaged over different effective areas ranging from 0.27 m^2 (i.e. group of 2 pressure taps) to 16.1 m^2 (i.e. group of 8 panels).

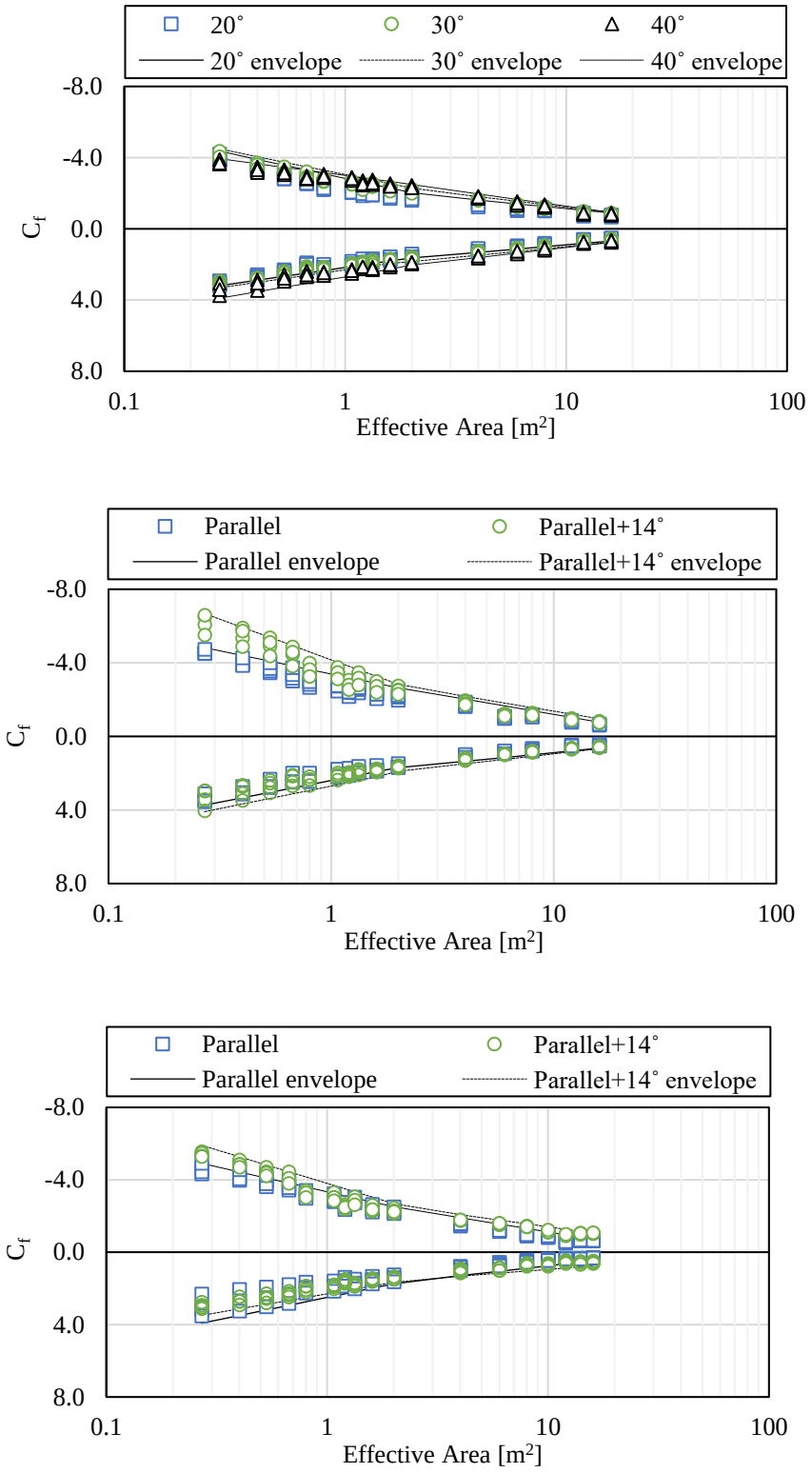

Figure 3-20. Enveloping curves for (a) flat roof, (b) gable roof and (c) hip roof.

As can be observed from Figure 3-20a, for flat roof models with effective area less than 1 m^2 there is only a slight difference between the enveloping curves generated for 20˚, 30˚ and 40˚ tilt angle models for both maximum and minimum force coefficients. When areas larger than 1 m^2 are considered, increasing the tilt angle leads to higher positive and negative enveloping curve. However, this variation of peaks is not large enough to require separate design enveloping curves for 20˚, 30˚ and 40˚ tilt angles, and so for simplification only two curves should be suggested for flat roof models; one for maximum and one for minimum pressure coefficients. As can be observed from Figure 3-20b and c, the gable and hip roof models follow quite similar patterns in regard to both maximum and minimum enveloping curves. While maximum curves in both gable and hip roof models lay relatively close for parallel and parallel+14 tilt angles, for minimum values enveloping curve of 14˚ tilted panels lay well above the one for parallel panels.

The summary of the enveloping curves is presented in Figure 3-21. All flat roof tilt angles are depicted with a single pair of curves whereas the gable and hip roof curves are split into two groups; i.e. tilt angles more than 10˚ are considered as “high” while the tilt angles less than 10˚ are referred to as “low”. As can be observed from this figure the maximum enveloping curves for all cases fall almost in the same range, so a single curve would adequately stand for the maximum force coefficient. In the case of minimum force coefficient, the results of gable and hip roof type with high tilt angle are close enough to be represented by a single curve, while another curve can be applied to flat roof models along with gable and hip roof models with low tilt angle. Taking into consideration these observations the need to codify the experimental findings in a simple format, the final suggested design curves can be reduced to the ones presented in Figure 3-22.

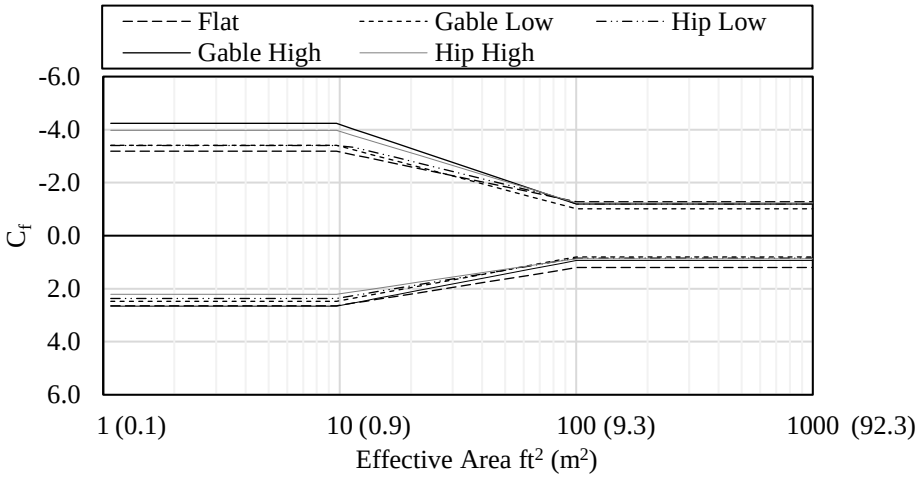

Figure 3-21. Enveloping curves grouped based on roof type and tilt angle.

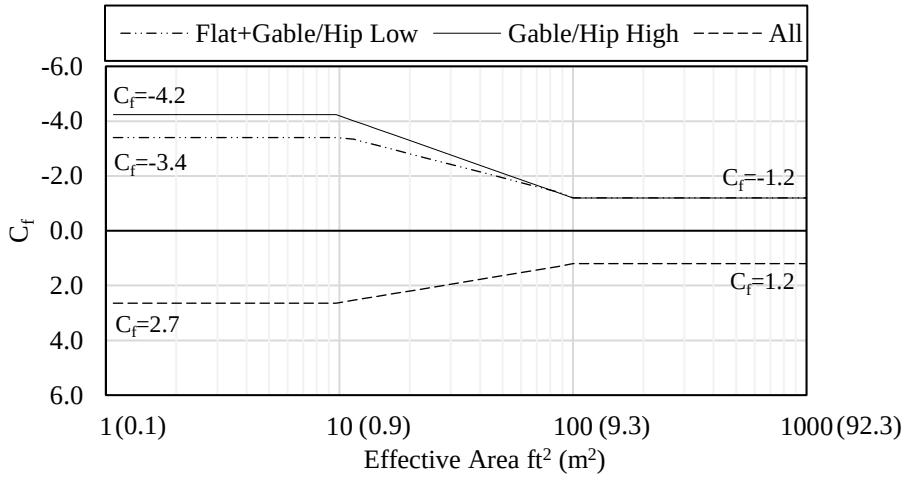

Figure 3-22. Recommended enveloping curves for codification purposes.

3.7. Discussion and comparison with other studies

In this section, a comparison is made between the conclusions obtained from this study and the previously performed researches on PV panels mounted on low rise buildings. In this study, it was shown that the panel tilt angle has significant effect on wind induced pressures on PV panels. This observation was in agreement with the previous studies (18,19). Also, it was shown that the clearance distance beneath the panels and roof

surface had a rather small effect on wind loads acting on the panels. The studies performed by Ginger et al. (18) and Geurts and Blackmore (14) resulted to the same conclusion, while Stenabaugh et al. (23) came to the opposite one. The reason for this discrepancy can be the fact that clearance distances investigated in Stenabaugh et al. included very small distances (0-0.2 m) compared to Ginger et al. (i.e. 0.1-0.2 m) and this study (i.e. 0.3-0.45 m). On the other hand, in Geurts and Blackmore although the clearance started from small distances (0.025 m), the small scale of 1:100 did not allow for accurate simiulation of panel thickness, which might have affected the reported results. These discrepnacies suggest that the effect of small clearance distances might need to be further investigated.

Figure 3-23, compares the suggested minimum force coefficient enveloping curves from the current study (see also Figure 3-22) to those reported by previous studies and the limited building codes. For the purpose of comparison only suggested force coefficients obtained from roof mounted PV panel studies were selected. All presented force coefficients in Figure 3-23, were reported based on the maximum 3-second gust speed, except for the Dutch standard (4), which was originally reported based on a 10-minute mean wind speed. Since it was important to present even a rough comparison of the design force coefficient for PV panel suggested by all existing standards, the 10-minute force coefficient was converted into 3-second force coefficient using figure C26-5.1 of ASCE 7-2010 (5). Furthermore, for the purpose of comparison, the highest force coefficient (related to the most critical roof zone and wind angle) reported by each of these references is presented. The first and most notable observation that can be made from Figure 3-23, is the considerable discrepancy among the force coefficient suggested by different studies and the two building codes. This observation affirms the need for further investigation of

wind loads on PV panels and uniform effort for development of consistent design force coefficient for these systems. The second notable fact is the considerably higher force coefficient suggested by the current study for small areas (i.e. smaller than a single panel area - 2 m^2), compared to most of the comparable studies. The higher force coefficients can be attributed to the following reasons. The large scale in the current study allowed for installation of 15 pressure tap sets per single PV panel. This resulted in a very fine pressure resolution that was no possible in previous smaller scale studies. In addition, the smaller scale studies did not allow for proper simulation of the actual turbulent cavity flow beneath the PV panels, while for the current study the large model scale made it possible to model such detail. Another possible reason for the observed discrepancies is related to the effect of high local suctions near the roof edges, which have been omitted from almost all the other studies by either considering a conservative setback from roof edges or low resolution of pressure taps. In the current study, the panels were installed as close as possible to the roof edges (0.2 m. distance) and high resolution of pressure taps allowed for measuring high local pressures. The tests carried out by Kopp (15) were designed for a commercial building with 1.22m setback from roof edges. SEAOC standard is also developed based on the studies performed on commercial building with considerably larger plan dimensions and long enough set back from roof edges. The provision for PV panels wind load in AS/NZS 1170-2 (3) is developed based on the study at James Cook University (18). Although this study was designed for residential buildings and considered small setback from roof edges, it was incapable of in capturing the local effects due to low resolution of pressure taps (only two locations were tapped for the 1.7 m x 1 m PV panel). The design force coefficient for PV panels in Dutch standard (4) was initially obtained in the study by

Geurts et al. (14). In this study only a 1.5 m x 1.2 m area of the PV array, which was close to building edge, got instrumented and only four tap locations were considered for this area. The only other study that reported results for near roof edge was Stenabaugh et al. (23) and this resulted in considerably higher force coefficient compared to the rest of the studies.

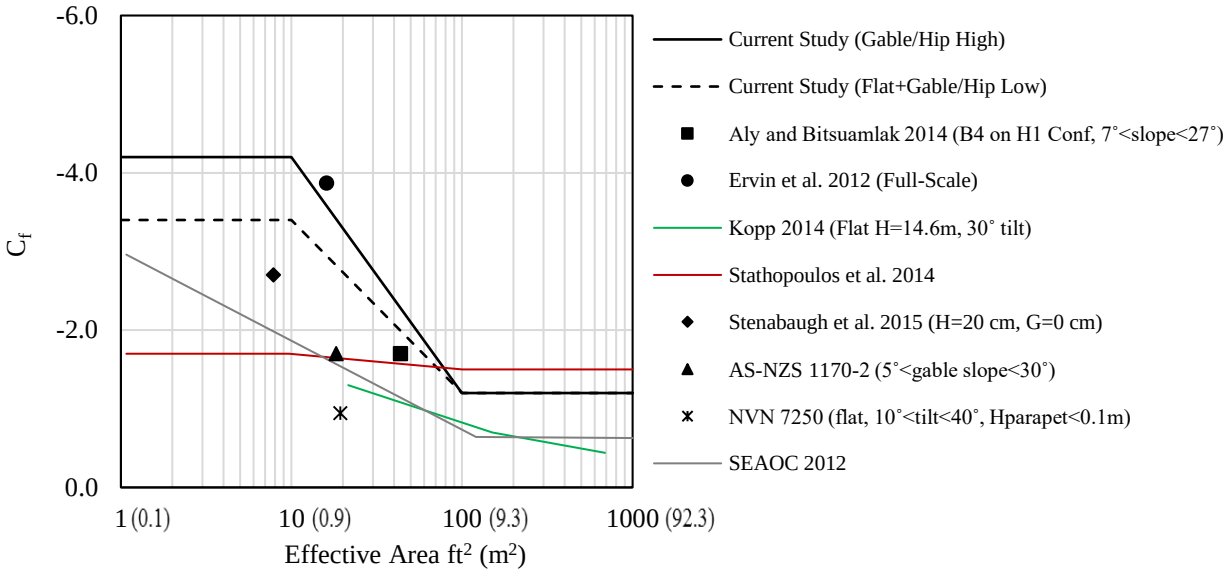

Figure 3-23. Comparison of the suggested enveloping curves with the design force coefficients of previous studies and existing standards.

3.8. Conclusions

In this study the wind-induced effect on PV panels, mounted on different types of residential building roofs, was investigated. Different geometrical properties, including panel tilt angle, clearance height, building height and roof type, were examined to assess the most significant parameters affecting the wind pressures on PV panels. Generally, it can be concluded that the tilt angle and roof type are the most important parameters that affect the wind forces on roof mounted PV panels, while the effect of clearance distance and building height was not significant. Also, it was observed that, depending on whether

the panels are tilted or parallel to the roof, the critical wind direction, location of critical peak pressures and mechanism leading to those peaks can be different. However, tilted panels experienced higher wind pressure compared to parallel panels. In summary, the following conclusions can be inferred:

- For tilted panels, the highest maximum net peaks occur at wind direction where the lower surface of the panels is leeward to the wind flow which leads to high suctions at lower surface of leading panels along with higher downward pressures at top surface of the panels. The wind angle that generates this condition is 315˚ for flat and gable roof and 337.5˚-0˚ for hip roof models.
- For parallel panels, the highest maximum net peaks usually happen at wind directions and on locations where the building generated turbulence reaches its maximum values. For parallel panels mounted on gable roof models the highest maximum pressures occurred at 247.5 ˚ wind direction and for hip roof models at 180˚ wind direction.
- For tilted panels, the highest suction net peaks occur at 225˚ wind angle of attack, where the building generated turbulent flow attacks the bottom surface of the leading panels and get separated at its edges and cause high suctions on top surface of the panels. The locations of critical panels for flat, gable and hip roof are windward corner of the roof, ridge and gable end edge intersection and ridge and hip line intersection, respectively. For parallel panels mounted on both gable and hip roof models the highest suction net peaks occur at 180˚ wind direction and at panels close to the ridge. These high suctions can be due to the high uplift pressures on top surface of the panels which are generated by flow separation at roof ridge.

- The design force coefficients for smaller effective areas resulted from the current study were found to be noticeably higher when compared to those from previous studies and the limited existing codes. This discrepancy may be attributed firstly to the scaling issue and the fact that the most of the previous studies could not model accurate flow characteristics due to small dimensions of the models. Moreover, the majority of the previous studies were performed on the panels located at a conservative set back from the roof edges and as a result could not in capture the high pressures that are mainly observed at near edge zones.

3.9. Acknowledgements

The authors would like to express their appreciation to Florida Division of Emergency Management (DEM) and International Hurricane Research Center (IHRC) at FIU for funding this research. Special thanks are also due to Walter Conklin and Roy Liu-Marques for the technical support during this study.

3.10. References

1. MITei. Future of Solar Energy Study. Energy Initiative Massachusetts Institute of Technology; 2015.
2. SEAOC. Report PV2-2012: Wind Loads on Low Profile Solar Photovoltaic Systems on Flat Roofs. Sacramento, California, USA: SEAOC Wind Subcommittee on Solar Photovoltaic Systems; 2012.
3. AS/NZS. Amendment No. 2 to AS/NZS 1170.2: Structural Design Actions - Part 2: Wind Actions. Sydney, Australia: Standards Australia/Standards New Zealand; 2012.
4. NEN. NVN 7250: Solar Energy Systems – Integration in Roofs and Facades_Building Aspects. Rotterdam, Netherlands: Netherlands Standardization Institute; 2007.

5. ASCE 7-10. Minimum Design Loads for Buildings and Other Structures [Internet]. Reston, Virginia: American Society of Civil Engineers; 2010. Available from: https://doi.org/10.1061/9780784412916

6. Stathopoulos T. Wind loads on solar panels: Reviews of research progress. In Phoenix, AZ: American Society of Civil Engineers; 2016.

7. Aly AM, Bitsuamlak G. Aerodynamics of ground-mounted solar panels: Test model scale effects. Journal of Wind Engineering and Industrial Aerodynamics. 2013 Dec 1;123:250–60.

8. Bitsuamlak GT, Dagnew AK, Erwin J. Evaluation of wind loads on solar panel modules using CFD. In: 5th International Symposium on Computational Wind Engineering (CWE2010), Chapel Hill, NC, USA [Internet]. 2010 [cited 2017 Oct 9]. Available from: https://www.researchgate.net/profile/G_Bitsuamlak/publication/267263612_Evaluation_of_wind_loads_on_solar_panel_modules_using_CFD/links/5496233e0cf2ec13375b2e95.pdf

9. Kopp GA, Farquhar S, Morrison MJ. Aerodynamic mechanisms for wind loads on tilted, roof-mounted, solar arrays. Journal of Wind Engineering and Industrial Aerodynamics. 2012 Dec 1;111:40–52.

10. Stathopoulos T, Zisis I, Xypnitou E. Local and overall wind pressure and force coefficients for solar panels. Journal of Wind Engineering and Industrial Aerodynamics. 2014 Feb 1;125:195–206.

11. Banks D. The role of corner vortices in dictating peak wind loads on tilted flat solar panels mounted on large, flat roofs. Journal of Wind Engineering and Industrial Aerodynamics. 2013 Dec 1;123:192–201.

12. Browne MTL, Gibbons MPM, Gamble S, Galsworthy J. Wind loading on tilted roof-top solar arrays: The parapet effect. Journal of Wind Engineering and Industrial Aerodynamics. 2013 Dec 1;123:202–13.

13. Cao J, Yoshida A, Saha PK, Tamura Y. Wind loading characteristics of solar arrays mounted on flat roofs. Journal of Wind Engineering and Industrial Aerodynamics. 2013 Dec 1;123:214–25.

14. Geurts C, Blackmore P. Wind loads on stand-off photovoltaic systems on pitched roofs. Journal of Wind Engineering and Industrial Aerodynamics. 2013 Dec 1;123:239–49.

15. Kopp Gregory A. Wind Loads on Low-Profile, Tilted, Solar Arrays Placed on Large, Flat, Low-Rise Building Roofs. Journal of Structural Engineering. 2014 Feb 1;140(2):04013057.

16. Pratt RN, Kopp GA. Velocity measurements around low-profile, tilted, solar arrays mounted on large flat-roofs, for wall normal wind directions. Journal of Wind Engineering and Industrial Aerodynamics. 2013 Dec 1;123:226–38.

17. Wood GS, Denoon RO, Kwok KCS. Wind loads on industrial solar panel arrays and supporting roof structure. Wind and Structures. 2001;4(6):481–94.

18. Ginger J, Payne M, Stark G, Sumant B, Leitch C. Investigations on wind loads applied to solar panels mounted on roofs. Rep TS821. 2011;

19. Erwin James, Bitsuamlak Girma, Chowdhury Arindam Gan, Barkaszi Stephen, Gamble Scott. Full Scale and Wind Tunnel Testing of a Photovoltaic Panel Mounted on Residential Roofs. Advances in Hurricane Engineering [Internet]. [cited 2017 Aug 16]; Available from: http://ascelibrary.org/doi/abs/10.1061/9780784412626.041

20. Fu T-C. Development of Effective Approaches to the Large-Scale Aerodynamic Testing of Low-Rise Building [Internet]. 2013. Available from: http://digitalcommons.fiu.edu/etd/986

21. Mooneghi MA, Irwin P, Chowdhury AG. Partial turbulence simulation method for small structures. In: Proc, 14th Int Conf on Wind Engineering [Internet]. 2015 [cited 2017 Aug 15]. Available from: https://www.researchgate.net/profile/Maryam_Asghari_Mooneghi/publication/306394907_Partial_Turbulence_Simulation_Method_for_Small_Structures/links/57bc85ba08aebc3b71fe6d23.pdf

22. Aly AM, Chowdhury AG, Bitsuamlak G. Wind profile management and blockage assessment for a new 12-fan Wall of Wind facility at FIU. Wind & Structures. 2011;14(4):285–300.

23. Stenabaugh SE, Iida Y, Kopp GA, Karava P. Wind loads on photovoltaic arrays mounted parallel to sloped roofs on low-rise buildings. Journal of Wind Engineering and Industrial Aerodynamics. 2015 Apr 1;139:16–26.

24. Asghari Mooneghi M, Irwin P, Gan Chowdhury A. Partial turbulence simulation method for predicting peak wind loads on small structures and building appurtenances. Journal of Wind Engineering and Industrial Aerodynamics. 2016 Oct;157:47–62.

25. Naeiji A., Raji F., Zisis I. Large-Scale Wind Testing of Photovoltaic Panels Mounted on Residential Roofs. Structures Congress 2015 [Internet]. [cited 2017 Aug 15]; Available from: http://ascelibrary.org/doi/abs/10.1061/9780784479117.161

CHAPTER 4

EXPERIMENTAL ANALYSIS OF WIND-INDUCED VIBRATION ON ROOF-MOUNTED SOLAR PANELS

(A paper to be submitted to ASCE Journal of Structural Engineering)

CHAPTER 4. EXPERIMENTAL ANALYSIS OF WIND-INDUCED VIBRATION ON ROOF-MOUNTED SOLAR PANELS

Amir Naeiji[4], Ioannis Zisis[5], Arindam Gan Chowdhury[6], Peter Irwin[7]

4.1. Abstract

Despite the recent interest in the study of the wind effects on solar photovoltaic (PV) panels, there exists very limited information regarding the dynamic response of these systems to the wind fluctuations.

This study aimed to investigate the wind-induced vibrations on residential scale roof-mounted solar panels. Two full-scale experimental setups were used, a model with real panels (flexible model) instrumented with accelerometers and a pressure tapped model made out of wood (rigid model). Both models were instrumented with load cells at the connections of racking system to the mounting building. Additionally, a pressure-tapped 1:5 scale model was built and tested to evaluate the scaling effects.

Net force coefficients were calculated based on the pressure data resulted from the pressure-tapped model as well as reaction forces obtained from load cells. The mean and minimum force coefficient comparisons between the flexible and the rigid models showed

[4] [Corresponding author] Department of Civil and Environmental Engineering, Florida International University, Miami, FL, USA. E-mail: anaeiji@fiu.edu

[5] Department of Civil and Environmental Engineering, Florida International University, Miami, FL, USA. E-mail: izisis@fiu.edu

[6] Department of Civil and Environmental Engineering, Florida International University, Miami, FL, USA. E-mail: chowdhur@fiu.edu

[7] Department of Civil and Environmental Engineering, Florida International University, Miami, FL, USA. E-mail: peairwi@fiu.edu

good agreement. However, the maximum force coefficient values were lower for the flexible model compare to the rigid model.

Comparing to the force coefficient spectra obtained from the load cell records of the flexible and the pressure taps of the rigid model, it was shown that at the frequency of 10.5 Hz (fundamental natural frequency of the system) the resonance effect results in the amplification of the response spectra of flexible model.

In addition, the Dynamic Amplification Factor was calculated based on the response spectra of the models. Finally, the wind-induced forces were compared to ASCE 7-16.

Keywords: Photovoltaic panel, Fluid-structure interaction, Wind load, Wind-induced vibration, Dynamic analysis, Pressure coefficient, Force coefficient.

4.2. Introduction

Reduction in construction and installation costs of solar panels and inverters has led to widespread use of residential rooftop PV modules. Most recent developments even include mandatory installation of solar panels in new construction (1). Propagation of solar energy harvesting and development of more efficient PV systems have increased the attention toward the structural design aspect of these systems and, in particular, the design for wind forces. Over the past decade, numerous studies have been performed and guidelines for estimating wind loads on industrial and residential structures have started to be included in some building codes and wind standards. Photovoltaic (PV) module vibrations under wind action have been found to be significant during full-scale tests while current design standards and building codes do not address this unfavorable behavior.

Preliminary studies showed that the effect of PV-system vibration should be considered in the design of mounting structure. Moreover, the <1 Hz fundamental natural frequency criterion used in current standards (2–4) to determine whether wind-induced dynamic effects should be considered or not, may not be applicable to PV systems. The goal of this study is to expand the understanding of the dynamic behavior of PV systems exposed to wind-induced loads. More specifically, the study examines the vibration on the PV panels and the supporting system due to turbulent action of wind.

Scaled rigid models are not suitable for investigating the dynamic effects, because such models do not simulate the dynamic properties of the systems and are unable to capture resonant response. For this study, an actual full-scale PV panel system (i.e. flexible panels) was mounted on a low-slope roof and instrumented using accelerometers and load cells. Then an identical rigid full-scale PV panel system was tested under the same conditions. In addition to the full-scale flexible and rigid models, an identical large-scale pressure-tapped model was built. All models were tested at the Wall of Wind Experimental Facility at Florida International University (FIU). Comparison of pressure and force coefficients between the different experimental setups are reported herein. Also, the dynamic response of the flexible system was investigated in detail and an estimation of its Mechanical Admittance Function (MAF) was attempted.

4.3. Previous studies

Due to the considerable expansion of solar photovoltaic (PV) systems, the evaluation of wind loads acting on these systems plays a very important role from the practical design viewpoint. For the very first time, ASCE 7-16 (2) provides provisions for

the design of roof-mounted PV systems. These provisions are offering design values (i.e. net pressure coefficients) that are developed based on several previous experimental and numerical studies.

Numerical and experimental studies on ground-mounted solar arrays investigated the effects of pressure equalization and array generated turbulences (i.e. model scale, wind direction, tilt angle, lateral and longitudinal spacing between panels) on the wind-induced loads and pressure distributions (5–12). The net flow-induced loads on the solar panel are partially affected by the cavity pressures generated by the cavity flow (the flow passing through the ground and the panel). The pressure equalization results from this phenomenon and is frequently referred to explain the net pressure distribution on roof pavers, canopies, solar panels etc. (13–20).

Most of the previous studies evaluated the wind-induced loads on the solar panels mounted on large flat roofs. These studies evaluated the building generated turbulence as well as the influential parameters, i.e. building height, array setback from the roof edge, parapet height, corner vortices (9,21–27). However, there are a few studies investigating the distribution of loads and pressures throughout the panels mounted on the roof of low-rise residential buildings. It has been shown that roof type (i.e. gable, hipped, mansard, gambrel, flat) and shape (e.g. slope) can effectively alter the wind load distribution on the mounted solar panels (18,28–33).

Almost all of the previous wind tunnel studies evaluated the load on solar panels by utilizing pressure-tapped rigid models and they naturally cannot capture the vibration effects on the prototype. Since the solar arrays are slender structures, and are repeatedly

placed in rows, they are potentially vulnerable to the effects of von Karman vortex streets. Vortices that are shed along the panel surfaces are producing crosswind fluctuating forces. These effects can result in significant vibrations on the surface of the panels as shown by previous studies (34–36).

Strobel and Banks (34) investigated the effects of vortex shedding in arrays of ground-mounted solar panels. They have challenged the building standards (ASCE 7-05 (4) and ASCE 7-10 (3)) criteria for definition of dynamically sensitive structures (e.g. ground-mounted solar arrays of photovoltaic panels) by calculating the power spectra of hinge moment coefficients. The total hinge moment was calculated by applying the Miles' approximation (37) and Davenport equation (38). They found damping of the support structure, location and tilt angle of the panel, and wind direction are important parameters affecting the excitation.

Moravej et al. (35) investigated the wind-induced vibrations on a roof-mounted solar panel. They presented the force coefficients on the full-scale flexible and small-scale rigid models and reported that the force coefficients on full-scale model are significantly magnified compared to the small-scale model. A mechanical admittance function was used as a transfer function to estimate the force coefficient based on the rigid model.

The mentioned studies investigated the ground-mounted and flat roof-mounted panels. The purpose of this study is evaluating the wind-induced vibrations on the residential roof-mounted solar panels and examining the significance of the dynamic behavior of the actual PV panels.

4.4. Test Setup

4.4.1. Model Configuration

In order to investigate the dynamic response of roof-mounted solar PV panels, it was decided to mount the PV system on a mono-slope roof building with full-scale mean roof height of 2.13 m and roof pitch angle of 10˚. The tests were performed using three setups including two full-scale models (flexible and rigid) and one 1:5 scaled model (Figure 4-1). The full-scale models were tested to investigate the effect of vibrations of the panels. Therefore, three actual PV panels were mounted on the racking system (named flexible model throughout this paper) while for the other tests the panels were built out of wood to represent the response of rigid system to the turbulent wind loading. The research hypothesis was that the rigid model would not experience any vibration effects while the flexible model would experience across-the-plane vibrations and possible dynamic amplification of the support reactions along with amplified acceleration at wind gust frequencies close to the system natural frequencies. The scaled down model provided the opportunity of investigating the scaling effects on the wind induced pressures by comparing its results to the results of full-scale rigid model.

Three monocrystalline solar modules were used as the flexible models (Figure 4-1a). The module dimensions are 1971 by 982 mm. The thickness and weight of each module is 46 mm and 23 kg respectively. The full-scale rigid panels were built out of wood with the same dimensions and mounted on the same racking system as the flexible model (Figure 4-1b). The large-scale rigid panels were also made out of wood with 1:5 scaled down dimensions (Figure 4-1c).

(a) (b) (c)

Figure 4-1. Three models were used in this study: (a) full-scale flexible model, (b) full-scale rigid model, and (c) 1:5 rigid model

4.4.2. Instrumentation

Load cells and accelerometers were installed on the PV panel system to monitor the dynamic response of the system during the wind loading. Dytran 3263A series accelerometers were selected for monitoring the panel acceleration due to their light weight. In order to decide on the location of the accelerometers the numerical model of the system was created using SAP 2000 and the critical points that were subjected to the maximum deformations in the vibration mode shapes were selected (Figure 4-2). Figure 5-7 displays the location of accelerometers installed on the PV panel modules.

The PV mounting system consisted of two aluminum rails that were supported by eight pedestals. Since it was decided to keep the 25-cm gap between the panels and the roof surface the load cells were mounted under the pedestals as connecting links between the pedestals and the roof trusses. The locations and the numberings of the load cells are illustrated in Figure 5-8.

Once the model was mounted on the racking system and got instrumented with the accelerometers, hammer tests were performed to investigate the dynamic characteristic of

the PV system including the fundamental frequencies. Considering the required impact intensity for exciting the PV module, a force-instrumented hammer, PCB Piezotronics model 086C01 impulse hammer, was selected for the experimental tests (Figure 5-9).

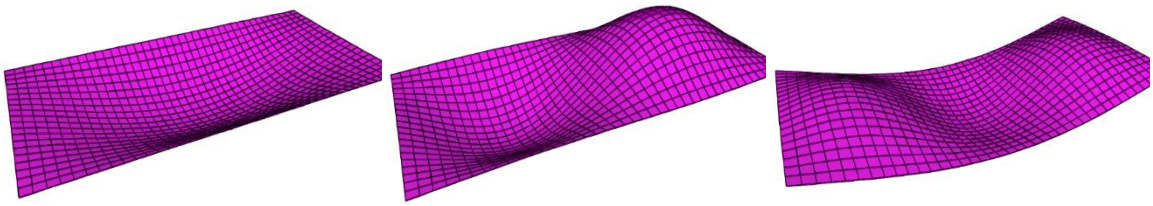

Mode 1 *Mode 2* *Mode 3*

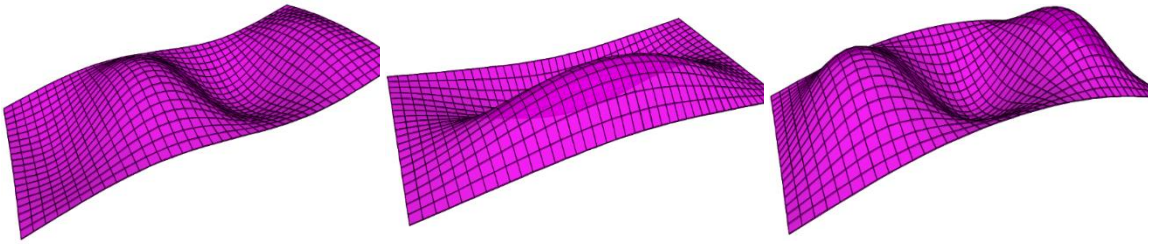

Mode 4 *Mode 5* *Mode 6*

Figure 4-2. Mode shapes based on numerical model

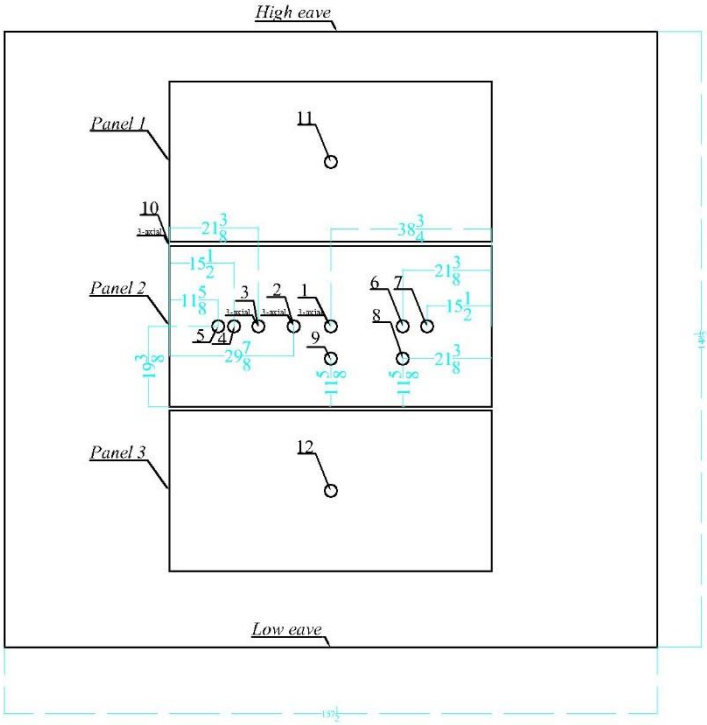

Figure 4-3. Location and numbering of the accelerometers on the PV modules

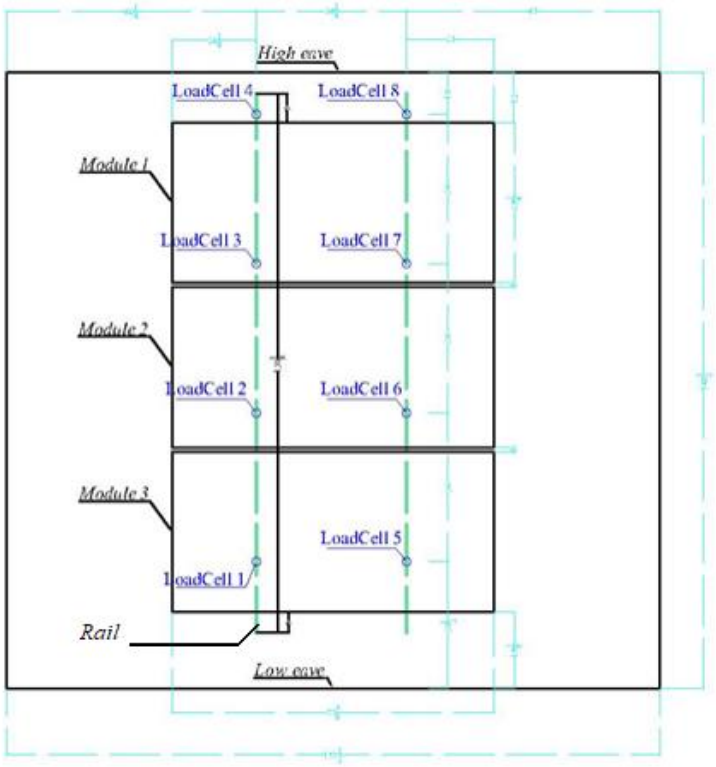

Figure 4-4. PV modules and load cell location and numbering on the roof

Figure 4-5. Impulse hammer (PCB model 086C01)

The upper and lower layers of the full-scale rigid panels were instrumented by 210 pressure taps (35 taps on each side on each panel). While only 90 taps were installed on the 1:5 scale model.

4.4.3. Flow Characteristics

All experiments were carried out at the 12-fan Wall of Wind Experimental Facility at Florida International University (FIU) (Figure 4-6) assuming an open terrain simulation. Details on the specification of the Wall of Wind Experimental Facility and the wind flow characteristics can be found in (39). All tests were performed at 30% fan throttle (i.e. 19 m/s mean wind speed and 7% turbulence intensity at mean roof height) except for the full-scale flexible model tests that were performed at 60% (i.e. 38 m/s at mean roof height) and 80% fan throttle (i.e. 51 m/s at mean roof height) in addition to 30% fan throttle to investigate the effect of wind speed on the dynamic response of the PV systems. The full-scale tests with 30% throttle were performed at the Reynolds number equal to 3.5×10^5.

The mean wind speed and turbulence intensity profiles were calculated by using Pitot-static tubes and Cobra probes mounted at different heights at the center of the test section at the Wall of Wind Experimental Facility without the model in place. The corresponding mean wind speed and longitudinal turbulence intensity profiles are shown in Figure 4-7 as a function of height.

Figure 4-6. Wall of Wind Experimental Facility

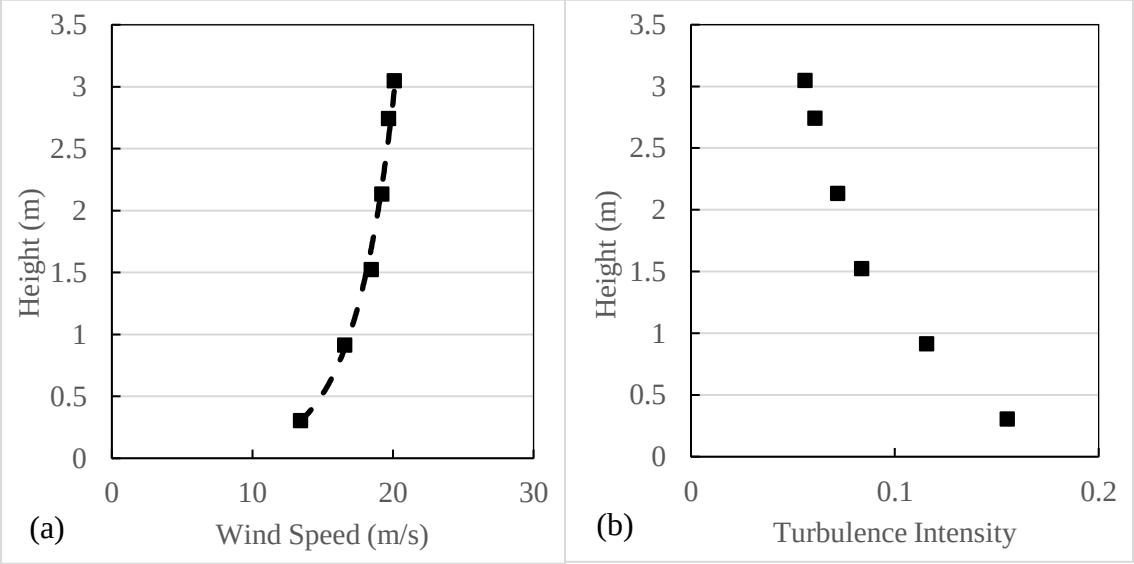

Figure 4-7. (a) Mean wind speed and (b) turbulence intensity profiles

The longitudinal power spectral density of the generated flow is compared to the von Karman spectrum ($I_u = 0.2$ and $xL_u = 20$ m) in Figure 4-8. The comparison suggests the surface roughness parameter of 0.02 m. which corresponds to open terrain exposure.

Both full-scale models (flexible model and rigid model) were tested for 24 wind angles from 0˚ to 345˚ with 15˚ increments. For the large-scale model, the experimental

tests were performed for 66 wind angles from 0˚ to 195˚ with 3˚ increments. Figure 4-9 shows the direction convention for the experimental tests.

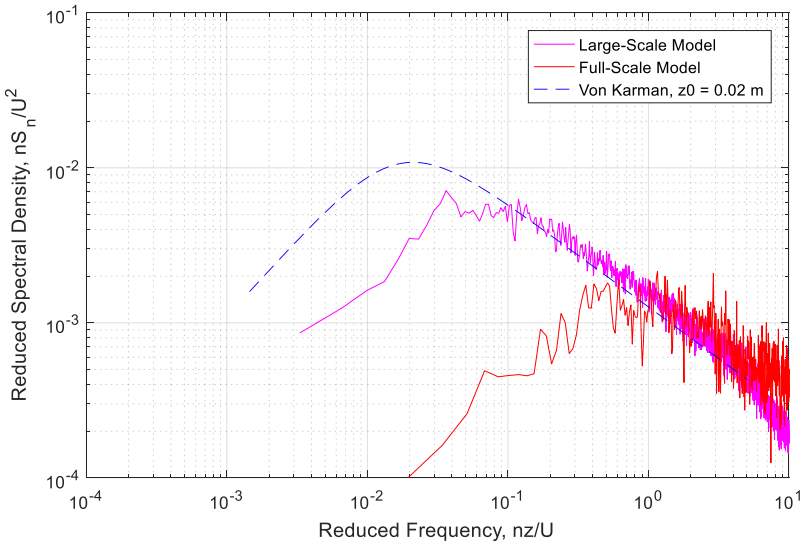

Figure 4-8. Wind speed spectra (at the height of full- and large- scale models) at Wall of Wind and von Karman spectrum for z_0=0.02 m

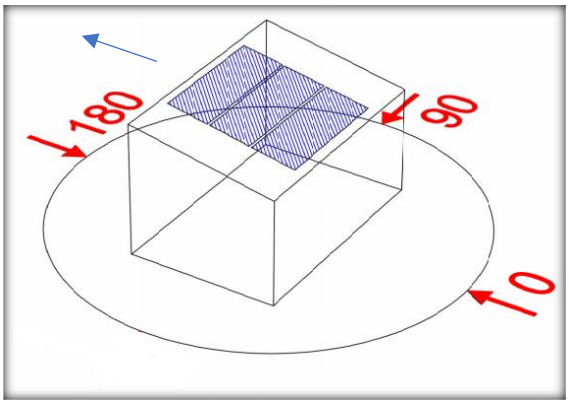

Figure 4-9. Reference wind directions.

4.5. Results

4.5.1. Impulse Hammer Testing

The natural frequency of the flexible model was determined using impulse hammer tests with different excitations and the response functions as the resultant motion were

measured at the location of the accelerometers. Figure 4-10 shows the time history of the impact load applied by the hammer at the location 1 and Figure 4-11 shows the corresponding accelerometer time history at location 2 (see Figure 4-3 for locations). The measurements lasted for 31 seconds and the sampling frequency was 1000 Hz. The power spectra of the acceleration response at location 2 caused by the hammer impact at location 1 is presented in Figure 4-12. The spectrum indicates a distinct amplification of response amplitude at the natural frequencies of the model. The first noticeable peak is detected at 10.5 Hz and corresponds to the fundamental natural frequency of the solar panels.

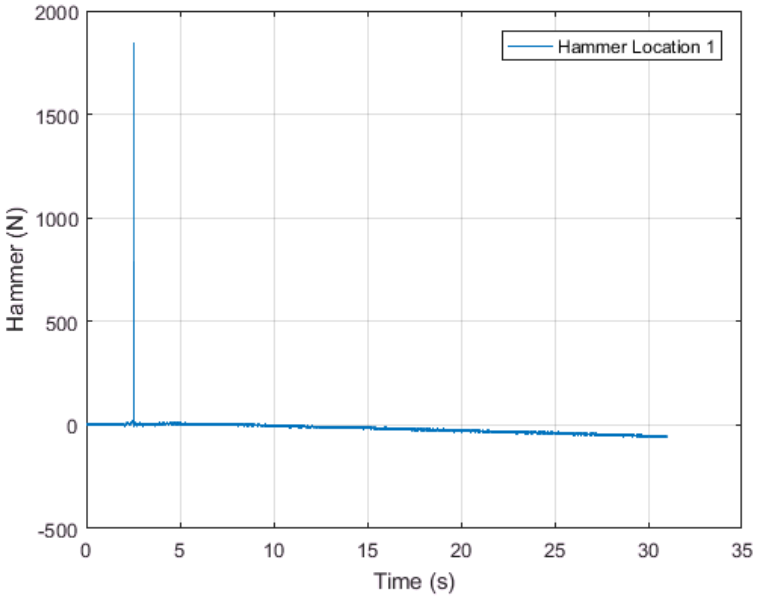

Figure 4-10. Time history of hammer load data

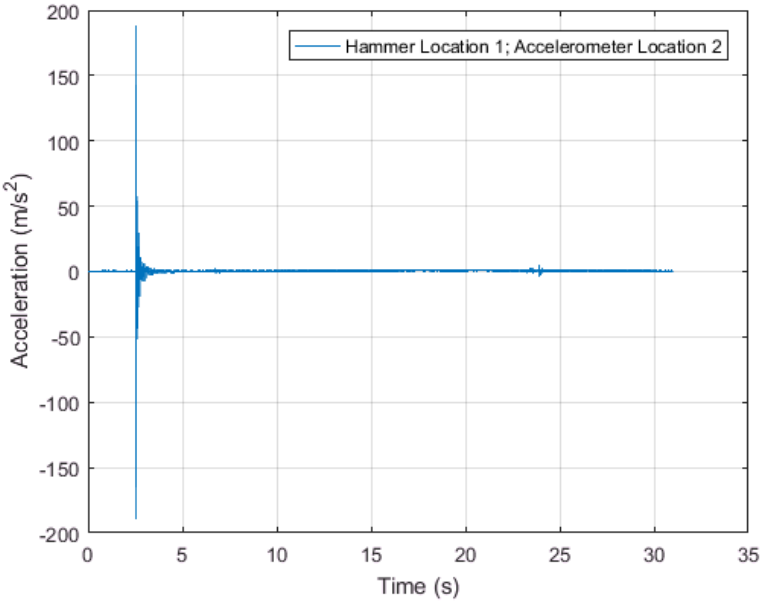

Figure 4-11. Time history of accelerometer 2 when location 1 was excited by the impact hammer

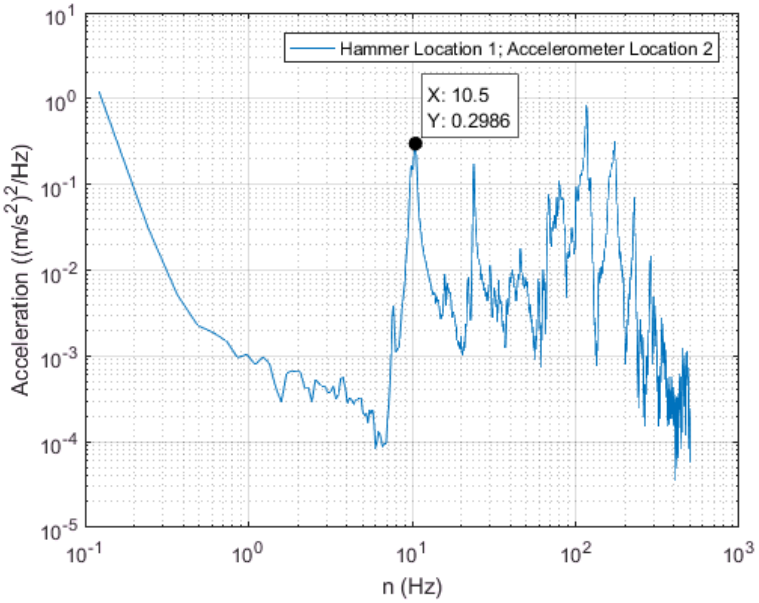

Figure 4-12. Spectrum of accelerations due to the hammer hit.

4.5.2. *Dynamic Response*

During the tests, the load cells were recording the wind-induced reactions at the eight pedestals (i.e. supports of the racking system). A representative record from the flexible model tests, is presented in Figure 4-13 and shows the load time history for load cell 1 at 30% throttle and for 0° wind direction. To estimate the total force (F(t)) on each module the following equations were used:

$$F_{LC}^{j}(t) = F_{LCRaw}^{j}(t) - B^{j} \quad (1)$$

$$F(t) = \sum_{j=1}^{8} F_{LC}^{j}(t) \quad (2)$$

where, $F_{LC}^{j}(t)$ is the net load time history of jth load cell which is calculated by removing the mean of the baseline (B^{j}) from the raw load data ($F_{LCRaw}^{j}(t)$).

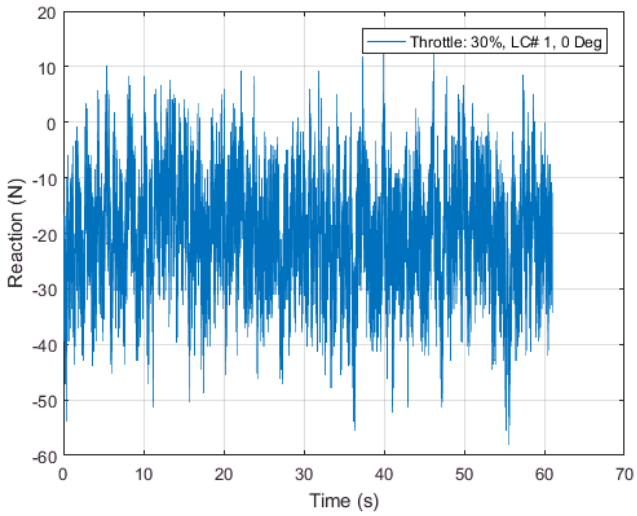

Figure 4-13. The time history of load cell 1 with 30% throttle, flexible model in 0° wind direction.

The force coefficient was calculated based on the following formula:

$$C_F(t) = \frac{F(t)}{(1/2)\rho_a {V_m}^2 A} \quad (3)$$

where, $F(t)$ is total force (N), ρ_a is mass density of air (kg/m^3), V_m is mean wind speed (m/s) at the mean roof height and A is the corresponding area (m^2).

Figure 4-14 compares the mean, maximum and minimum force coefficients for 30% (blue), 60% (yellow) and 80% (red) fan throttle at different wind angles on the full-scale flexible model. The values are the average force coefficient over three panels. As can be observed from this figure, the mean force coefficient results obtained at different throttles are following the same pattern while the peak force coefficients show some discrepancies for specific wind directions. For instance, the minimum force coefficients in the range of 0^o-120^o are significantly influenced by the oncoming wind speed. On the other hand, when the critical peak coefficients are observed (i.e. worst values regardless of wind direction) the discrepancies are minimal.

The comparison of the mean, maximum and minimum force coefficient values calculated based on rigid model load cell results, flexible model load cell results and rigid model pressure tap results is presented in Figure 4-15. Overall, the comparison does not show any significant difference between the force coefficient values obtained from the flexible versus the rigid model tests. When specific wind directions are considered (e.g. 0^o-60^o), the flexible model experiences considerably higher force coefficient values when compared to the rigid model pressure tap results. These cases were considered to test for the central hypothesis of this research, regarding the dynamic amplification of the response due to panel vibrations. When the rigid model is considered only and the force coefficient

results obtained from the load cells and the pressure taps are compared, some discrepancies are identified. This can be partially justified by the area-averaging approach used with the pressure tap analysis – a corresponding area is assigned to each pressure tap and it is assumed that this area experiences the same pressure time history as the point where the tap is located. As can be observed on these graphs, the minimum force coefficients occur when the wind pressures on the back of the panels increase due to the northern (180^o) wind directions.

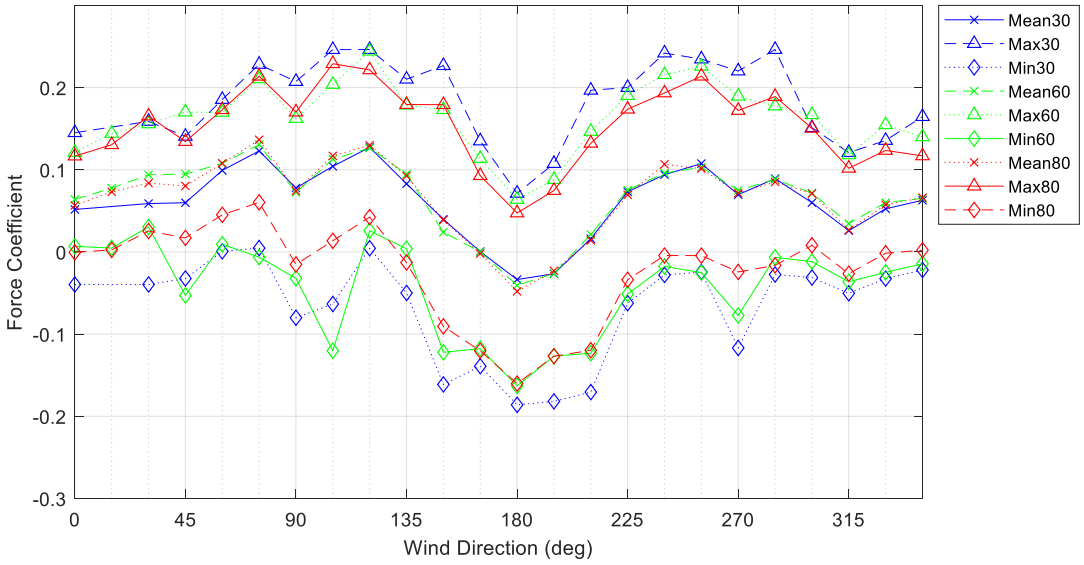

Figure 4-14. Mean, maximum and minimum force coefficient (at 30, 60 and 80 percent fan throttles) on the flexible model (calculated using load cell data) at different wind angles of attack

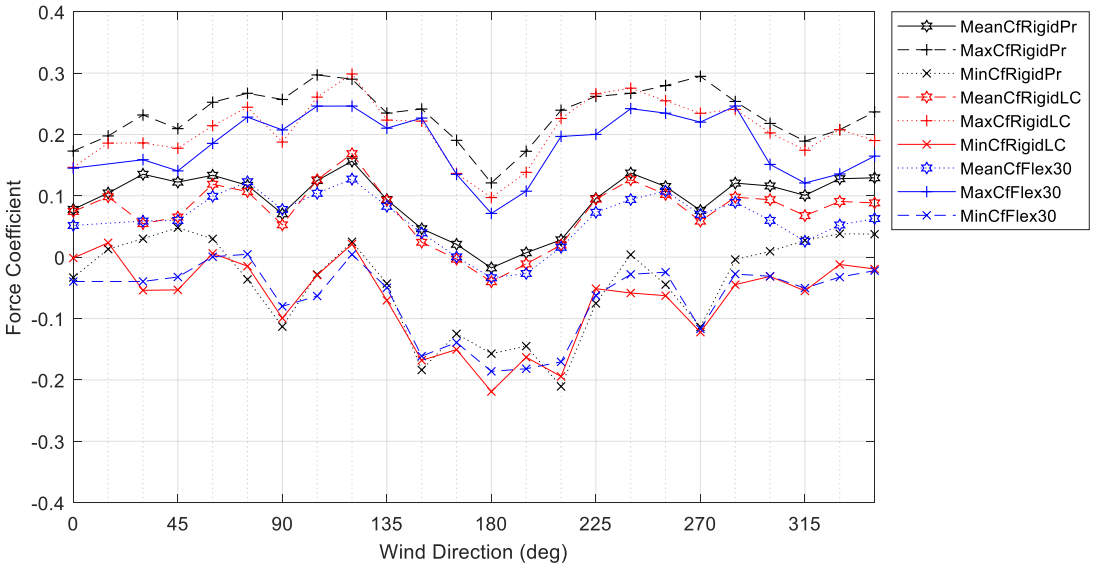

Figure 4-15. Mean, maximum and minimum force coefficient on the flexible model (blue), rigid model using load cells' data (red) and rigid model using pressure taps' data (black) at different wind angles of attack

Figure 4-16 provides the comparison of the force coefficient values between the full-scale rigid model and large-scale model. For both models, the force coefficient values are calculated using the pressure tap data. The results indicate a good match between the large-scale and full-scale mean force coefficient values. However, for the maximum and minimum peaks the large-scale model has resulted in lower values. These discrepancies were expected since the wind power spectra at different scales do not match the expected full-scale power spectrum (see Figure 4-8). Accounting for this mismatch, the Partial Turbulence Simulation (PTS) has been developed and verified by Wall of Wind researchers (40). Figure 4-17 presents 3-second maximum and minimum values for the large- and full-scale rigid models when the PTS method is implemented. The results indicate a significantly improved agreement in both maximum and minimum force coefficients.

However, the large-scale minimum force coefficient values still show a considerable deviation from the full-scale data.

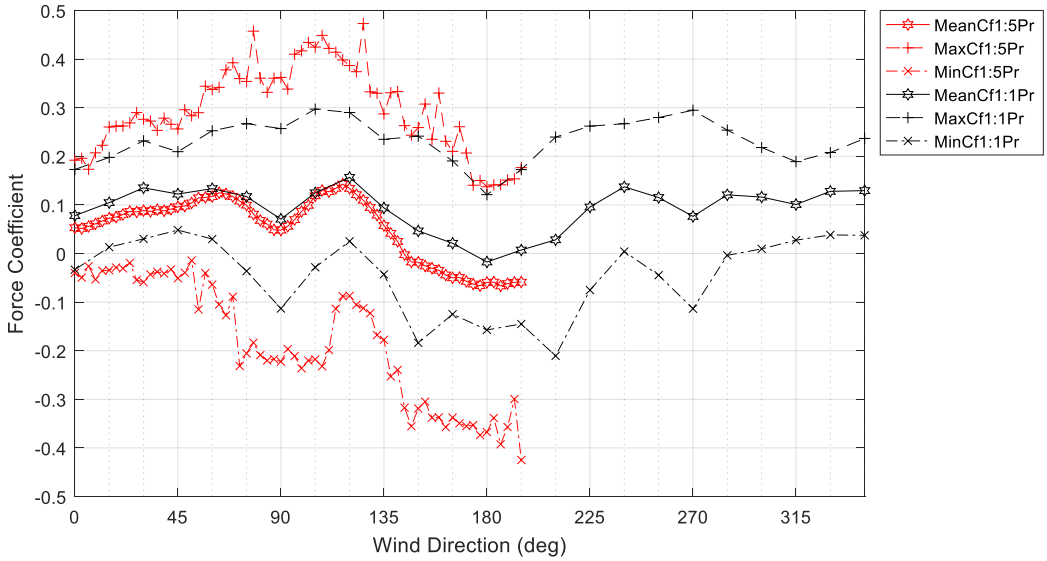

Figure 4-16. Mean, maximum and minimum force coefficient on the full-scale and large-scale rigid models using pressure taps' data

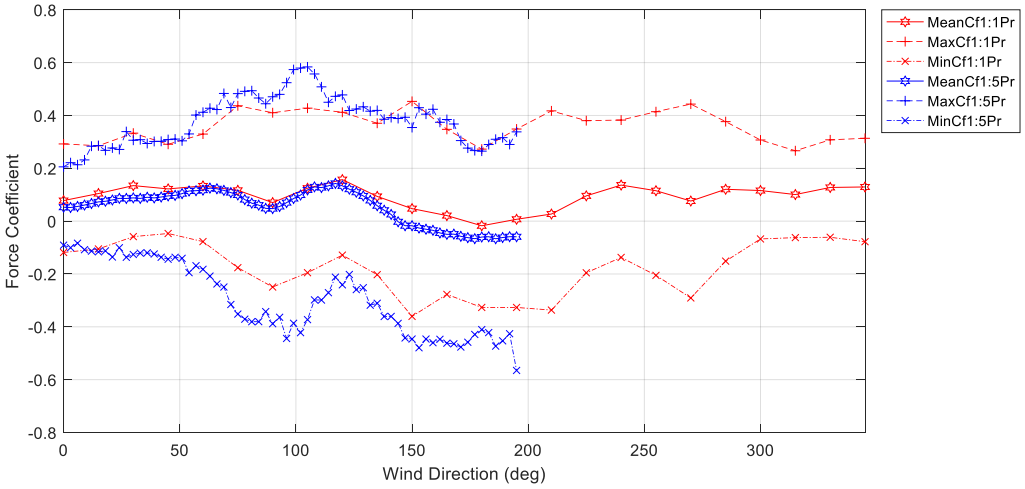

Figure 4-17. Mean, and PTS 3-sec peak force coefficient on the full-scale and large-scale rigid models using pressure taps' data

To further investigate the dynamic response of the PV modules and the racking system, the force coefficient power spectra were plotted. Figure 4-18 shows the power spectra of the force coefficients calculated based on the reaction force at location 1 on the flexible model during the 0˚ wind angle test with 30% throttle. The resonant response of the system at the first natural frequency is quite notable by the illustrated peak at nb/U=1.098. Setting the wind speed (U) equal to 19.9 m/s and panel length of 2.13m, the excitation frequency was calculated by:

$$n = 1.098 * \frac{19.2}{2.13} = 10\ Hz \tag{4}$$

This value is very close to the module's fundamental natural frequency of 10.5 Hz which was established by the hammer tests. Figure 4-19 compares the force power spectra between the flexible model and the rigid model at 0˚ wind direction and at 30% fan throttle. The peak on the flexible model graph indicates the resonance on the reaction force coefficient spectra which is the result of response amplification at the frequencies around the fundamental natural frequency of the structure. Except for the illustrated peak at the first natural frequency there is not any significantly effective variation between the two spectra.

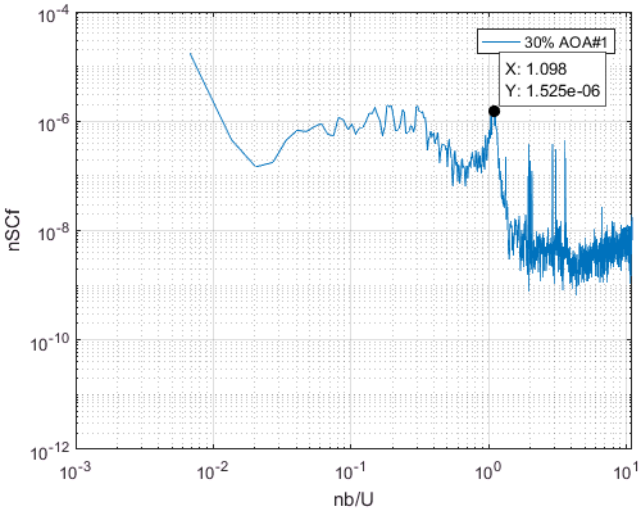

Figure 4-18. Force spectrum of the flexible model for 30% fan throttle at 0° angle of attack (AOA)

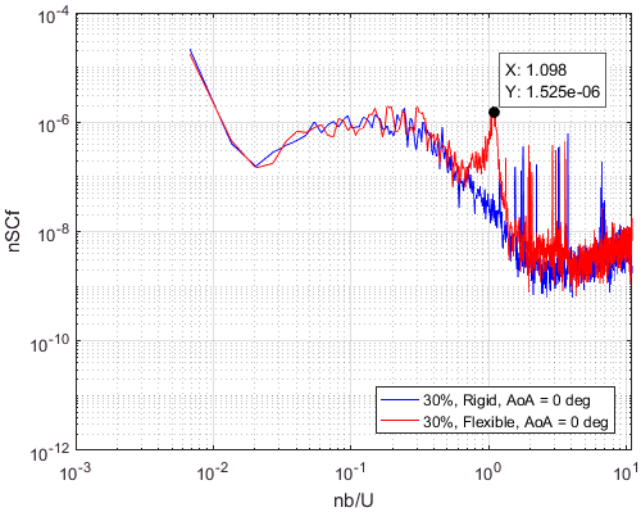

Figure 4-19. Comparison of force spectra of flexible and rigid models at 0° angle of attack (AOA)

Figure 4-20 shows the spectra of force coefficients calculated and averaged on all three PV panels based on the flexible model (red), load-cells on full-scale rigid model (blue), and pressure taps on full-scale rigid model (green). As can be observed from this figure, for the reduced frequency (nb/U) values greater than 0.3 the load cell spectra (both

flexible and rigid models) dramatically decrease while this is not the case for the spectrum resulted from the pressure taps data. The reduced spectral density values resulted from the load cells (blue and red curves in Figure 4-20) in comparison to the spectral values calculated based on the pressure taps (green curve in Figure 4-20) implies the lower dynamic reaction forces compared to the applied wind-induced loads. This phenomenon can be resulted either from the intrinsic damping and stiffness of the support structure which is composed of the racking system, timber truss and the building frame or the local damping caused by installation defects of one of the load cells. These findings called for a more thorough analysis of the obtained results using individual load cells as will be discussed in the following paragraphs.

Seo et al. (41) presented some equivalent viscous damping ratios in wooden frame buildings. According to this study, the damping ratios varied from 13% to 27%. Considering such a high percentage of damping, the observed dramatic decrease of spectral density may be partially justified. Figure 4-21 displays the spectra of all eight load cells at 0° wind direction at 30% fan throttle. For all the load cell curves, the same pattern of decreased spectral density at nb/U greater than 0.3 can be observed. This observation does not indicate any defective connection in any of the load cells to the roof trusses. Stiffness of the racking system is another parameter that can participate on this phenomenon.

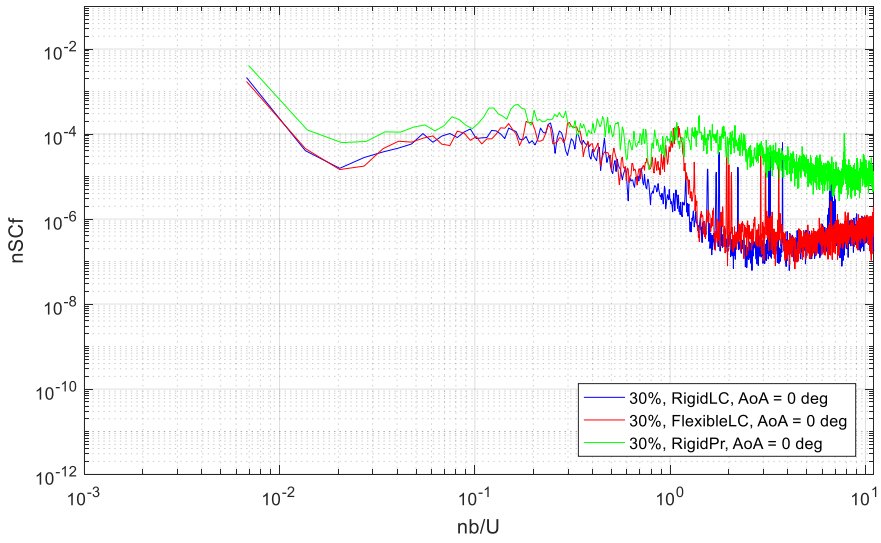

Figure 4-20. Comparison of spectra for the full-scale models based on the data from load cells and pressure taps

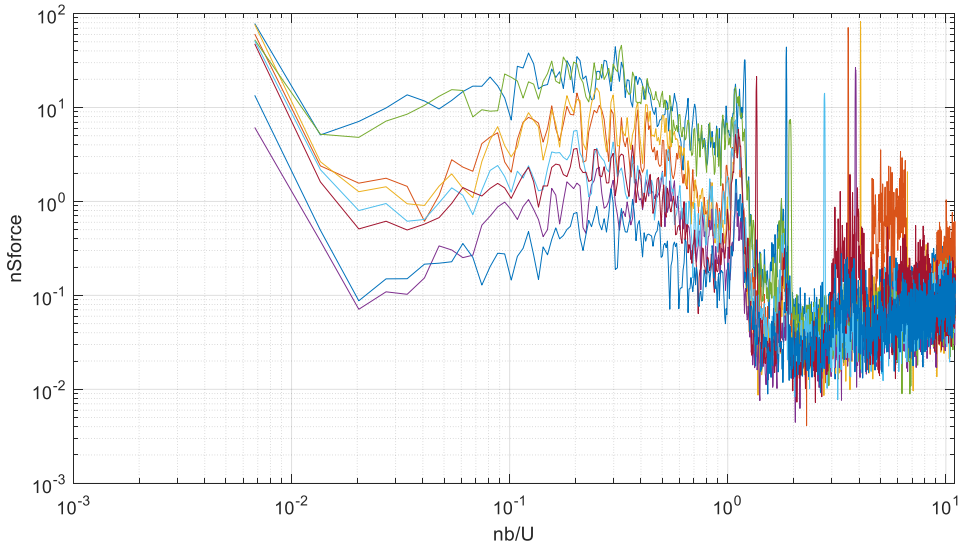

Figure 4-21. Spectra of all eight load cells at 0° wind direction at 30% fan throttle

4.5.3. Dynamic Amplification

In this section, the implementation of the dynamic amplification is explored by investigating the use of the Mechanical Admittance Function (MAF). The MAF is used to

estimate the amplification of the flexible model response, compared to that of the equivalent rigid model (load cell data), at its fundamental natural frequency and is defined as:

$$|H(n)|^2 = \frac{1}{[1-(n/n_1)^2]^2 - 4\eta^2(n/n_1)^2} \quad (5)$$

where n is the desired frequency, n_1 is the natural frequency of the system (10.5 Hz) and η is the damping ratio. Figure 4-22 presents the MAF for the first vibration mode of the PV system. The rigid model spectrum (see Figure 4-23) is generated by multiplying the original spectrum to the square of Mechanical Admittance Function:

$$S_{Cf(B+R)} = |H(n)|^2 . S_{Cf(B)} \quad (6)$$

where $S_{Cf(B+R)}$ is the modified spectrum, and $S_{Cf(B)}$ is the rigid model spectrum. The modified rigid model spectrum compares well to the flexible model which confirms the validity of using the MAF to account for the dynamic amplification.

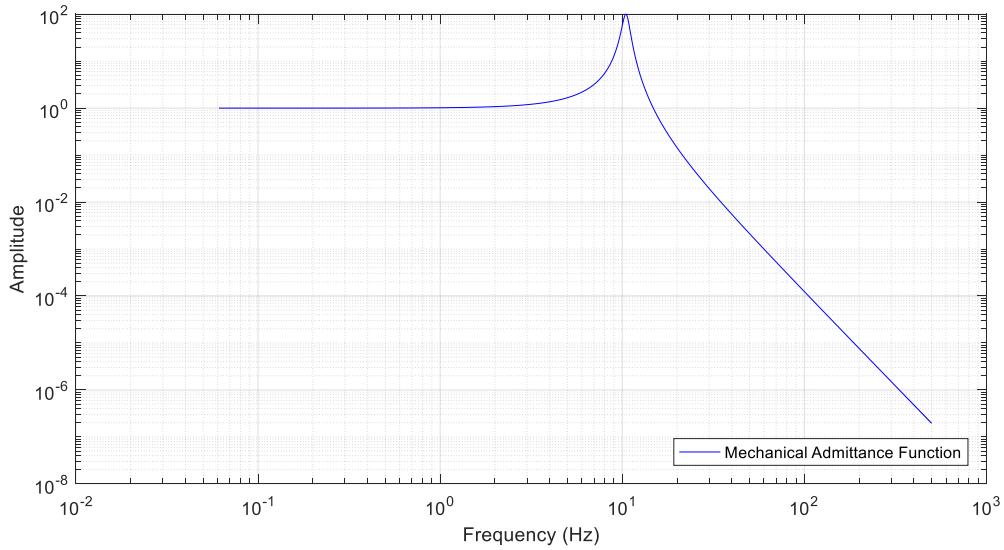

Figure 4-22. Mechanical Admittance Function for the first vibration mode of PV system

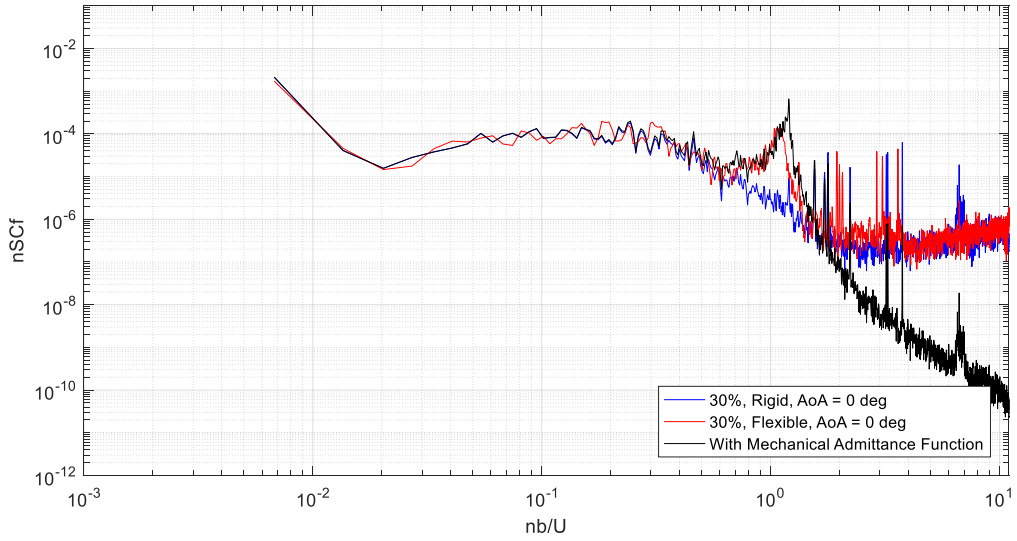

Figure 4-23. The modified rigid model spectrum by incorporating the Mechanical Admittance Function

To estimate the maximum and minimum force coefficient from the modified spectrum the following equations can be used:

$$\widehat{C_f} = \overline{C_f} + \sqrt{g^2{}_B.B + g^2{}_R.R} \quad (7)$$

$$g_R = \sqrt{2\ln(n_1 T)} + \frac{0.577}{\sqrt{2\ln(n_1 T)}} \quad (8)$$

$$g_R = \sqrt{2\ln(10.5 * 3600)} + \frac{0.577}{\sqrt{2\ln(10.5 * 3600)}} = 4.64 \quad (9)$$

In the above equation, the g_B is assumed equal to 3.4, using the suggested value in ASCE 7-16 (2). Based on the spectra of the flexible and rigid models the background and resonant components are calculated for four representative wind directions (see

Table 4-1).

The mean, maximum and minimum force coefficients are presented in Table 4-2, Table 4-3 and Table 4-4 respectively. The dynamic amplification factor is applied to the rigid model force coefficients calculated based on the load-cell data. The implementation of the MAF resulted in mixed findings. Although it improved the agreement in certain wind directions, it also resulted in higher discrepancies for several cases.

However, in general, the presented peak force coefficient values (both from flexible, and rigid amplified results) are relatively in a very low range. These low values are resulted from area averaging over the surface of three panels and as a result the dynamic amplification effect seems to be faded.

Table 4-1. Background and resonant components of force coefficient spectra

Wind Direction (deg)	B ($\times 10^{-5}$)	R ($\times 10^{-5}$)	$\sqrt{g^2{}_B.B + g^2{}_R.R}$
0	6.16	2.7	0.036
45	47	5.9	0.082
90	60.9	13.4	0.100
135	51.9	1.4	0.079

Table 4-2. $C_{f,mean}$ for total area (i.e. 3 PV panels on the single racking system)

Wind Direction	Flexible 1:1	Rigid 1:1
	Load Cells	Load Cells
0	0.051	0.074
45	0.060	0.065
90	0.078	0.053
135	0.083	0.093

Table 4-3. $C_{f,max}$ for total area (i.e. 3 PV panels on the single racking system)

Wind Direction	Flexible 1:1	Rigid 1:1	
	Load Cells	Load Cells	
		No H(f)	H(f)
0	0.145	0.146	0.182
45	0.159	0.177	0.259
90	0.207	0.188	0.288
135	0.210	0.223	0.302

Table 4-4. $C_{f,min}$ for total area (i.e. 3 PV panels on the single racking system)

Wind Direction	Flexible 1:1	Rigid 1:1	
	Load Cells	Load Cells	
		No H(f)	H(f)
0	-0.040	-0.001	-0.037
45	-0.032	-0.053	-0.135
90	-0.080	-0.100	-0.200
135	-0.050	-0.070	-0.149

4.6. Comparison to ASCE 7-16

The results from the current study are compared to the recently published ASCE 7-16 Standard (2). It should be noted that ASCE 7-16 design values for PV arrays were predominantly based on studies of larger installations on flat roof commercial buildings whereas the focus of this study was on low-rise residential buildings.

The following equations were used based on sections 26.10.2 and 29.4.4 of the code:

$$q_h = 0.613 K_z K_{zt} K_d K_e V^2 \quad (10)$$

$$p = q_h (GC_p) \gamma_E \gamma_a \quad (11)$$

where q_h velocity pressure for all surfaces evaluated at mean roof height, h, (GC_p) is external pressure coefficient, γ_E is array edge factor, and γ_a is solar panel pressure equalization factor. The velocity pressure estimation and the corresponding results for a single PV panel and a 3 PV panel array are presented in Table 4-5 and

Table 4-6.

Table 4-5. Estimation of velocity pressure

Directionality Factor, K_d	0.85
Exposure Coefficient, K_z	0.85
Ground Elevation Factor, K_e	1.0
Topographic Factor, K_{zt}	1.0
Basic Wind Speed, V (m/s)	40
Velocity Pressure, q_z (N/m2)	708

Table 4-6. Design wind pressure

Case/Parameters	One panel	Three panels
Area (m2)	1.9	5.8
Array Edge Factor, γ_E	1.0	1.0
Solar Panel Pressure Equalization Factor, γ_a	0.6	0.5
External Pressure Coefficient, (GCp)	-2.0	-0.8
Design Wind Pressure, P (N/m2)	840	280

In the current study, the critical (i.e. regardless of wind direction) minimum force coefficient on the flexible model for the three-panel array is -0.2, which is lower than the

proposed value (-0.8) by ASCE 7-16. When the pressure tap results are considered (PTS method on the full-scale rigid model), the values are ± 0.4 which are closer to the ASCE 7-16. Finally, the large-scale model is providing values even closer which are ± 0.6 approximately.

4.7. Summary and Conclusions

Past studies (34–36) indicated that wind-induced vibration might become a concern in the structural design of PV system. Therefore, a detailed experimental study was carried out to evaluate the wind-induced response of photovoltaic (PV) panel arrays mounted on top of low-rise residential buildings. The focus of the study was on the dynamic response of the PV panel array and vibration issues that are induced even at lower wind speeds. Three models were tested at the Wall of Wind Experimental Facility at FIU, including a full-scale real PV panel array (i.e. flexible model), a full-scale rigid panel array (i.e. wood model) and a large scale rigid panel array (i.e. plexiglass model). In summary, the main achievements of this study are as follows:

- The mean force coefficient results obtained from the flexible model tests appear to be independent of the wind speed. The peak force coefficient values show some discrepancies for specific wind directions.
- In general, no significant differences were found between the mean and minimum force coefficient values obtained from the flexible versus the rigid model tests. However, the maximum force coefficient values were higher for rigid model compared to the flexible model for most wind directions.

- When the force coefficient values are calculated using the pressure tap data the results indicate a good match between the large-scale and full-scale mean values. The peak force coefficient values show significant discrepancies which are though reduced when the partial turbulence simulation is used.
- The resonant response of the PV array at the first natural frequency (approx. 10 Hz) is very close to the module's fundamental natural frequency of 10.5 Hz which was established by the hammer tests.
- The implementation of the MAF resulted in mixed findings. Although it improved the agreement in certain wind directions, it also resulted in higher discrepancies for several cases.
- The findings compare well with the current wind standard recommendations. The best agreement is established when the force coefficient values are estimated using the pressure data.

Overall, this study is expected to provide valuable information for the enhancement of wind design guidelines for residential scale PV panel arrays. The majority of the current building codes and wind standards that include design guidelines for PV systems are based predominantly on tests that considered scaled models of large commercial PV array systems on flat industrial size buildings. These configurations are significantly different than a typical low-rise building therefore the current study is expected to add knowledge and assist in the development of more accurate design recommendation for residential scale PV installations. Recent growth of residential roof-mounted solar panels, demands for development of safe and efficient design tools for rooftop solar arrays. Furthermore, the

findings related to the wind-induced vibration on the PV panels provide important insight on the dynamic response of the system. This type of information would not be possible to be extracted from small-scale rigid model tests and such knowledge will further improve our understanding of the wind-induced performance of solar arrays and assist in the development of more comprehensive building code guidelines.

4.8. References

1. South Miami set to become first city in Florida to mandate solar panels on new homes [Internet]. The Real Deal Miami. 2017 [cited 2017 Aug 28]. Available from: https://therealdeal.com/miami/2017/07/13/south-miami-becomes-first-city-in-florida-to-mandate-solar-panels-on-new-homes/

2. ASCE 7-16. Minimum Design Loads and Associated Criteria for Buildings and Other Structures [Internet]. Reston, Virginia: American Society of Civil Engineers; 2016. Available from: https://doi.org/10.1061/9780784414248

3. ASCE 7-10. Minimum Design Loads for Buildings and Other Structures [Internet]. Reston, Virginia: American Society of Civil Engineers; 2010. Available from: https://doi.org/10.1061/9780784412916

4. ASCE 7-05. Minimum Design Loads for Buildings and Other Structures [Internet]. Reston, Virginia: American Society of Civil Engineers; 2005. Available from: https://doi.org/10.1061/9780784408094

5. Aly AM, Bitsuamlak G. Aerodynamics of ground-mounted solar panels: Test model scale effects. Journal of Wind Engineering and Industrial Aerodynamics. 2013 Dec 1;123:250–60.

6. Jubayer CM, Hangan H. A numerical approach to the investigation of wind loading on an array of ground mounted solar photovoltaic (PV) panels. Journal of Wind Engineering and Industrial Aerodynamics. 2016 Jun 1;153:60–70.

7. Abiola-Ogedengbe A, Hangan H, Siddiqui K. Experimental investigation of wind effects on a standalone photovoltaic (PV) module. Renewable Energy. 2015 Jun 1;78:657–65.

8. Warsido WP, Bitsuamlak GT, Barata J, Gan Chowdhury A. Influence of spacing parameters on the wind loading of solar array. Journal of Fluids and Structures. 2014 Jul 1;48:295–315.

9. Stathopoulos T, Zisis I, Xypnitou E. Local and overall wind pressure and force coefficients for solar panels. Journal of Wind Engineering and Industrial Aerodynamics. 2014 Feb 1;125:195–206.

10. Jubayer CM, Hangan H. Numerical simulation of wind effects on a stand-alone ground mounted photovoltaic (PV) system. Journal of Wind Engineering and Industrial Aerodynamics. 2014 Nov 1;134:56–64.

11. Aly AM. On the evaluation of wind loads on solar panels: The scale issue. Solar Energy. 2016 Oct 1;135:423–34.

12. Kopp GA, Surry D, Chen K. Wind loads on a solar array. Wind and Structures. 2002;5(5):393–406.

13. Suresh Kumar K. Pressure equalization of rainscreen walls: a critical review. Building and Environment. 2000 Feb 1;35(2):161–79.

14. Choi ECC, Wang Z. Study on pressure-equalization of curtain wall systems. Journal of Wind Engineering and Industrial Aerodynamics. 1998 Mar 4;73(3):251–66.

15. Bienkiewicz Bogusz, Endo Munehito. Wind Considerations for Loose-Laid and Photovoltaic Roofing Systems. Structures Congress 2009 [Internet]. [cited 2017 Aug 17]; Available from: http://ascelibrary.org/doi/abs/10.1061/41031%28341%29282

16. Oh JH, Kopp GA. Modelling of spatially and temporally-varying cavity pressures in air-permeable, double-layer roof systems. Building and Environment. 2014 Dec 1;82:135–50.

17. Zisis Ioannis, Raji Farzaneh, Candelario Jose D. Large-Scale Wind Tunnel Tests of Canopies Attached to Low-Rise Buildings. Journal of Architectural Engineering. 2017 Mar 1;23(1):B4016005.

18. Naeiji A, Raji F, Zisis I. Wind loads on residential scale rooftop photovoltaic panels. Journal of Wind Engineering and Industrial Aerodynamics. 2017 Sep 1;168:228–46.

19. Oh JH, Kopp GA. An experimental study of pressure distributions within an air-permeable, double-layer roof system in regions of separated flow. Journal of Wind Engineering and Industrial Aerodynamics. 2015 Mar 1;138:1–12.

20. Asghari Mooneghi M, Irwin P, Gan Chowdhury A. Large-scale testing on wind uplift of roof pavers. Journal of Wind Engineering and Industrial Aerodynamics. 2014 May 1;128:22–36.

21. Kopp GA, Farquhar S, Morrison MJ. Aerodynamic mechanisms for wind loads on tilted, roof-mounted, solar arrays. Journal of Wind Engineering and Industrial Aerodynamics. 2012 Dec 1;111:40–52.

22. Banks D. The role of corner vortices in dictating peak wind loads on tilted flat solar panels mounted on large, flat roofs. Journal of Wind Engineering and Industrial Aerodynamics. 2013 Dec 1;123:192–201.

23. Pratt RN, Kopp GA. Velocity measurements around low-profile, tilted, solar arrays mounted on large flat-roofs, for wall normal wind directions. Journal of Wind Engineering and Industrial Aerodynamics. 2013 Dec 1;123:226–38.

24. Cao J, Yoshida A, Saha PK, Tamura Y. Wind loading characteristics of solar arrays mounted on flat roofs. Journal of Wind Engineering and Industrial Aerodynamics. 2013 Dec 1;123:214–25.

25. Browne MTL, Gibbons MPM, Gamble S, Galsworthy J. Wind loading on tilted roof-top solar arrays: The parapet effect. Journal of Wind Engineering and Industrial Aerodynamics. 2013 Dec 1;123:202–13.

26. Kopp Gregory A. Wind Loads on Low-Profile, Tilted, Solar Arrays Placed on Large, Flat, Low-Rise Building Roofs. Journal of Structural Engineering. 2014 Feb 1;140(2):04013057.

27. Wood GS, Denoon RO, Kwok KCS. Wind loads on industrial solar panel arrays and supporting roof structure. Wind and Structures. 2001;4(6):481–94.

28. Stenabaugh SE, Iida Y, Kopp GA, Karava P. Wind loads on photovoltaic arrays mounted parallel to sloped roofs on low-rise buildings. Journal of Wind Engineering and Industrial Aerodynamics. 2015 Apr 1;139:16–26.

29. Aly Aly Mousaad, Bitsuamlak Girma. Wind-Induced Pressures on Solar Panels Mounted on Residential Homes. Journal of Architectural Engineering. 2014 Mar 1;20(1):04013003.

30. Naeiji A., Raji F., Zisis I. Large-Scale Wind Testing of Photovoltaic Panels Mounted on Residential Roofs. Structures Congress 2015 [Internet]. [cited 2017 Aug 15]; Available from: http://ascelibrary.org/doi/abs/10.1061/9780784479117.161

31. Geurts C, Blackmore P. Wind loads on stand-off photovoltaic systems on pitched roofs. Journal of Wind Engineering and Industrial Aerodynamics. 2013 Dec 1;123:239–49.

32. Leitch CJ, Ginger JD, Holmes JD. Wind loads on solar panels mounted parallel to pitched roofs, and acting on the underlying roof. Wind and Structures. 2016;22(3):307–28.

33. Erwin James, Bitsuamlak Girma, Chowdhury Arindam Gan, Barkaszi Stephen, Gamble Scott. Full Scale and Wind Tunnel Testing of a Photovoltaic Panel Mounted on Residential Roofs. Advances in Hurricane Engineering [Internet]. [cited 2017 Aug 16]; Available from: http://ascelibrary.org/doi/abs/10.1061/9780784412626.041

34. Strobel K, Banks D. Effects of vortex shedding in arrays of long inclined flat plates and ramifications for ground-mounted photovoltaic arrays. Journal of Wind Engineering and Industrial Aerodynamics. 2014 Oct 1;133:146–9.

35. Moravej M, Chowdhury A, Irwin P, Zisis I, Bitsuamlak G. Dynamic effects of wind loading on photovoltaic systems. In: 14th International Conference in Wind Engineering, At Porto Alegre, Brazil [Internet]. 2015 [cited 2017 Aug 18]. Available from: https://www.researchgate.net/profile/Mohammadtaghi_Moravej/publication/279770545_Dynamic_effects_of_wind_loading_on_photovoltaic_systems/links/56d770ae08aee1aa5f75cbc1.pdf

36. Cain J, Banks D. Wind Loads on Utility Scale Solar PV Power Plants. In: SEAOC CONVENTION PROCEEDINGS. Seattle, WA; 2015.

37. Miles JW. On Structural Fatigue Under Random Loading. Journal of the Aeronautical Sciences. 1954;21(11):753–62.

38. Davenport AG. Note on the distribution of the largest value of a random function with application to gust loading. Proceedings of the Institution of Civil Engineers. 1964;28(2):187–196.

39. Aly AM, Chowdhury AG, Bitsuamlak G. Wind profile management and blockage assessment for a new 12-fan Wall of Wind facility at FIU. Wind & Structures. 2011;14(4):285–300.

40. Asghari Mooneghi M, Irwin P, Gan Chowdhury A. Partial turbulence simulation method for predicting peak wind loads on small structures and building appurtenances. Journal of Wind Engineering and Industrial Aerodynamics. 2016 Oct;157:47–62.

41. Seo J-M, Choi I-K, Lee J-R. Static and Cyclic Behavior of Wooden Frames with Tenon Joints under Lateral Load. Journal of Structural Engineering. 1999 Mar;125(3):344–9.

CHAPTER 5

ANALYTICAL EVALUATION OF WIND-INDUCED VIBRATION ON ROOF-MOUNTED SOLAR PANELS

(A paper to be submitted to ASCE Journal of Structural Engineering*)*

CHAPTER 5. ANALYTICAL EVALUATION OF WIND-INDUCED VIBRATION ON ROOF-MOUNTED SOLAR PANELS

Amir Naeiji[8], Farzaneh Raji[9], Ioannis Zisis[10]

5.1. Abstract

Considering the growing application of the PV systems in the recent decade the resilience design of these systems has necessitated the accurate estimation of their response to wind loads. Although several previous wind tunnel studies have shed light on the wind load acting on PV system, very little attention has been dedicated to the dynamic behavior of these systems under wind loading.

In this study, it was tried to develop an analytical model to numerically simulate the dynamic behavior of PV system under wind loads. The results of the analytical model were compared to the experimental results and it was shown that the dynamic deflection of the supporting structure can attenuate the acceleration response and reaction forces of the PV system.

5.2. Introduction

In recent years, several experimental (1–14) and computational (15–17) studies have been accomplished to elucidate the effect of wind load on solar Photovoltaic (PV)

[8] [Corresponding author] Department of Civil and Environmental Engineering, Florida International University, Miami, FL, USA. E-mail: anaeiji@fiu.edu

[9] Department of Civil and Environmental Engineering, Florida International University, Miami, FL, USA. E-mail: fraji@fiu.edu

[10] Department of Civil and Environmental Engineering, Florida International University, Miami, FL, USA. E-mail: izisis@fiu.edu

systems. Almost all of these experimental studies have used rigid models to measure the wind pressures applied to the panel surface during wind tunnel tests. In these type of experimental simulations, the dynamic behavior of the system is not a concern and the rigid models cannot in capture the vibration effects. However, in the case of the solar panels, since they are lightweight and flexible structures, the wind-induced vibrations may play a role in the overall behavior of the system. So, there is a need to further investigate PV system vibration not only in extreme wind events but also during operational wind conditions.

Strobel and Banks (18) and Moravej et al. (19) investigated the wind-induced vibration effects on solar panels. They concluded the solar panels are dynamically sensitive structures affected by wind-induced turbulence.

The study by Kilikevičius et al. (20) is amongst the very few studies performed on dynamic characteristics of PV modules. The study included analytical and experimental evaluation of the PV system reaction to different dynamic loads. The authors concluded that the static analysis of the PV modules is not sufficient for fulfilling the safety and stability of the system and further attention should be dedicated to the dynamic effects. This study did not account for the effect of PV racking system and boundary layer wind effects.

In the current study, it was tried to develop an experimentally verified analytical model to investigate the dynamic response of solar panels and their mounting system to boundary layer wind effects.

5.3. Methodology

The objective of this paper is developing an analytical model of a PV system in order to investigate the structural response of the system to wind loadings. The analytical model was validated by the experimental tests performed at 12-fan Wall of Wind Experimental Facility. Two different experimental models were tested one with pressure taps to obtain the actual wind loads affecting the structure and another one equipped with accelerometers and load cells to in capture the response of the system. The results of the experimental tests were used to validate the analytical model. Once the analytical model was calibrated it was used to further understand the response of the PV system.

5.4. Experimental Test Setup

5.4.1. Testing Facility

The experimental tests were performed at the 12-fan Wall of Wind Experimental Facility at Florida International University (FIU) (Figure 5-1) at 30% fan throttle resulting in 42 mph wind speed at mean roof height). For further information about the specification of the Wall of Wind Experimental Facility and the wind flow characteristics please refer to (21). Figure 5-2 shows the mean wind speed and turbulence intensity profiles at different heights.

Figure 5-1. Wall of Wind facility

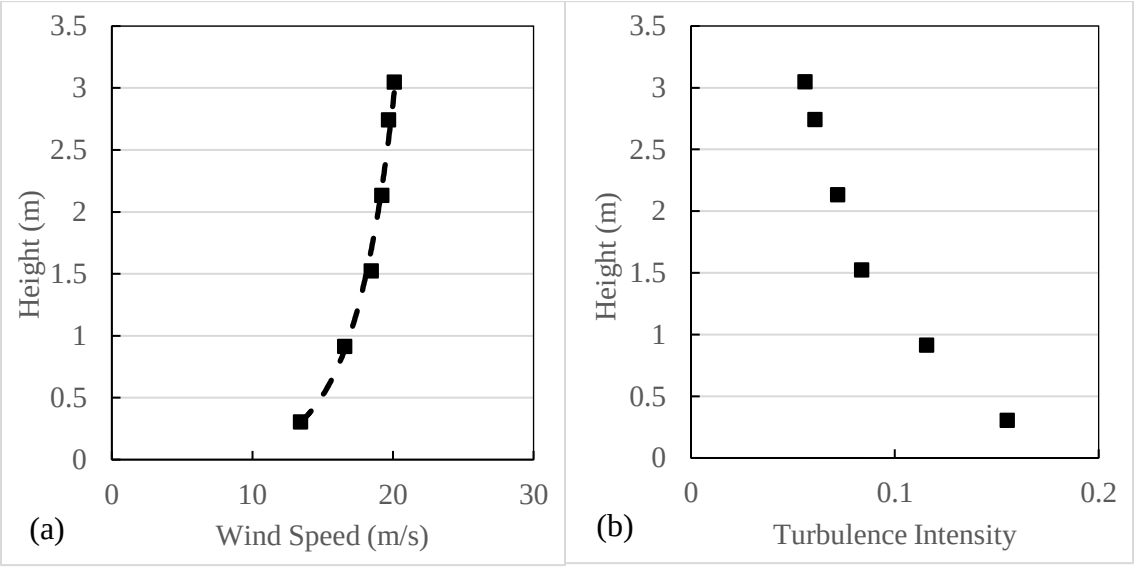

Figure 5-2. (a) Mean wind speed and (b) turbulence intensity profiles

5.4.2. Building model

The investigated PV system was mounted on a full-scale wood frame building model. The building model had a mono-slope roof with a pitch angle of 10˚ and 0.3 m overhangs. Figure 5-3 displays the dimensions of the building model.

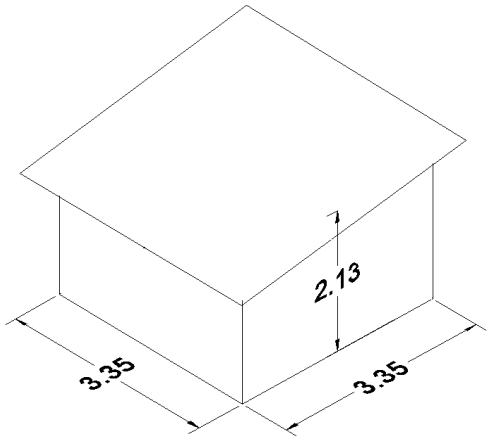

Figure 5-3. Dimensions of the full-scale building model (dimensions in m)

5.4.3. Pressure taped model

As shown in the PV panels of the pressure tap model was made from wood with the same width and length of the real panels (0.983 m × 1.008 m). However, the thickness of the modeled PVs was not the same as actual modules (0.05 m to allow for pressure tap tubing). This model was supposed not to deform under wind loads and so it is referred to as "Rigid Model" for the rest of this paper.

Figure 5-4. Full-scale rigid model

Figure 5-5 shows the locations of the pressure taps on one PV module. The same pressure tap locations were selected for all three panels. There was a total of 210 taps evenly distributed on the upper and lower surfaces of the three panels.

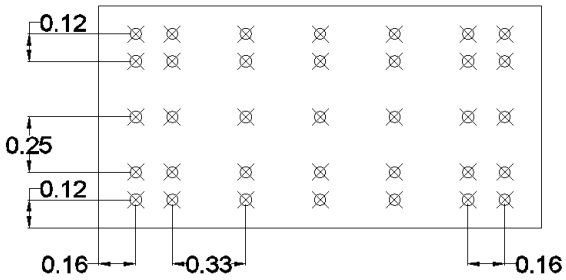

Figure 5-5. Pressure tap locations (dimensions in m)

This model was subjected to 0˚ wind direction (the lower ever of the building windward to the wind flow) and the time history of the obtained pressure data was applied to the analytical model as will be discussed in "Loading" section.

5.4.4. Model with accelerometer and load cells

Three real PV modules were mounted on the same racking system as the rigid model and got equipped with accelerometers and load cells. This model was supposed to deform while dynamically responding to the wind loads and so is referred to as "Flexible Model" for the rest of this paper. Dytran 3263A series accelerometers were used for acceleration measurement. The accelerometers where attached at several locations to the lower surface of the PV modules as displayed in Figure 5-7.

Figure 5-6. Full-scale flexible model

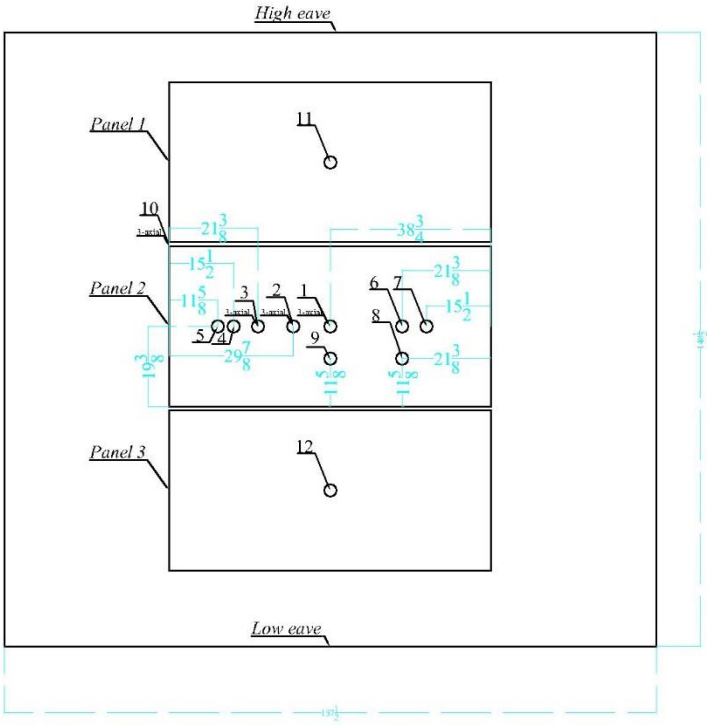

Figure 5-7. Location and numbering of the accelerometers on the PV modules

In order to measure the reaction forces at racking system support eight high accuracy s-beam load cells were installed. Figure 5-8 shows the location of the load cells installed at the racking system supports.

The results of the flexible model to 0˚-degree wind direction was used for verification of the numerical model as will be later discussed.

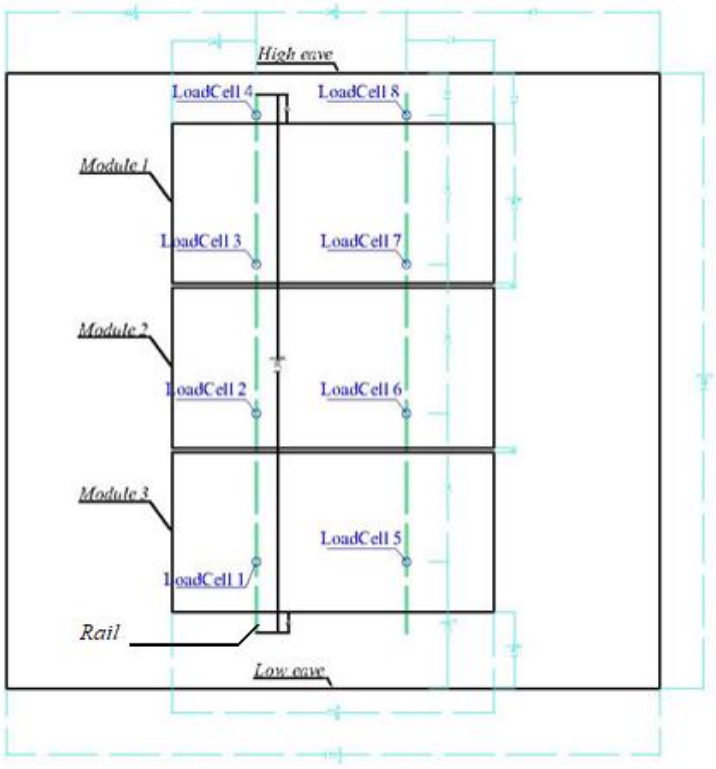

Figure 5-8. PV modules and load cell location and numbering on the roof

5.5. Numerical Simulation

5.5.1. Structural Modeling

To numerically simulate the response of the PV system to wind loading, the structural model of the PV system was created using ANSYS and the time history of the pressures data obtained from the experimental pressure taped model was applied to the model. The analytical model used BEAM188 element for modeling the PV module frame as well as the rail where the three modules where mounted. The PV panel surface was modeled using SHELL281 elements. The PV panel frame was connected to the rail by constraining the translational degrees of freedom at PV frame and the rail at connection points. The connection of the rail to the building roof was modeled by pinned restrained at pedestal locations.

The analytical model was verified by comparing the modal frequencies to the natural frequencies of the experimental model obtained from the hammer tests. The modal frequencies of the numerical model are presented in Table 5-1. Figure shows the mode shapes of the analytical model.

Table 5-1. Modal frequencies obtained from analytical model

Mode No.	Natural Frequencies (Hz)
1	9.0
2	9.0
3	9.0
4	14.5
5	14.5
6	14.5
7	21.2
8	21.7
9	22.1
10	28.0
11	28.9
12	29.5

In order to experimentally obtain the natural frequencies of the model the hammer tests were performed while the accelerometers were mounted at several locations under the surface of the central panel (Figure 5-7). These locations were selected based on the model analysis of the analytical model at nodes where the maximum displacement associated with different mode shapes occurred. PCB Piezotronics model 086C01 impact hammer was used for the hammer tests (Figure 5-9). Different tests were performed with the hammer hitting the different selected locations. This method would allow the hammer tests to in capture the acceleration peaks associated to all the desired modes. Table 5-2 displays the

associate mode to some of the selected locations (refer to for Figure 5-7 for location number).

Figure 5-9. Impulse hammer (PCB model 086C01)

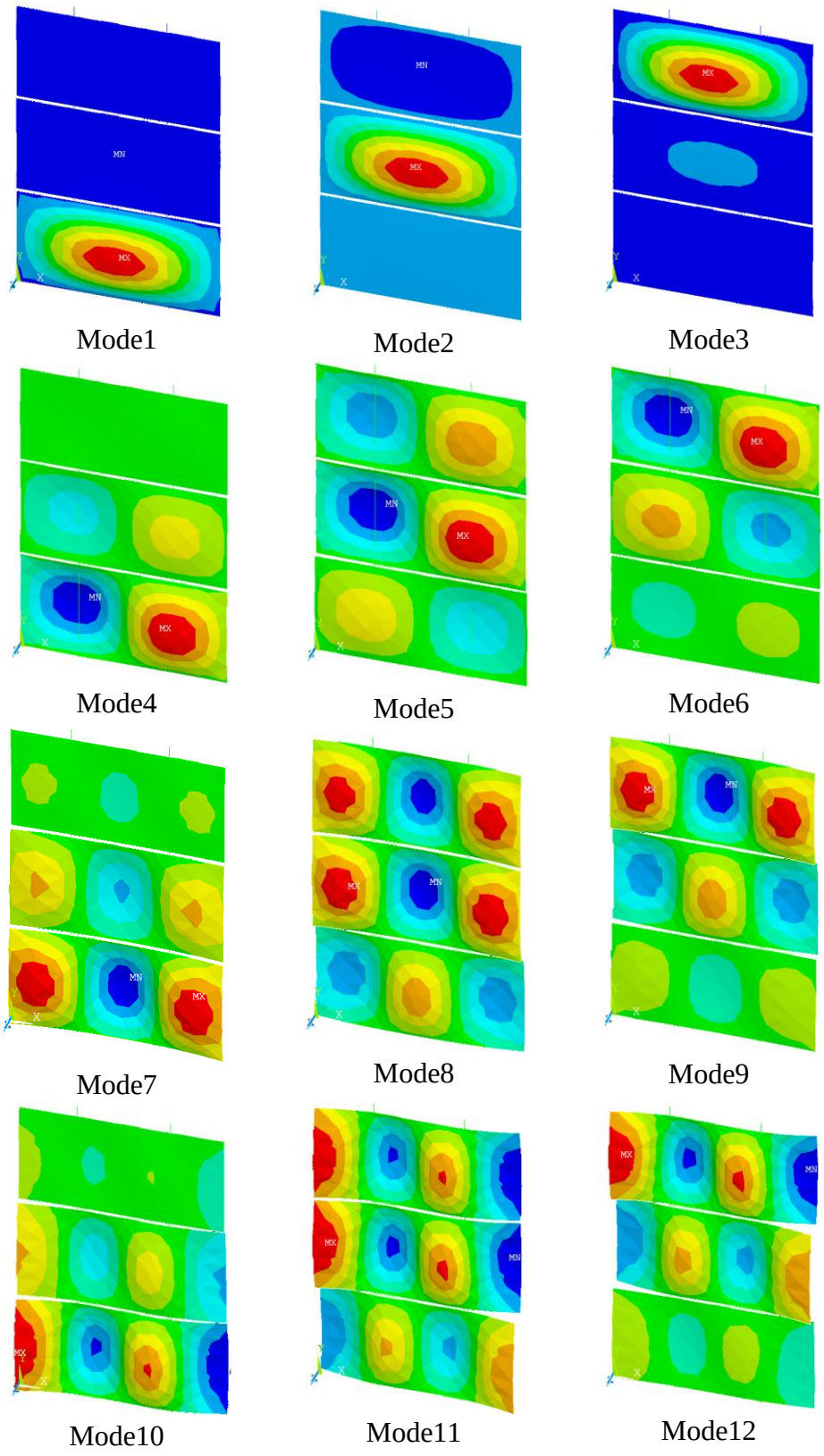

Figure 5-10. Mode shapes

Table 5-2. Associated modes to the selected locations

Location No.	Associated modes
1	1-3
2	10-12
3	4-6
4	7-9
5	10-12
6	2
7	3

Figure 5-1 displays the power spectra of the acceleration response to hammer impact at location 1 (refer to for Figure 5-7 for location number). The observed peaks correspond to the natural frequencies of the excited modes. As was expected from the modal shapes (Figure 5-10) modes 1-3 and 7-9 are the ones that get excited by hitting the center of the panel (location 1) while modes 4-6 and 10-12 are not expected to get excited. So, it is predictable to observe peaks at 9 and 21 Hz frequencies. The expected trend is notable from the figure and it can be inferred that the first peak at 10 Hz is associated to the modes 1-3, while the second peak at 23 Hz is related to modes 7-9.

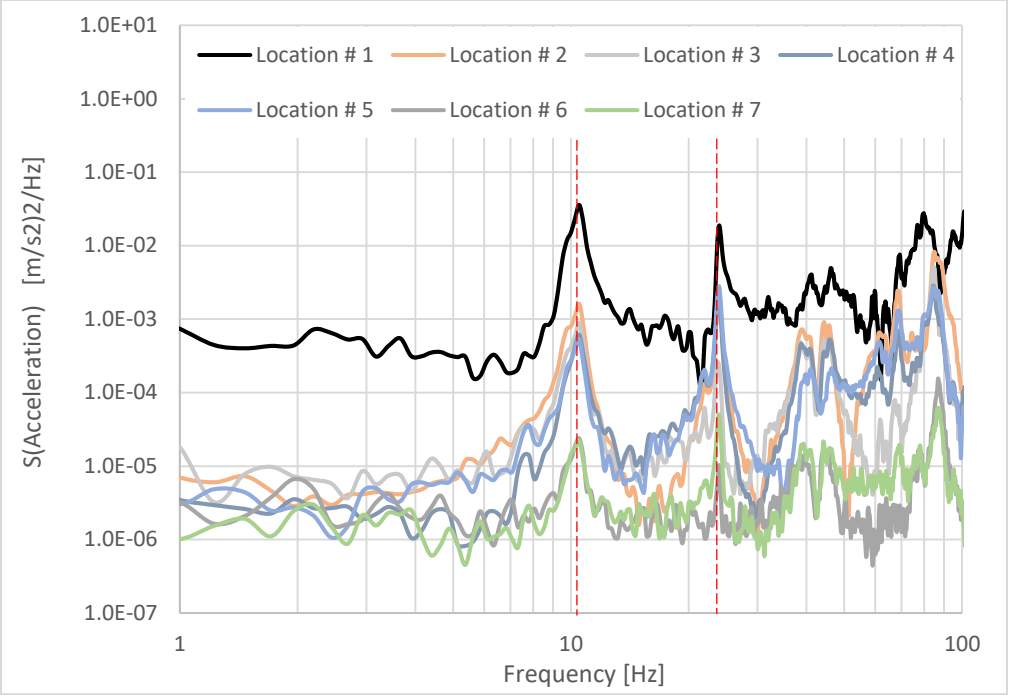

Figure 5-11. Power spectra of the acceleration at different locations on the panel due to hammer impact at location 1

The results of hammer impact at location 3 is presented in figure 3. This is the location where the maximum displacement of modes 4-6 occurs, so based on the modal analysis it is predictable that location two experience high peaks at 14.5 Hz (modal frequency associated to modes 4-6). The experimental results agree with this expectation. On the other hand, since the displacement of location 1 is equal to zero for modes 4-6, it can be expected that this location does not get highly excited at 14.5 Hz frequency by hitting the hammer at location 3. This expectation is also satisfied by the experimental tests.

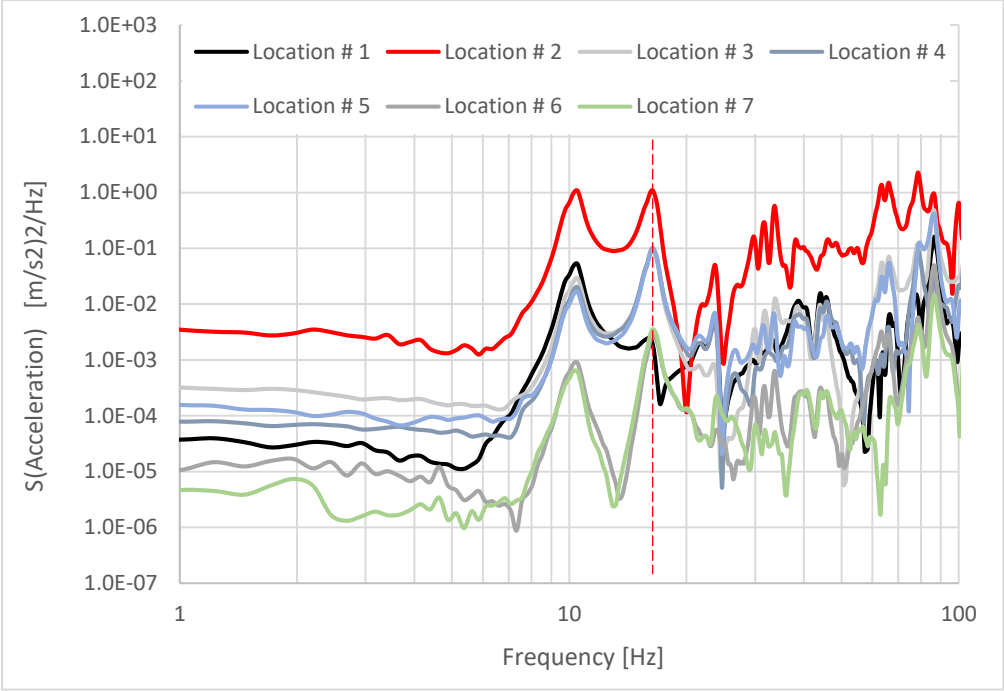

Figure 5-12. Power spectra of the acceleration at different locations on the panel due to hammer impact at location 3 is presented in

5.5.2. Loading

In order to obtain the dynamic response of the structure the time history of the wind pressure was applied to the analytical model. The net pressure results at each tap location was applied to the model as surface pressure acting on the tributary area associated to that tap location. Figure 5-13 displays the tributary area assigned to different tap locations on one panel. The same pattern of tributary area was applied to all three panels of the rigid model.

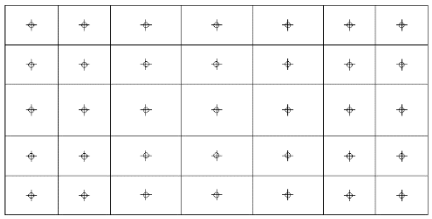

Figure 5-13. Tributary area associated to different tap locations

5.6. Comparison of analytical and experimental results

Figure 5-14 compares the power spectra of the acceleration at location 1 between the experimental and the numerical model. As can be observe the results are in relatively good agreement.

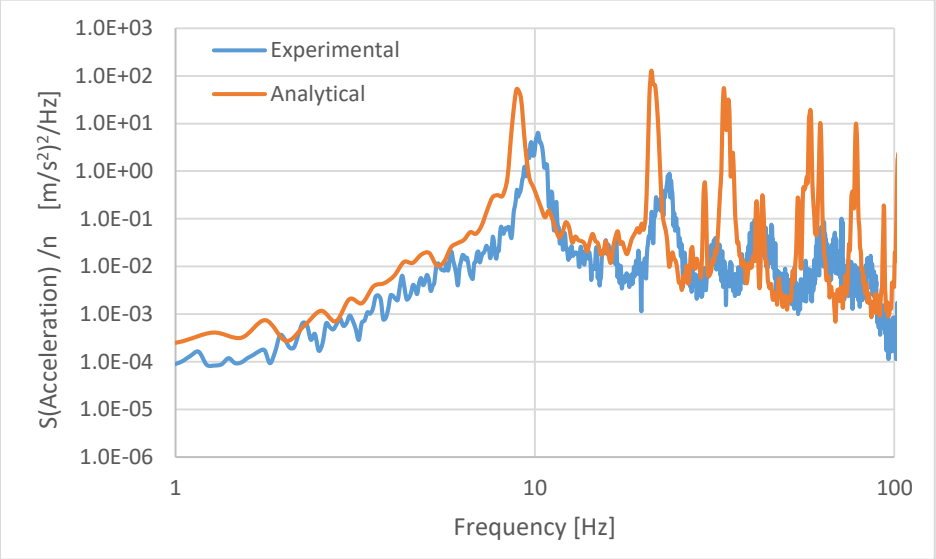

Figure 5-14. Power Spectra of the acceleration response

Figure 5-15 shows the total reaction force at the load cells versus the sum of the reactions at analytical model supports. There is a considerable discrepancy between the experimental and analytical results. Figure 5-16 displays the reaction force at each of the load cells separately. As can be noted from this figure for all the load cells there is a drop of reaction force at around Hz. This similar pattern rejects the assumption of construction defects in some of the load cells connection to the roof.

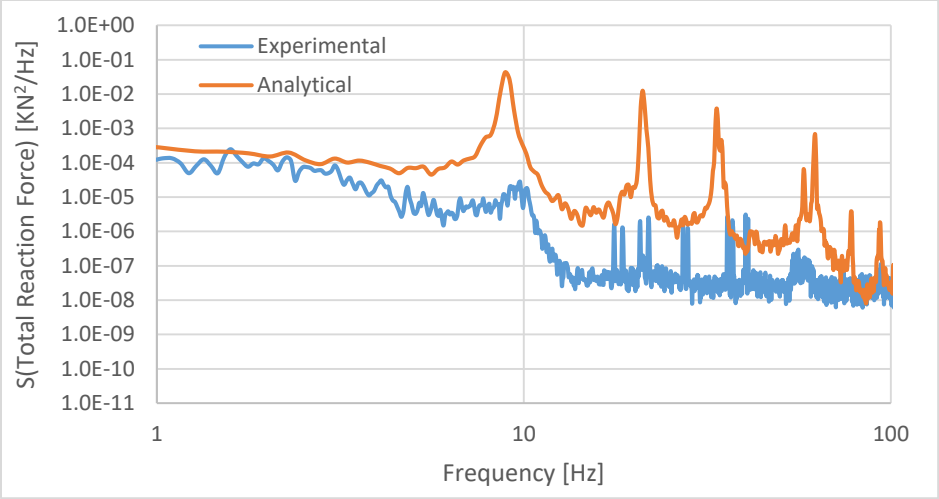

Figure 5-15. Power spectra of the reaction forces

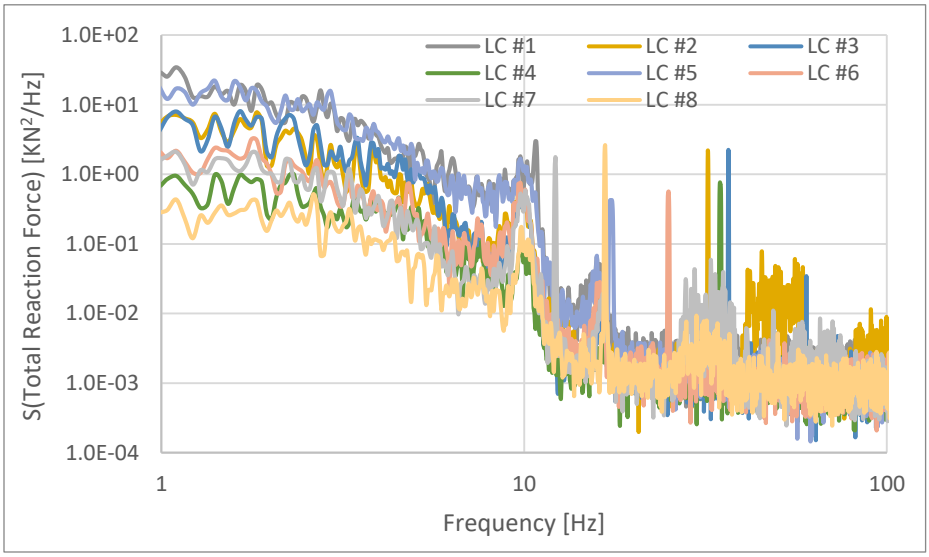

Figure 5-16. Power spectra of each load cell obtained from the experimental tests

In the analytical model, the pinned restrains were assumed at the support nodes, however in reality the system is mounted on the wood frame building that can dynamically deform under the transferred load from the PV system. As a result of support system deformation, the reaction response of the PV system recorded by load cells can differ from the analytical reaction forces. Since the high peaks of the analytical model have attenuated in the real system it can be assumed that the support building is acting like a spring and damper system. With this assumption, linear spring and dampers were added at the support

of the analytical model and the dynamic response of the system was investigated. This analytical model with additional spring at support is name modified analytical model throughout this paper.

Figure 5-17 compares the acceleration response of the modified analytical model and experimental model. As can be observed there is a better agreement between this analytical model and the experimental acceleration results.

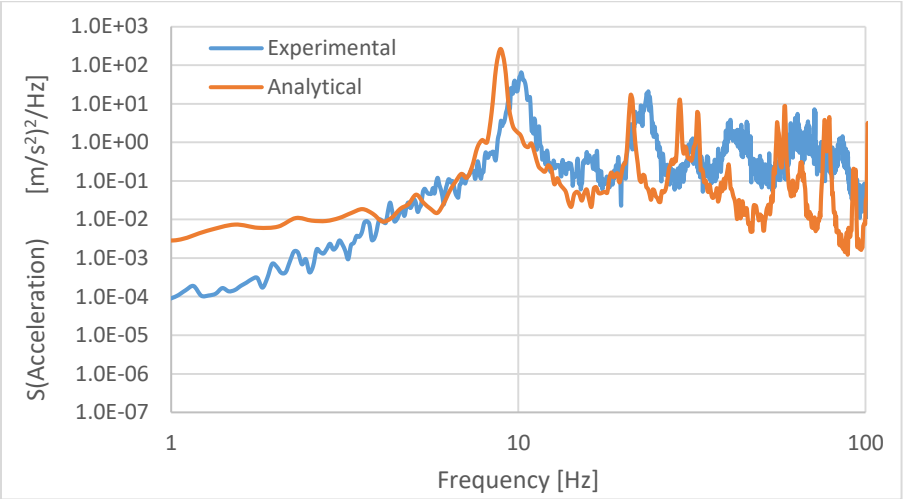

Figure 5-17. Power Spectra of the acceleration response

The comparison of the modified analytical model and experimental total reaction force is presented in Figure 5-18. As can be noted the application of spring and damper sets at the PV system support nodes has significantly improved the results and a much better match to experimental results is achieved by this modification. This observation agrees with the assumption of the building deformation being the source of attenuation in both acceleration and reaction force responses.

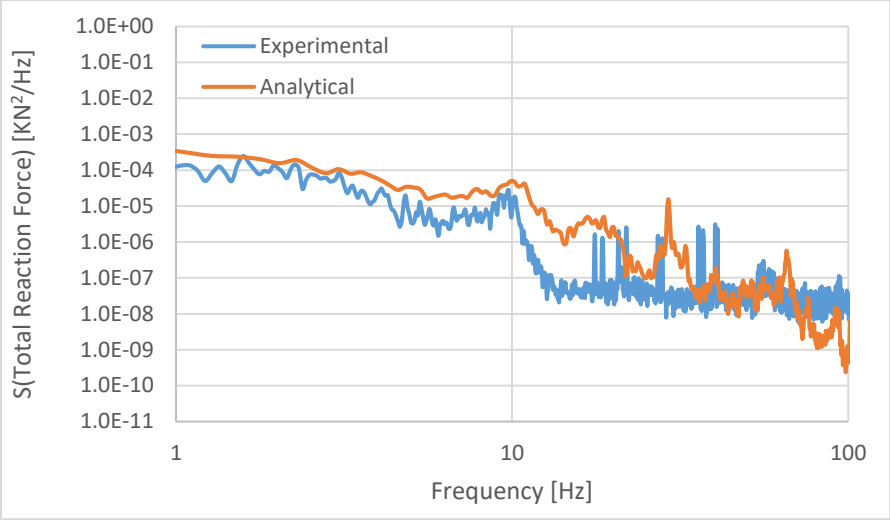

Figure 5-18. Power spectra of the reaction forces

5.7. Conclusions

At the first step of the numerical simulation the analytical model was developed and validated based on the experimental hammer test results. The validated model was then subjected the time history of the wind pressures obtained from the experimental pressure taped model and the acceleration and reaction responses resulted from the numerical dynamic analysis were compared to the experimental responses obtained from the accelerometers and load cells installed on the full-scale model. It was noted that although the analytical model could successfully simulate the modal frequencies of the PV system it could not correctly reproduce the dynamic response of the system once it got subjected to the wind pressures and there was a notable inconsistency between the reaction forces obtained from the numerical and experimental models. It was suggested that in practice the deflection of the supporting building can result in the attenuation of the acceleration and reaction responses of the system.

In the second step, it was tried to in capture the effects of the supporting building by application of spring and damper sets at the supports of the PV racking system. The

modified analytical model was then analyzed and the results showed a much better consistency with the experimental acceleration and reaction responses. The improvement of the results can confirm the effects of the supporting building on the dynamic response of the PV system.

5.8. References

1. Abiola-Ogedengbe A, Hangan H, Siddiqui K. Experimental investigation of wind effects on a standalone photovoltaic (PV) module. Renewable Energy. 2015 Jun 1;78:657–65.

2. Stathopoulos T, Zisis I, Xypnitou E. Local and overall wind pressure and force coefficients for solar panels. Journal of Wind Engineering and Industrial Aerodynamics. 2014 Feb 1;125:195–206.

3. Kopp GA, Farquhar S, Morrison MJ. Aerodynamic mechanisms for wind loads on tilted, roof-mounted, solar arrays. Journal of Wind Engineering and Industrial Aerodynamics. 2012 Dec 1;111:40–52.

4. Cao J, Yoshida A, Saha PK, Tamura Y. Wind loading characteristics of solar arrays mounted on flat roofs. Journal of Wind Engineering and Industrial Aerodynamics. 2013 Dec 1;123:214–25.

5. Browne MTL, Gibbons MPM, Gamble S, Galsworthy J. Wind loading on tilted roof-top solar arrays: The parapet effect. Journal of Wind Engineering and Industrial Aerodynamics. 2013 Dec 1;123:202–13.

6. Wood GS, Denoon RO, Kwok KCS. Wind loads on industrial solar panel arrays and supporting roof structure. Wind and Structures. 2001;4(6):481–94.

7. Kopp Gregory A. Wind Loads on Low-Profile, Tilted, Solar Arrays Placed on Large, Flat, Low-Rise Building Roofs. Journal of Structural Engineering. 2014 Feb 1;140(2):04013057.

8. Erwin James, Bitsuamlak Girma, Chowdhury Arindam Gan, Barkaszi Stephen, Gamble Scott. Full Scale and Wind Tunnel Testing of a Photovoltaic Panel Mounted on Residential Roofs. Advances in Hurricane Engineering [Internet]. [cited 2017 Aug 16]; Available from: http://ascelibrary.org/doi/abs/10.1061/9780784412626.041

9. Naeiji A., Raji F., Zisis I. Large-Scale Wind Testing of Photovoltaic Panels Mounted on Residential Roofs. Structures Congress 2015 [Internet]. [cited 2017

Aug 15]; Available from: http://ascelibrary.org/doi/abs/10.1061/9780784479117.161

10. Stenabaugh SE, Iida Y, Kopp GA, Karava P. Wind loads on photovoltaic arrays mounted parallel to sloped roofs on low-rise buildings. Journal of Wind Engineering and Industrial Aerodynamics. 2015 Apr 1;139:16–26.

11. Naeiji A, Raji F, Zisis I. Wind loads on residential scale rooftop photovoltaic panels. Journal of Wind Engineering and Industrial Aerodynamics. 2017 Sep 1;168:228–46.

12. Leitch CJ, Ginger JD, Holmes JD. Wind loads on solar panels mounted parallel to pitched roofs, and acting on the underlying roof. Wind and Structures. 2016;22(3):307–28.

13. Geurts C, Blackmore P. Wind loads on stand-off photovoltaic systems on pitched roofs. Journal of Wind Engineering and Industrial Aerodynamics. 2013 Dec 1;123:239–49.

14. Aly Aly Mousaad, Bitsuamlak Girma. Wind-Induced Pressures on Solar Panels Mounted on Residential Homes. Journal of Architectural Engineering. 2014 Mar 1;20(1):04013003.

15. Aly AM, Bitsuamlak G. Aerodynamics of ground-mounted solar panels: Test model scale effects. Journal of Wind Engineering and Industrial Aerodynamics. 2013 Dec 1;123:250–60.

16. Jubayer CM, Hangan H. A numerical approach to the investigation of wind loading on an array of ground mounted solar photovoltaic (PV) panels. Journal of Wind Engineering and Industrial Aerodynamics. 2016 Jun 1;153:60–70.

17. Reina GP, De Stefano G. Computational evaluation of wind loads on sun-tracking ground-mounted photovoltaic panel arrays. Journal of Wind Engineering and Industrial Aerodynamics. 2017 Nov 1;170(Supplement C):283–93.

18. Strobel K, Banks D. Effects of vortex shedding in arrays of long inclined flat plates and ramifications for ground-mounted photovoltaic arrays. Journal of Wind Engineering and Industrial Aerodynamics. 2014 Oct 1;133:146–9.

19. Moravej M, Chowdhury A, Irwin P, Zisis I, Bitsuamlak G. Dynamic effects of wind loading on photovoltaic systems. In: 14th International Conference in Wind Engineering, At Porto Alegre, Brazil [Internet]. 2015 [cited 2017 Aug 18]. Available from: https://www.researchgate.net/profile/Mohammadtaghi_Moravej/publication/279770545_Dynamic_effects_of_wind_loading_on_photovoltaic_systems/links/56d770ae08aee1aa5f75cbc1.pdf

20. Kilikevičius A, Čereška A, Kilikevičienė K. Analysis of external dynamic loads influence to photovoltaic module structural performance. Engineering Failure Analysis. 2016 Aug 1;66(Supplement C):445–54.

21. Aly AM, Chowdhury AG, Bitsuamlak G. Wind profile management and blockage assessment for a new 12-fan Wall of Wind facility at FIU. Wind & Structures. 2011;14(4):285–300.

CHAPTER 6

SUMMARY AND CONCLUSION

CHAPTER 6. SUMMARY AND CONCLUSION

This study aimed to investigate the wind forces acting on the residential roof mounted PV panels along with the dynamic response of these structures. The research consisted of three main phases.

The first phase focused on investigating the effects of different geometrical configurations on the wind induced pressures acting on PV panels. The investigated geometrical configurations included building height, roof type, PV panel tilt angle and clearance distance from the roof surface. This investigation shed light on the most important geometrical parameters affecting the wind induced pressures as well as the most critical locations on the roof surface with respect to maximum pressure and suction wind forces.

In the second phase, it was tried to evaluate the effects of dynamic response of the PV system to wind induced vibration. To assess the dynamic response of the PV panel array and vibration issues that are induced even at lower wind speeds, three models were mounted on building and tested at the Wall of Wind Experimental Facility at FIU, including a full-scale real PV panel array (i.e. flexible model), a full-scale rigid panel array (i.e. wood model) and a large scale rigid panel array (i.e. plexiglass model). By comparing the support reactions of rigid model and flexible model the effects of dynamic vibration of the PV panels was investigated.

The last phase of the research was dedicated to numerical simulation of wind induced vibration on the PV systems. The analytical model of the PV panel was developed and validated by experimental hammer test results. The validated model was then subjected

to the time history of the experimentally recorded wind pressures and dynamically analyzed to obtain the response of the system to boundary layer wind. In overall, this research extends the knowledge of wind effects on PV systems and their supporting structures which can improve the design criteria to achieve a cost efficient, safe and stable PV system implementation. Following is a list of the findings and conclusions of each research phase.

6.1. Geometrical Configurations

Wind pressure measurement on the roof mounted solar panel surfaces, showed that the tilt angle and roof type are the most important parameters affecting the load on the panels while the clearance and building height was not significantly changed the wind force on the solar panels. At different tilt angles the critical wind direction, and location of peak pressures on the arrays can be varied.

The flat roof mounted panels experience the highest suctions when the building generated turbulent flow from northern or northern cornering (180˚ to 240˚) wind pushes the lower surface of the panels and the flow separation occurs on the upper surface. The panels located on the windward corner of the roof are experiencing the highest loads. The highest net wind forces on the gable and hip roof mounted panels are the winds attacking from back of the arrays (180˚). The panels that are located near the gable (or hip) ridge and the gable end edge (or hip line) are experiencing the highest loads. The uplift pressures due to the flow separation of the roof edges are mainly responsible for these effects.

This study suggests the enveloping curves based on the measured pressures and the resulted force coefficients applicable to the structural design of solar PV systems, including

the panels, racking and mounting systems, and the building roof structure. Since the number of the solar panels can be varied, enveloping curves are the useful tool incorporating in the design codes and standards.

The comparison is made between the proposed enveloping curves and the force coefficients suggest by previous researches as well as codes and standards. The values for smaller effective areas resulted from the current study were found to be noticeably higher when compared to those from previous studies and the limited existing codes. The main reason for this discrepancy can be attributed to the set back of the arrays from the roof edges. Because of the modelling and scale issues the previous studies could not in capture the high pressures that are mainly observed at near edge zones.

6.2. Experimental Vibration Analysis

It was observed that the mean force coefficient results were independent of the wind speed, while there were some discrepancies among the peak force coefficient recorded at different wind speeds for specific wind directions.

Mean and minimum force coefficient values obtained from the rigid and flexible models showed a good agreement while the maximum force coefficients obtained from the rigid model were generally higher than the flexible model.

The mean force coefficient values calculated based on pressure tap results were similar for large-scale and full-scale tests. However, there was a notable discrepancy between the peak force coefficients obtained from these two models. It was shown that partial turbulence simulation can help reduce this discrepancy.

The observed peak in the response spectra of the model at near 10 Hz frequency is justified by the resonant effect at 10.5 Hz fundamental frequency of the model.

The experimental observations were in agreement with the current wind standard recommendations particularly when the force coefficients were calculated based on pressure data.

6.3. Analytical Vibration Analysis

The analytical model was validated with experimental hammer tests so that its modal frequencies matched the natural frequencies of the PV system. However, the validated analytical model was incapable of accurately simulating the dynamic response of the system under wind induced pressures once the effect of supporting building was not considered for the analytical modeling.

To correctly simulate the dynamic response of the system, spring and damper sets were added to the analytical model to represent the deflection of the supporting building. This modification significantly improved the results of the analytical model.

It was concluded that supporting structure can considerably affect the dynamic response of the PV system to wind induced vibrations and should be considered for accurate evaluation of the wind effects.

VITA

AMIR NAEIJI

Born, Tehran, Iran

2004 - 2008	B.Sc., Civil Engineering, Iran University of Science and Technology, Tehran, Iran.
2009 - 2012	M.Sc., Structural Engineering, University of Tehran, Tehran, Iran
2013 - 2017	Ph.D., Structural/Wind Engineering, Florida International University, Miami, FL

PUBLICATIONS AND PRESENTATIONS

Naeiji, A., Raji, F., and Zisis, I. (2017). Wind loads on residential scale rooftop photovoltaic panels. Journal of Wind Engineering and Industrial Aerodynamics, 168, 228-246.

Naeiji, A., Matus, M. and Zisis, I. (2016). Wind-induced Loads on Canopies Attached to Medium-rise Buildings. Proceedings of 4th American Association for Wind Engineering Workshop (4AAWE), Miami FL, USA.

Zisis, I., Naeiji, A. and Matus, M. (2016). Wind-induced Loads on Canopies Attached to Mid-rise Buildings. Final Report submitted to The State of Florida Division of Emergency Management.

Naeiji, A., Raji, F., Zisis, I., Chowdhury, A., Irwin, P. (2015). Wind-induced Pressures and Forces on Solar Panels Mounted on Flat, Gable or Hip Roof Residential Buildings. In 14th International Conference in Wind Engineering Proceedings, Porto Alegre, Brazil.

Candelario, J., Raji, F., Naeiji, A., Zisis, I., Chowdhury, A. (2015). Large-scale wind testing on canopies attached to residential buildings. In 14th International Conference in Wind Engineering Proceedings, Porto Alegre, Brazil.

Naeiji, A., Moravej, M., Chowdhury, A., Zisis, I. (2015). Experimental Study of Dynamic Behavior of Photovoltaic Systems. Final Report submitted to The State of Florida Office of Insurance Regulations.

Naeiji, A., Raji, F., & Zisis, I. (2015). Large-scale Wind Testing of Photovoltaic Panels Mounted on Residential Roofs. In ASCE Structures Congress 2015 (pp. 1868-1878), Portland, Oregon.

Zisis, I., Naeiji, A. and Raji, F. (2014). Codification of Wind-induced Loads on Rooftop Solar Panels. Final Report submitted to The State of Florida Division of Emergency Management.